AFCRL-64-917 ASE-759

A RESEARCH PROGRAM TO INVESTIGATE ARTIFICIALLY INJECTED TRAPPED RADIATION

R. GIACCONI
F. R. PAOLINI
W. C. HADLEY
R. TALBOT, JR.

American Science and Engineering, Inc.
11 CARLETON STREET
CAMBRIDGE, MASSACHUSETTS
02142

CONTRACT NO. AF 19 (628)-2799
PROJECT NO. 8630
TASK NO. 860006

FINAL REPORT

30 OCTOBER 1964

PREPARED FOR

AIR FORCE CAMBRIDGE RESEARCH LABORATORIES
OFFICE OF AEROSPACE RESEARCH
UNITED STATES AIR FORCE
BEDFORD, MASSACHUSETTS

Requests for additional copies by Agencies of the Department of Defense, their contractors, and other Government agencies should be directed to the:

DEFENSE DOCUMENTATION CENTER (DDC)
CAMERON STATION
ALEXANDRIA, VIRGINIA 22314

Department of Defense contractors must be established for DDC services or have their "need-to-know" certified by the cognizant military agency of their project or contract.

All other persons and organizations should apply to the:

U. S. DEPARTMENT OF COMMERCE
OFFICE OF TECHNICAL SERVICES
WASHINGTON, D. C. 20230

AFCRL-64-917 ASE-759

A RESEARCH PROGRAM TO INVESTIGATE ARTIFICIALLY INJECTED TRAPPED RADIATION

Authors: R. Giacconi, F. R. Paolini
W. C. Hadley, R. Talbot, Jr.

American Science and Engineering, Inc.
11 Carleton Street
Cambridge, Massachusetts 02142

CONTRACT NO. AF 19 (628) - 2799

Project No. 8600

Task No. 860006

FINAL REPORT

30 October 1964

Prepared for

AIR FORCE CAMBRIDGE RESEARCH LABORATORIES
OFFICE OF AEROSPACE RESEARCH
UNITED STATES AIR FORCE
BEDFORD, MASSACHUSETTS

FOREWORD

This document is the final report on Contract AF 19 (628) - 2799. It describes an experimental program devoted to the study of the particle population trapped in the Earth's magnetic field and injected into it by either natural cause or by high altitude nuclear bursts. Instruments were constructed in this program according to the designs developed under two other Air Force contracts. The proton-alpha detector and the proton spectrometer were developed under Contract AF 19 (604) - 7347, and the electron and gamma detector was developed under Contract AF 19 (628) - 252. The description of these instruments is abstracted from the final report on these programs.

Instruments identical to the ones constructed were flown on an Air Force Satellite, 1962 βk, on 26 October 1962, under Contracts AF 19 (628) - 252 and AF 19 (604) - 7347.

The analysis of the data obtained by this instrumentation has been carried out as part of this program, and the procedures are here given. The results of this analysis have been presented to the scientific community in several publications, of which the most recent are enclosed.

ABSTRACT

This document describes an experimental research program to measure the intensity, angular distribution, and energy spectra of particles trapped in the Earth's magnetic field. Particular attention has been focused on the measurement of particles artificially injected by high altitude nuclear detonations during the series of nuclear tests conducted by the USSR and the USA during the summer and fall of 1962. A detailed description of the instrumentation and calibration procedures are given. Measurements obtained by instrumentation identical to the one here described, flown on an Air Force satellite (1962 βk) are given. The method of data handling is discussed and machine programs for data reduction are described. Results from these measurements have appeared in several documents, a listing of which is included in the text. A summary of the results and conclusions is given.

TABLE OF CONTENTS

LIST OF APPENDICES

TABLE OF FIGURES

1.0 INTRODUCTION

The radiation trapped in the Earth's magnetic field has been the subject of intense study for the past several years. Experiments have been prompted by the intense scientific interest in this important geophysical phenomenon as well as by the practical importance of its effects. Possible danger to manned and unmanned spacecraft exposed to the trapped radiation flux has been a primary practical consideration. Instruments to detect and study the trapped particle environment had been designed and flown by several groups by the time of the resumption of high altitude nuclear testing in 1962. From the understanding which had been reached on the behavior of the natural radiation belts, it was realized that large yield high altitude nuclear detonations would significantly alter the particle distribution in the belts by injecting copious numbers of the charged particles produced by the detonation. The artificial radiation belts thus created were in fact intense enough to cause damage to solar cells of orbiting spacecraft and to present a real hazard for manned space missions.

An important difference exists between natural and artificial belts. Artificial injections result in a sudden increase of the particle intensities in localized regions of the magnetosphere. This increase can be so large that the flux of artificially produced particles is orders of magnitude greater than the natural flux. The pitch angle distribution and energy spectrum of the radiation may also be radically changed. With time, conditions return to the natural levels. Depending on the characteristics of the injection and on the processes which determine the removal of trapped radiation, the

characteristic times for return to the "normal" can vary by large factors. Estimates of these times prior to the tests varied from months to decades. The purpose of the research program described in this report was to study the nature of the radiation, its angular distribution, its energy spectrum, and its temporal and spatial variation.

Several mechanisms play an important role in the injection of trapped particles produced by nuclear detonation. One can easily understand how the decay of neutrons or of radioactive debris can result in trapping. The relative importance of the various processes is, however, harder to determine and depends critically on the depth in the atmosphere at which the detonation occurs.

The low atmospheric density at the altitude at which Shot Star Fish Prime was detonated permitted the debris to expand to great distances. In the upward direction the major force acting to restrict this expansion was due to the interaction of the charged debris with the geomagnetic field. As a consequence, this expansion continued until one or a combination of the following conditions occurred. The debris was brought to rest, its energy having been converted to magnetic energy and stored in the compressed field; or the debris was guided along the field lines of the magnetic bottle to the Southern Hemisphere; or the debris de-ionized and the subsequent trajectory of each particle was determined by the gravitational force until a β-decay event occurred; or the expansion became turbulent with the debris breaking up into separated blobs. The downward expansion was controlled principally by the exponentially increasing atmosphere.

Several ways exist to permit the debris to expand to large distances from the source. Each debris β-decay event results in the injection of an electron into the magnetosphere. What happens to the electron depends

on its energy, the altitude of injection, and the pitch angle of injection. For each altitude electrons injected over a certain portion of the solid angle can be trapped. The contribution by this process of debris decay to the artificial belts is believed to have been predominant over other processes and in particular over neutron decay injection in the Star Fish event[1] In low altitude detonations occurring, for instance, at 30 km, the contribution to injection by the neutron decay process may become comparable or predominate over the debris decay injection process. Accurate measurements of the spectrum and anguiar distribution of artificially trapped radiation could permit discrimination between the different injection models.

Of great importance for the understanding of the dynamics of the trapped radiation and for its practical consequences is the determination of the removal times associated with the artificial radiation belts. The measurements obtained up to date seem to indicate a rapid initial decay followed by a slower exponential decay with characteristic decay times of the order of months. It would also appear that scattering of the trapped particles on atmospheric constituents is the major cause for removal.[3]

The results of the program here described have been published in various forms. In this report a brief summary of results and of the major conclusions are given. The instrumentation and calibration procedures are described in detail.

2.0 INSTRUMENTATION

The instrumentation constructed under this contract had been designed and developed under other contracts. It included three instruments:

1. A proton spectrometer for the energy region of 6 to 70 Mev, developed under Contract AF 19 (604) - 7347. The detector and pertinent calibrations are described in Appendix A.

2. A proton and alpha particle detector for the region from 1 to 10 Mev also developed under Contract AF 19 (604) - 7347 and described in Appendix B.

3. An electron and γ -ray measuring instrument package developed under Contract AF 19 (628) - 252, which is described in Appendix C. This instrument contains two detectors sensitive to electrons and one sensitive to γ -rays, 0.05 to 5 Mev.

The three instruments were constructed under this program to replace identical instruments built under the AF 19 (628) - 252 and AF 19 (604) - 7347 programs and flown on an emergency basis on an Air Force satellite given the international designation 1962 βk, flown in the fall of 1962.

Part of this contract consists of the analysis of the data obtained by the instrumentation flown on this satellite. We therefore included in this report a description of the principle of operation and characteristics of the three instruments mentioned above.

3.0 DESCRIPTION OF SATELLITE MISSION

In the fall of 1962 an Air Force satellite, given the international designation 1962 βk, was launched into orbit. The satellite carried instrumentation to study artificial radiation belts created by the injection of electrons from nuclear detonations into the magnetosphere. Under the scientific direction of Air Force Cambridge Research Laboratories, a number of instruments were chosen for inclusion in the payload The instruments described in the preceding chapter were part of the payload.

The pertinent parameters for the satellite orbit at early times were the following: apogee, 3000 n.m.; perigee, 115 n.m.; orbit inclination, 71°; orbital period, 147 minutes; apsidal rate, 0.8° per day. Figure 1 illustrates these orbital parameters. The satellite pitch period was 127 seconds, and the roll period was 53 seconds. The satellite parameters were well suited to study the phenomena of interest. For example, the high eccentricity of the orbit enabled the acquisition of data at large L values near the equatorial plane. Slow tumbling rates, along with the chosen data sampling rate of about one per second, permitted the use of instruments which could measure accurately the angular distributions of trapped particles.

Figure 2 shows the projection of an early orbit on a dipole field. The coordinates are the usual "natural" B-L coordinates of McIlwain[2]. The squares and circles show regions of data acquisition in the 1.2 and 1.9 L-shells, shells of interest with respect to artificial radiation belts.

SATELLITE ORBIT

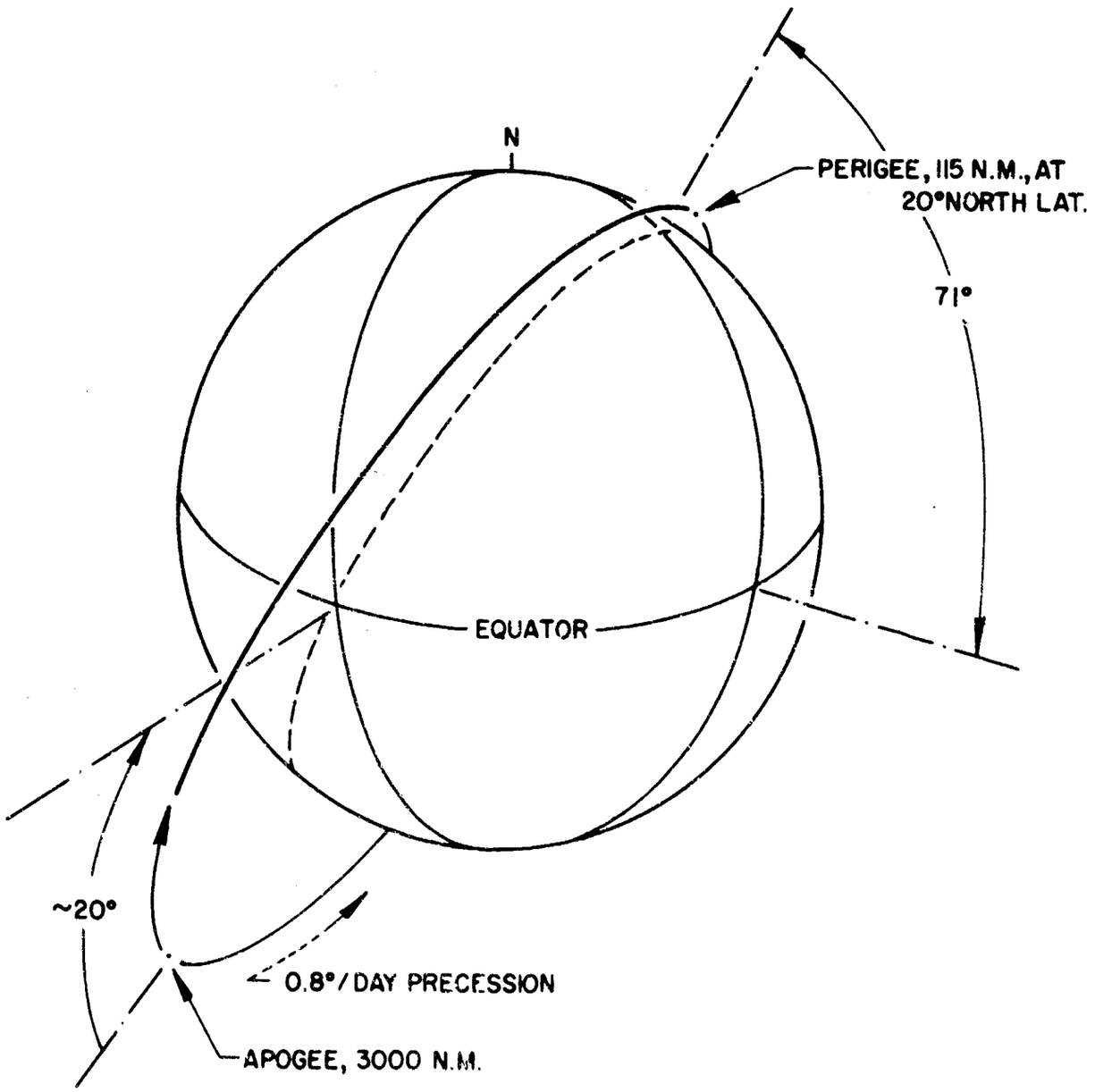

Figure 1

Figure 2

LOCUS OF AN ORBIT IN B-L SPACE
B (GAUSS)
.40
.30
.20
.14
.10
.06
.04
L
1.0
1.2
1.4
1.6
1.8
2.0
2.2
2.4
2.6
L
①
②
③
④
⑤
⑥

The instruments comprising the total payload were selected to yield redundant measurements in the energy range corresponding to fission electrons, and to include narrow acceptance angle detectors as well as omni-directional detectors. Instruments obtained their power from a large capacity battery pack to avoid degradation of the experiment due to possible solar-cell damage. Data could be acquired both by direct "real-time" read-out and by command read-out of a tape recorder capable of storing data from all instruments for a time longer than the orbital period.

The five scintillation detectors comprising the AFCRL-ASE portion of the payload were designated Beta-1, Beta-2, Gamma, P, and P-alpha. There is evidence that the P-alpha detector malfunctioned shortly after launch. The most salient features of the remaining four instruments are summarized in Table I.

It will be observed that detectors Beta-1, Beta-2, and Gamma have extremely wide fields of view for charged particles; (detector Gamma has essentially a 4π field for gamma radiation). These instruments were utilized in determining the gross aspects of the artificial belts. Detector P has an extremely narrow field of view, and is essentially a "directional differential intensity" detector. This detector was used in obtaining pitch angle distributions. Output channels most used for the data presented later in the report are marked with an asterisk.

Discrimination among types of particles (electrons, protons, or gammas) is achieved by a comparison of the observed counting rates and the rates of energy deposition in several channels, and by roll-modulation observations. In artificial radiation belts produced by high altitude nuclear detonations, the detected particles are predominantly electrons.

TABLE I

INSTRUMENT	FIELD OF VIEW		SCINTILLATOR	SHIELDING			DETECTOR THRESHOLD Mev		
	$\Delta\theta$ deg.	$\Delta A\Delta$ cm^2-ster	gm/cm^2	Window; Sides			γ	e	P
Beta-1 Beta-2	90°	1.8×10^{-2}	0.3 "E"	3 mg/cm^2 Al; $\geq 3 gm/cm^2$ Al	A	ϕ		0.5	2.0
					B	"		1.0	2.8
					C*	W		.05	1.4
Gamma	120°	1.8	4.5 CsI(Tl)	2gm/cm^2 Al; $\geq 4 gm/cm^2$ Al	A*	ϕ	0.5	4.5	40.+
					B	"	1.0	5.0	40.+
					C	W	.04	4.0	40.
P	6°	1.7×10^{-3}	12.5 CsI(Tl)	70 mg/cm^2 Al; 25. g/cm^2 Fe	A*	ϕ	1.0	1.0	6.2
					B	"	2.0	2.0	6.5
					C	"	4.0	4.0	7.6
					D	"	8.0	8.0	10.5
					E	"	20.	20.	21.
					F	"	30.	30.	31.
					G	"	50.	50.	51.
					H	"	70.	70.	70.
					J	W	.012	0.3	6.0

KEY

ϕ Flux Measurement

W Rate of Energy Deposition Measurement

A thru J: Channel Identification

4.0 DATA REDUCTION TECHNIQUES

The telemetered data from the satellite was digitized and merged with ephemeris information by Lockheed. This ephemeris information included B-L coordinates derived from McIlwain's model. Programs for the IBM 7090 computer were developed and used whenever possible in the data reduction. These programs are discussed in detail in Appendix D.

Digital Computer Processing. Outputs of the processing system included:

1. Straight listing or summary of telemetered information,
2. B - L matrix with detector counting rates as elements,
3. Pitch angle distribution printouts.

4.1 Time Correction

It was discovered that the universal times assigned to voltage points on the digitized tapes were in error. An initial assumption was then made to the effect that the time error was constant throughout a satellite orbit. Then two methods were used to determine time corrections:

1. From a knowledge of the satellite orbit, times of entry and exit from the Earth's shadow could be computed. This information was correlated with readings of the satellite's solar sensors to produce a time correction.

2. By studying the instrument readings, it was possible to determine when the satellite was passing through radiation belts. A radiation belt has a constant associated

L value. Since ephemeris quantity L was computed from universal time, which was in error, successive passages through the same radiation belt had apparent different L values. By adjusting universal time (and ephemeris) in such a manner as to yield consistent L values on each passage through the same radiation belt, a time correction could be computed.

Both methods yielded consistent results for any satellite phase. We have therefore used in data analysis universal times corrected by using Method 1.

4.2 Correcting Magnetometer Data

Figure 3 shows, as a function of time, a typical portion of the raw data from detector P and the corresponding calculated value of the cosine of the pitch angle θ. If we accept these pitch angle curves at face value, we would obtain inconsistent distributions from the left and right portions about a maximum or minimum of the cos θ curve. We demand consistency about maxima and minima in our analysis, attributing the apparent angular discrepancies to magnetometer error. This amounts to assuming axial symmetry about a B-field line.

There is little doubt that the magnetometer data are in error. The angular discrepancy is always greater in low B-field regions. Furthermore, if we plot the difference in absolute values between the magnetic field strength given in the ephemeris (calculated from the Jensen and Cain model) and the magnetic field strength derived from the magnetometers, we obtain an oscillatory function with a time behavior characteristic of the pitch- and roll behavior of the satellite. Such an apparent magnetometer error may be due to the residual magnetic field of the satellite or to magnetometer

TYPICAL DATA

PITCH ANGLE VARIATION

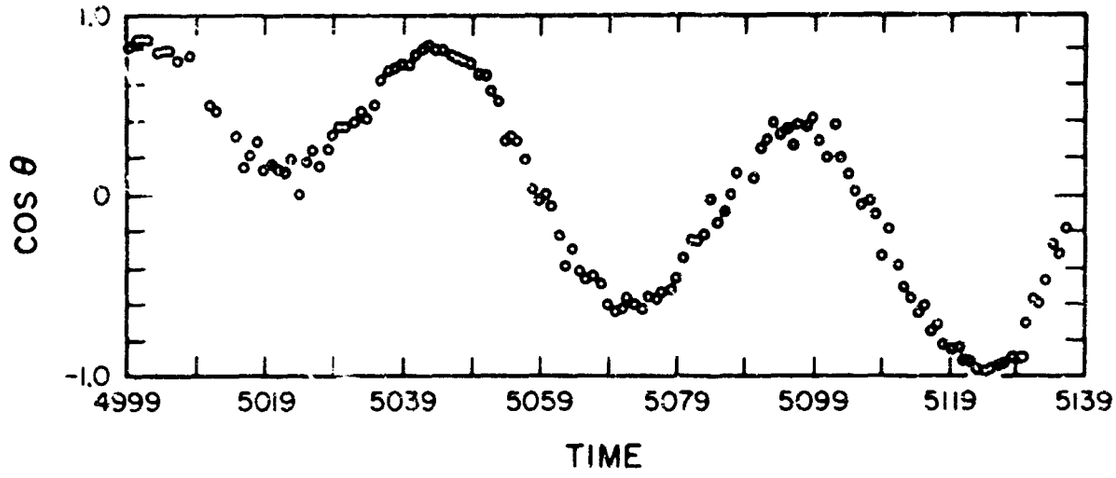

COUNTING RATE VARIATION

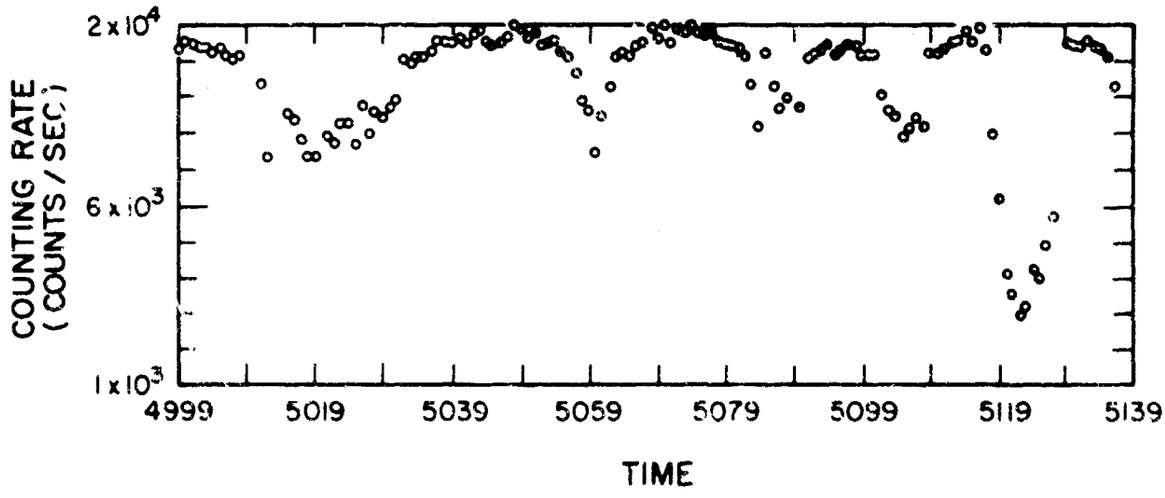

Figure 3

calibration drifts. The angular discrepancy does not seem to be due to timing errors since in the same orbit the angular shift required to bring about data consistency is just as apt to be positive as negative. All attempts to discover the source of the angular discrepancy, and correct for it, did not prove successful. We have, therefore, in our treatment of the data, shifted the aspect function by the amount required to bring about data consistency. The magnitude of such a shift seldom exceeds 6^{o} and, as stated, tends to be larger in the low B-field regions of the orbit.

ASE Document ASE-845 gives further details on the computer programs, on techniques used to make time corrections, and on attempts to make magnetometer corrections.

5.0 RESULTS AND RECOMMENDATIONS

After reduction, the data were analyzed to achieve the following aims:

1. To establish the time and location of the artificial injections occuring during the useful life of the spacecraft instrumentation,
2. To determine the angular distributions of the trapped particles, and
3. To study the temporal and spatial intensity variations.

The results obtained have been described in the several documents listed below to which ASE scientists have contributed under this program:

1. R. Giacconi and F. Paolini, "Preliminary Results Obtained by 1401 Instrumentation on the Artificial Radiation Belts", ASE Document ASE-341, 1 January 1963. SECRET
2. L. Katz, D. Smart, R. Giacconi, F. Paolini, and R. Talbot, Jr., "Preliminary Results on the Artificial Radiation Belts Since October 27, 1962, as Measured by Starad", in Symposium Proceedings: Beta Beta and Delta Gamma Programs, 6-7 March 1963, Armour Research Foundation of the Illinois Institute of Technology, Chicago, Illinois, DASA 1371, DASA Data Center Special Report 13, May 1963. SECRET-RESTRICTED DATA.
3. L. Katz, D. Smart, F. Paolini, R. Giacconi, R. Talbot, Jr., "Measurements on Trapped Particles Injected by Nuclear Detonations", in Symposium Proceedings: Trapped Radiation, 15-16 April 1963, Goddard Space Flight Center, Greenbelt, Maryland,

DASA 1394, DASA Data Center Special Report 16, August 1963. SECRET.

4. L. Katz, D. Smart, F. R. Paolini, R. Giacconi, and R. Talbot, Jr., "Recent Changes in the Artificial Radiation Belts", Presentation at the 44th Annual Meeting of the American Geophysical Union, Washington, D. C., 18 April 1963.

5. L. Katz, D. Smart, F. R. Paolini, R. Giacconi, and R. Talbot, Jr., "Measurements on Trapped Particles Injected by Nuclear Detonations", Space Research IV, Proceedings of the Fourth International Space Science Symposium, Warsaw, June 3-12, 1963, North-Holland Publishing Company, Amsterdam.

6. G. A. Kuck, "Time Behavior of Charged Particles Injected by 1962 High Altitude Russian Nuclear Tests", Thesis, Air Force Institute of Technology, August 1964.

Document 5 of this list is included as Appendix E of this report.

In summary, the results of the program were:

1. Detection of artificial belts due to Russian High Altitude Nuclear detonations on October 28 and November 1.

2. Measurement of angular distributions and lifetimes of the trapped radiation artificially injected by the Russian detonations from early times up to 45 days after the detonation.

The major difficulties encountered in the programs were:

1. Difficulty of interpretation of the data due to the broad response characteristics of the detectors with respect to different species and energies of particles.

2. Insufficient angular resolution of the electron detectors.

3. Incomplete coverage by the satellite of the times and regions of interest.

4. Insufficient timing and aspect accuracy.

Most of these difficulties were due to the fact that the instrumentation was not specifically designed for monitoring artificial radiation belts. The short times involved from conception to flight of 1962 βk (about 1 month) also did not permit modification of the detectors or adequate discussion and implementation of the timing and aspect requirements. Advanced planning, resulting in stand-by payloads specifically designed to detect artificially injected particles and ready to be flown for such missions is obviously the answer. This policy is presently being implemented by the Defense Atomic Support Agency.

A second difficulty which as yet has received inadequate attention is the poor coverage which one can obtain from polar orbiting satellites. A polar orbiter affords inspection of shells with a wide range of L values but poor coverage of each shell. An equatorial satellite with identical instrumentation with appropriately selected orbit could permit full time coverage from zero times.

REFERENCES

(1) Killeen, John, Wilmot N. Hess and Richard E. Lingenfelter, J. Geophys. Research 68, 4637 (1963).

(2) C. E. McIlwain, J. Geophys. Research 66, 3681 (1961).

(3) W. M. MacDonald and M. Walt, J. Geophys. Research 67, 5025 (1962).

APPENDIX A

"Proton Spectrometer"

Excerpt from G. Davidson, R. Giacconi, H. Gursky, et al., A Research Program to Investigate the Experimental Problems of Particle Measurements in Space, Final Report on Contract AF 19 (604) - 7347, ASE Document ASE-400, 27 May 1963. pp. 133-146.

3.4 PROTON SPECTROMETER

3.4.1 Introduction

The knowledge of the radiation environment in which satellite components have to survive is of particular interest for the design of long-lived systems. Due to the steepness of proton and electron spectra in the Van Allen belt, it is evident that most of the energy content is carried by low-energy particle fluxes. In particular, relatively low-energy protons (energies greater than 10 Mev) can traverse considerable thicknesses of shielding - for instance, 1 millimeter of aluminum - and lose their total residual energy in the next few grams of material. Damage to solar cells by such protons is therefore particularly extensive.

Such data must be known for satellites which spend a large portion of their orbit in the heart of the inner Van Allen belt where large fluxes of protons in this energy range are expected. The measurements available to date have been performed in the energy range above 60 Mev. These data indicate a steep power spectrum up to 320 Mev. If one extrapolates these results to the 10 Mev region, it can be shown that 10 Mev protons carry about 10^3 times more energy than 60 Mev protons. However, such an extrapolation is not known to be valid, and it is therefore of great importance to determine the differential spectrum of protons in this energy range to establish the existence or absence of a "knee" in the energy spectrum

The following sections describe an instrument which has been designed, constructed and flown primarily for the purpose of measuring the energy spectrum of protons in the energy region 6 to 100 Mev.

3.4.2 Theory of Design

The guiding philosophy in the design of this instrument

was to achieve the utmost simplicity consistent with the desired objective of measuring the spectrum of protons in the energy range between 6 and 100 Mev in the heart of the inner Van Allen belt. The spectrometer is a directional instrument which measures proton fluxes within a cone $\pm 5^{o}$ from its axis, and therefore is capable of further yielding information on pitch angle distributions.

The detector consists of a Thallium activated CsI crystal whose thickness in the direction of the incident beam is equivalent to the range of 90 Mev protons (11.5 gr cm^{-2}). This scintillator is surrounded by a stainless steel shield equivalent in thickness to about 100 Mev protons except in a narrow opening which defines the field of view. In the path of the incident particles and in front of the CsI(Tl) crystal an aluminum shield equivalent in thickness to the range of a 6 Mev proton (70 mg cm^{-2}) is placed. Figure 4 is a detailed drawing of the head design.

Protons of energy greater than 6 Mev and smaller than 90 Mev enter the crystal and are stopped in it. The crystal therefore has a response which is proportional to the total energy of the proton in the aforementioned energy range.

Protons of energy greater than 90 Mev traverse the crystal and are not stopped in it. The energy loss of these high-energy particles are not linearly proportional to their total energy, but equal the energy loss of some lower energy protons which do stop in the crystal. However, in any particular interval of energy between 6 and 100 Mev, the amount of contamination due to such high-energy protons will be less than 10 per cent due to the steepness of the proton energy spectrum. Figure 5 shows the relationship between the incident proton energy and the pulse height obtained from the photomultiplier viewing the CsI(Tl) crystal. The decrease in pulse height with increasing energy above 90 Mev is clearly evident.

PROTON SPECTROMETER ASSEMBLY

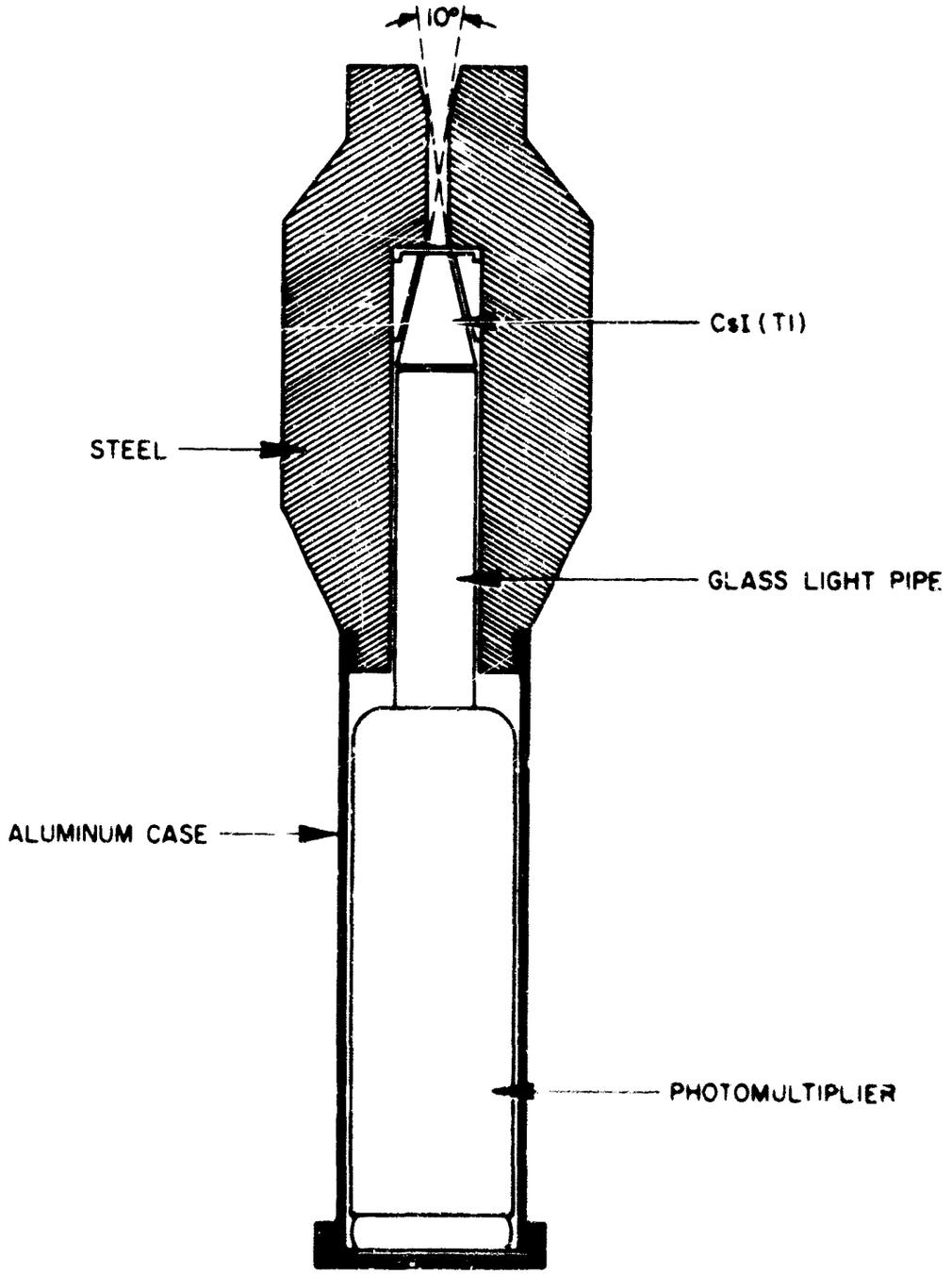

Figure 4

PROTON PULSE HEIGHT FROM A CsI(Tl) SCINTILLATION DETECTOR

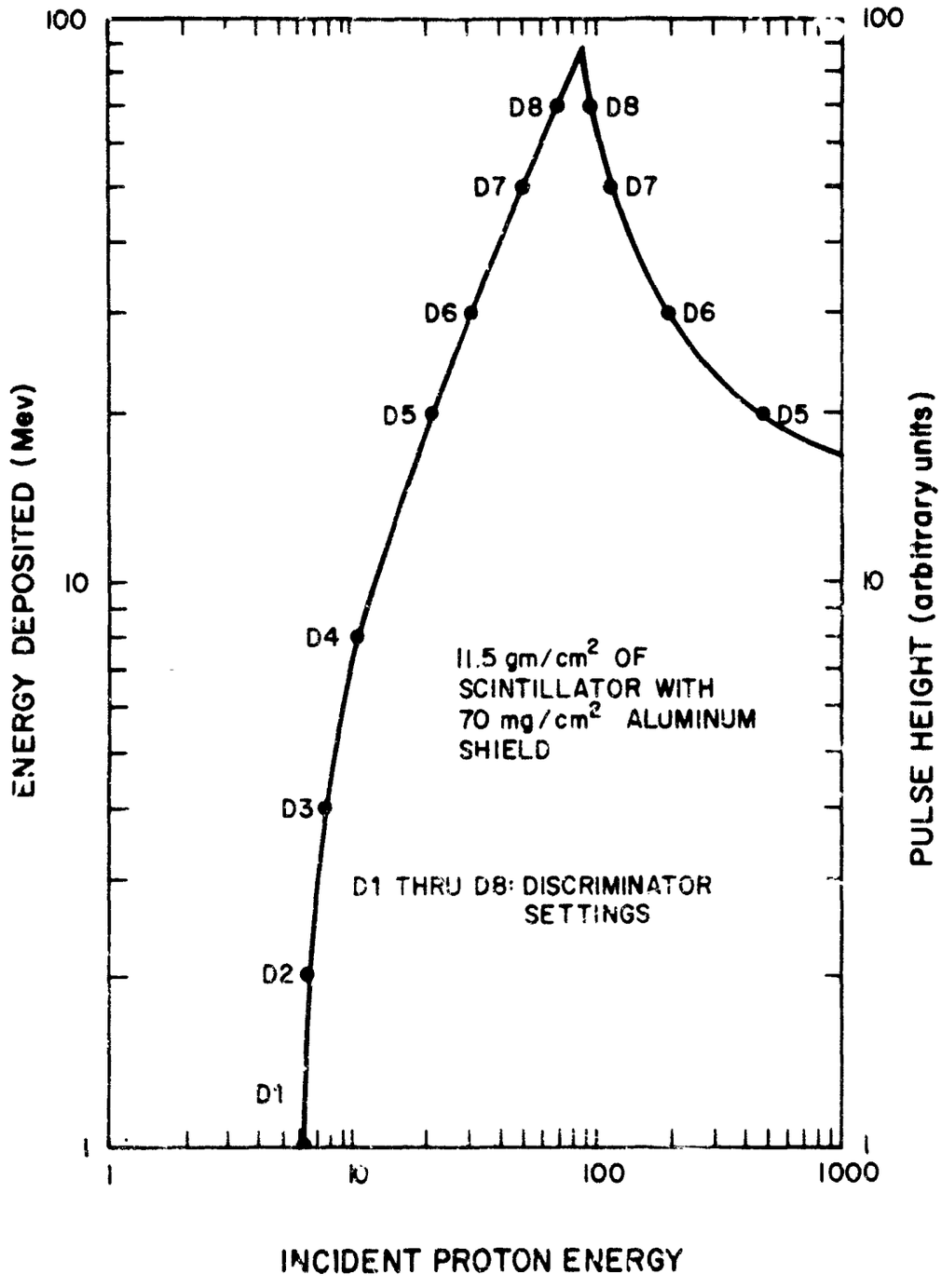

Figure 5

This detector is sensitive also to electrons of energy greater than 40 kev, which can penetrate the aluminum shield. However, since the flux of high-energy electrons is small compared to the proton flux of the same energy in the inner belt, it is felt that the electron background will not give rise to serious difficulties in the analysis of the data for this region of space. By performing pulse height analysis of the scintillator output it is therefore possible to determine the differential spectrum of protons between 6 and 100 Mev to reasonable accuracy. (Energy resolution is about 15% FWHM, and readout accuracy about $\pm$ 20%).

3.4.3 Description of the Instrument

Figure 6 is a photograph of the instrument. It occupies a volume of 6" x 6" x 12", and weighs about 12 pounds. The instrument has been tested to operate satisfactorily over a temperature range of 20°F to 165°F, and can withstand the vibration, shock, and acceleration environment specified for Midas vehicles.

Figure 7 gives a block diagram of the instrument. The scintillator is viewed by a ruggedized photomultiplier. The average dc current of the photomultiplier anode is monitored in addition to the single pulses and is therefore a measure of the total rate of energy deposition in the crystal. The dc current is fed to a dc amplifier which presents the information in analog form between 0 and 5 volts to a telemetering point.

Pulses are fed through two amplifiers with different gains. In the first, pulses corresponding to energy losses in the scintillator between 1 and 8 Mev are amplified to give pulse heights between 0.5 and 4.0 volts. In the second, pulses corresponding to energy losses between 20 Mev and 70 Mev are amplified to give pulse heights between 1.0 and 3.5 volts. The outputs of these two amplifiers are discriminated over eight ranges of pulse height corresponding to energy losses greater than 1, 2, 4, 8, 20, 30, 50 and 70 Mev. Figure 5 illustrates the relationship between incident proton energy, energy loss, and appropriate discrimination levels.

PROTON SPECTROMETER

BLOCK DIAGRAM OF PROTON SPECTROMETER

Figure 6

ure 7

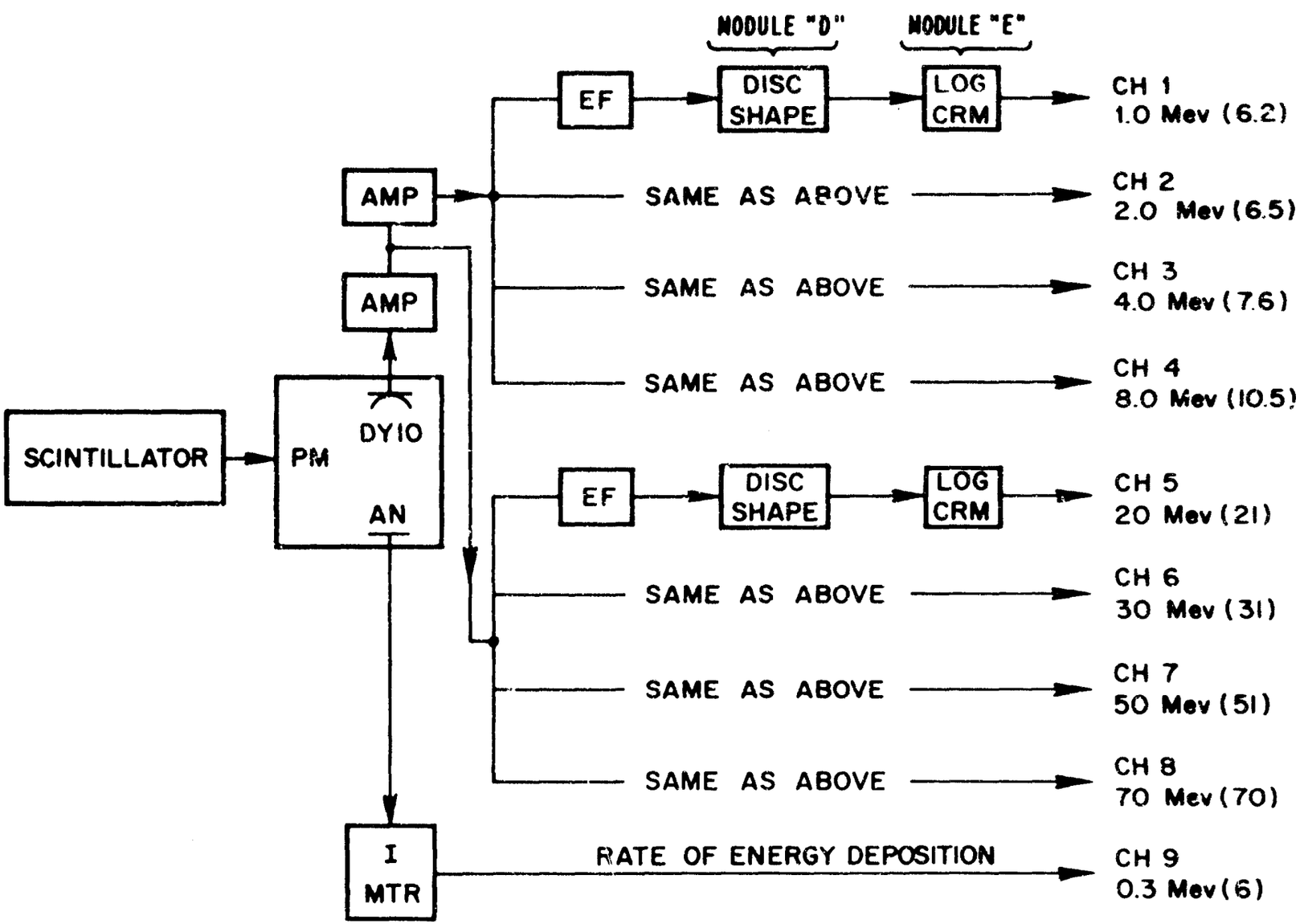
MODULE "D"
MODULE "E"
EF
DISC SHAPE
LOG CRM
CH 1
1.0 Mev (6.2)
AMP
SAME AS ABOVE
CH 2
2.0 Mev (6.5)
AMP
SAME AS ABOVE
CH 3
4.0 Mev (7.6)
SAME AS ABOVE
CH 4
8.0 Mev (10.5)
SCINTILLATOR
PM
DY10
AN
EF
DISC SHAPE
LOG CRM
CH 5
20 Mev (21)
SAME AS ABOVE
CH 6
30 Mev (31)
SAME AS ABOVE
CH 7
50 Mev (51)
SAME AS ABOVE
CH 8
70 Mev (70)
I
MTR
RATE OF ENERGY DEPOSITION
CH 9
0.3 Mev (6)
MODULE "S"

Figure

The output of each energy channel is fed to a logarithmic rate meter whose voltage is proportional to the logarithm of the counting rate over a dynamic range of 3 orders of magnitude. In the low-energy channels, this range extends from 10 to 10^4 counts per second while in high-energy channels it extends from 0.1 to 10^3 counts per second. The output of the logarithmic rate meters is in analog form between 0 and 5 volts. The different ranges in sensitivity were chosen to cover the expected possible variations in the measured intensities which might be encountered in the heart of the inner Van Allen belt.

Twelve telemetering points are needed to transmit the analog information. Additional telemetering points are used to monitor the photomultiplier high voltage and the transistor power supply voltage.

Circuit diagrams for the various elements comprising the instrument are identical to corresponding elements of the P-α detector, and will not be duplicated here. The power consumption of the total instrument is about 2 watts.

3.4.4 Calibration Procedures

Because of time limitations, it was impossible to calibrate the two instruments of this type with proton accelerators. Two accelerators would have been necessary - a low energy machine (such as the 8 Mev ONR Van de Graaff at M.I.T.) and a high energy machine (such as the 200 Mev Harvard Cyclotron) - for calibration of the low and high energy channels respectively.

For this reason, a Po^{210} alpha particle source was used for energy calibration. The source was in the shape of a very thin Po disk, one-eighth inch in diameter, covered with a thin protective film of evaporated gold, all mounted on an aluminum planchette. The energy of the alpha particles penetrating the gold was measured to be 5.2 Mev with a 0.2 Mev half-maximum width by the suppliers of the source. (The spread is caused by energy losses in the source and the protective gold foil.) This energy

spread is well within the resolution of scintillation detectors, and the source was therefore perfectly adequate for our purpose.

Calibration of the eight flux (counting rate) channels of each instrument was achieved as follows. The photomultiplier high voltage was preset. The gain of the amplifier feeding the four low energy channels was then adjusted until the amplifier pulses produced by the alpha source in contact with the scintillator were 1.65 volts high. Since a 5.2 Mev alpha particle gives the same pulse height in CsI(Tl) as a 3.3 Mev proton, this set an amplifier scale factor of 0.50 volts/Mev for protons. The photomultiplier was then disconnected from the amplifier input, and a pulse generator with a network to yield the same pulse shape as was obtained from the photomultiplier was substituted. The discriminators of the four low energy channels were then set to fire for amplifier output pulse heights of 0.5, 1.0, 2.0, and 4.0 volts, corresponding therefore to protons which give energy losses in the scintillator of 1, 2, 4, and 8 Mev respectively. The relationship between incident proton energy and energy loss in the scintillator (indicated in Figure 5 was calculated from proton range - energy relationships in the usual fashion, using the Univ. of Calif. Range-Energy Tables, UCRL-2301.

The gain of the amplifier feeding the four high energy channels was adjusted until the gain, relative to the low channel amplifier, was just 0.10. This was accomplished in practice by trimming this amplifier until a 0.5 volt pulse height output was obtained when the output from the low energy channel amplifier was 5.0 volts; the test pulser was used to furnish the input pulses. This procedure thus set the high energy channel amplifier scale factor to 0.05 volts/Mev for protons. The discriminators of the four high energy channels were then set to fire for amplifier output pulse heights of 1.0, 1.5, 2.5, and 3.5 volts, corresponding to protons which give energy losses in the scintillator of 20, 30, 50, and 70 Mev respectively. Since both amplifiers were tested to be linear within a few per cent over output pulse heights from 0.2 to 5.0 volts, this procedure resulted in a fairly accurate

calibration of the high energy channels despite the indirectness of the technique.

Calibration of the energy deposition channel was achieved as follows. The instrument was placed in a standard location in front of an opening in a lead house containing a 10. millicurie Co^{60} source. The rate of energy deposition in a standard shape CsI(Tl) crystal had previously been determined for this location in the following way. The crystal was mounted on a photomultiplier, run at a predetermined negative high voltage and the charge deposited by the Na^{22} 0.51 Mev annhilation photopeak was measured in the conventional way. This led to a "charge sensitivity constant", giving the number of coulombs deposited per ev of energy deposition by electrons. This number, of course, is also identical in magnitude to a "current sensitivity constant" giving the photomultiplier current (coulombs/second) produced per ev/second rate of energy deposition. The PM was then rewired for anode dc current measurement, and placed at the standard location before the Co^{60} source. The PM was run at the same high voltage as before, and the anode current was measured. Since the "current sensitivity factor" was known, this led directly to the rate of energy deposition in the standard CsI(Tl) crystal at the standard location before the source. Geometrical and shielding corrections were then calculated for the CsI(Tl) scintillator and shielding proper to the proton spectrometer to be calibrated. These were applied to derive a new source strength, in ev/sec, peculiar to this detector placed in the standard location. The signal output from this instrument's current meter was then recorded. This procedure calibrated one point for this channel, in an absolute fashion. To achieve calibration over the entire dynamic range of this channel, use was made of the fact that photomultiplier anode current (within space charge limitations) is linearly proportional to the rate of energy deposition in the scintillator. An intermediate calibration curve, of current meter signal output versus input current (generated by a calibrated laboratory current source) was first plotted. The recorded photomultiplier

signal obtained from the Co^{60} source led directly to the needed proportionality constant between PM anode current and rate of energy deposition. The current scale of the aforementioned intermediate calibration curve was then relabled in terms of the rate of energy deposition, resulting in an absolute calibration curve. The curve for a typical instrument is shown in Figure 8 .

The logarithmic count rate meters were calibrated by the use of the pulser utilized in the energy scale (discriminator) calibrations. Output signal versus the pulse repetition rate input was plotted for each of the eight flux channels of the instrument. Figure 9 shows a typical calibration curve.

3.4.5 Summary of Experimental Results

Up to the time of this report, one proton spectrometer has flown, and that one on a satellite given the international designation 1962$\beta\kappa$. The instrument operated satisfactorily. Analysis of the data obtained has not yet been completed. Preliminary results were reported at the NASA-DASA Symposium on Trapped Radiation, held at Goddard Space Flight Center in Greenbelt, Maryland, on April 15 and 16; and again at the 44th Annual Meeting of the American Geophysical Union held in Washington, D. C., on April 17 through 20.

Probably the most interesting data obtained from this instrument resulted from its capabilities as an electron spectrometer, rather than as a proton spectrometer. In this application, since the electron to proton pulse height ratio is very close to unity in CsI(Tl), and since the 70 mg/cm^2 aluminum shield in front of the scintillator results in negligible energy loss for high energy electrons, the first five discriminator levels correspond very nearly to electrons of incident energy 1, 2, 4, 8, and 20 Mev. (The last three discriminators will not respond to electrons since the maximum energy loss an electron can experience in the CsI(Tl) is about 25 Mev.) During flight, significant electron counting rates were

CALIBRATION CURVE
RATE OF ENERGY DEPOSITION CHANNEL
S MODULE OUTPUT

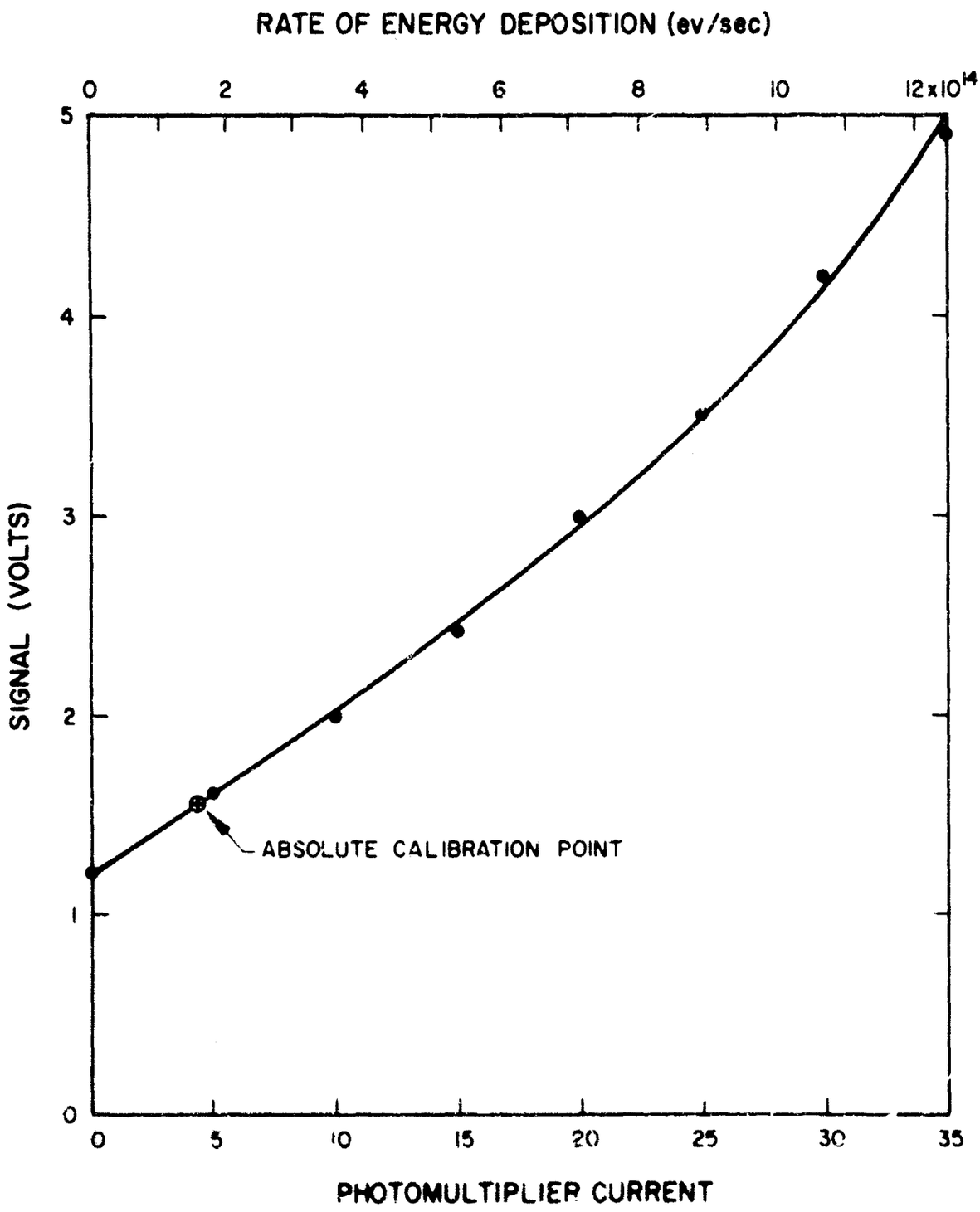

Figure 8

CALIBRATION CURVE
LOG RATEMETER 8 Mev CHANNEL
E-4 MODULE OUTPUT

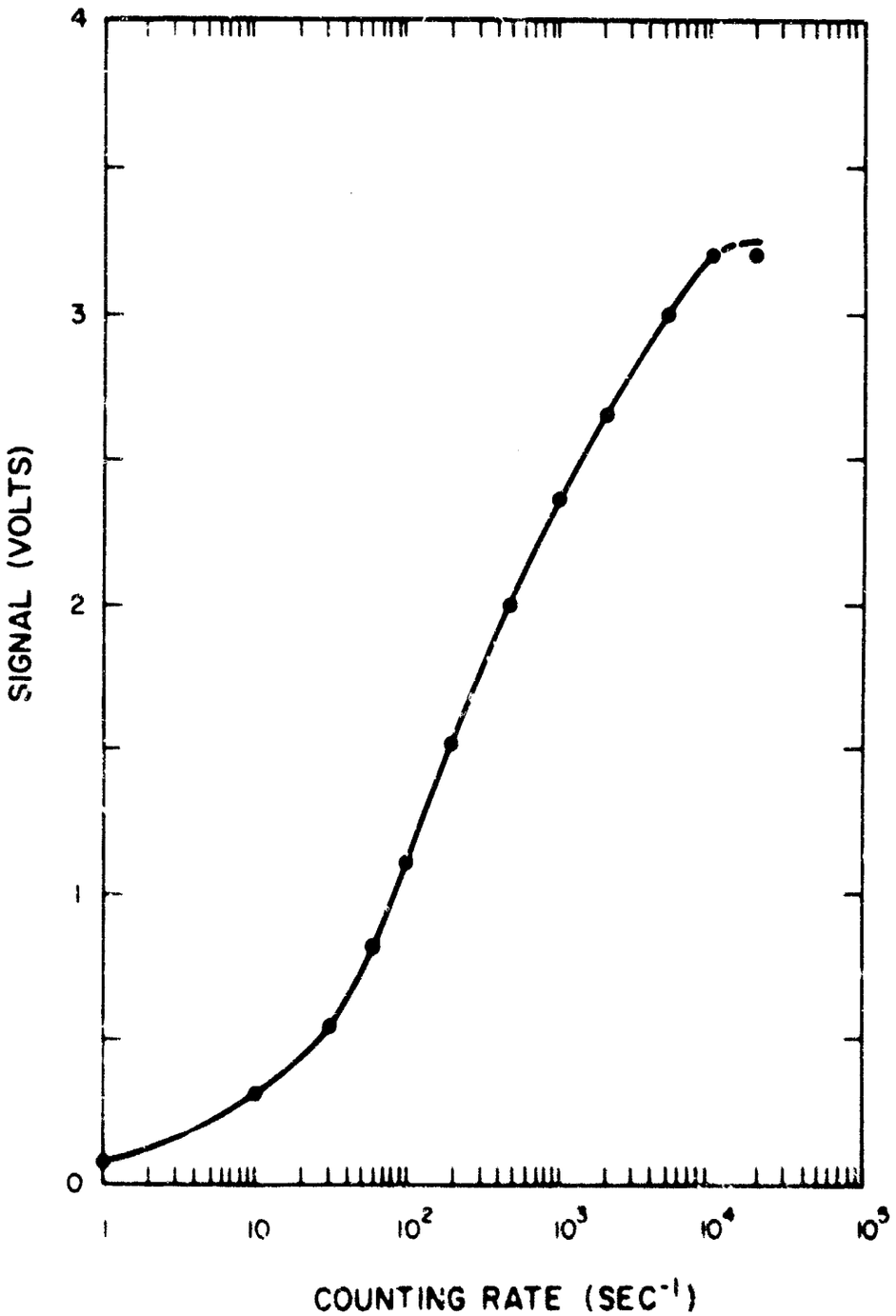

Figure 3

observed in the first three channels. Highest fluxes occurred when the satellite passed through the L = 1.83 shell, containing an artificial radiation belt. This L region is also the slot between the natural inner and outer radiation belts, known to be low in proton population. Correlation with outputs of other instruments flown established conclusively the identification of the particles beyond L = 1.8 as electrons. Protons were detected by the instrument in the region of the inner belt as expected, but data analysis for this region of the magnetosphere is incomplete.

APPENDIX B

"Proton-Alpha Experiment"

Excerpt from G. Davidson, R. Giacconi, H. Gursky, et al.,
A Research Program to Investigate the Experimental Problems
of Particle Measurements in Space, Final Report On
Contract AF 19 (604) - 7347, ASE Document ASE-400,
27 May 1963. pp. 58 - 89.

3.1.2 Instrumentation

The use of an artificial satellite as a vehicle imposed particular requirements on the weight, reliability, and ruggedness of the instrumentation necessary to perform the experiment. Classical solutions for mass discrimination such as magnetic separation had to be discarded owing to weight consideration. In order to exploit the benefits of long available times of observation, the power consumption requirements were kept to a minimum. Particular problems existed in the data transmission.

The experimental arrangements which are discussed in the following sections were designed to satisfy these requirements.

Emphasis was placed on simplicity of construction, reliability of operation, light weight, and low power requirements. A particular effort was spent to reduce to a minimum the requirements on the data-transmitting equipment.

The instrumentation required for the proposed experiment was designed to perform any or all of the following functions:

A. Detect protons, alpha particles, and other possible heavy components in the Mev energy range.

B. Distinguish between these particles.

C. Measure their energy.

The three functions are not independent from each other. In fact, to discriminate between different particles, a measurement of the energy together with another independent quantity, such as range, or rate of energy loss is required. Therefore, rather than discussing single components which could be used to perform one particular function, we prefer to discuss complete systems which can accomplish all three functions.

Each such system is built around a basic component, the detector. The characteristics of the detector and the type of information it can furnish dictated the choice for additional components which had to be used to perform the experiment. For the final design of the experiment, various possible systems built around adaptions of available detectors were studied in detail and a scintillator detector was selected as the basic detector.

3.1.3 Principle of Operation

Inorganic scintillators such as thallium-activated CsI will respond almost linearly to the energy loss within their volume. By using more than one scintillation detector, one could, therefore, measure both the specific energy loss and the total energy of the particle. In Figure 10a, a schematic arrangement is shown. The anti-coincidence detector, S_3, assures that the particles stop in S_2 and, therefore, that the pulse height in S_2 is a measure of the total energy, E. The pulse height in S_1 is a measure of the specific energy loss $\Delta E/\Delta x$. From these two measurements, the type and energy of the particle can be determined. This classical arrangement, however, is easily adapted only to the detection of particles of relatively high energy. For low-energy particles, the thickness of S_1 must be made smaller than the residual range of the particle. In the case of protons or alpha particles of energies of a few Mev, the residual ranges are of the order of microns, as shown in Figure 11.

The practical difficulties involved with a thin detector S_1 led to a consideration of other possible schemes. A different approach which was the one finally adopted consists in the measurement of maximum range (rather than $\Delta E/dx$) and energy. This arrangement is the one shown schematically in Figure 10b. The counter S_1 which previously was used

SCINTILLATION COUNTER SYSTEMS

Ⓐ MEASUREMENT OF SPECIFIC ENERGY LOSS $\Delta E/\Delta X$ AND ENERGY E

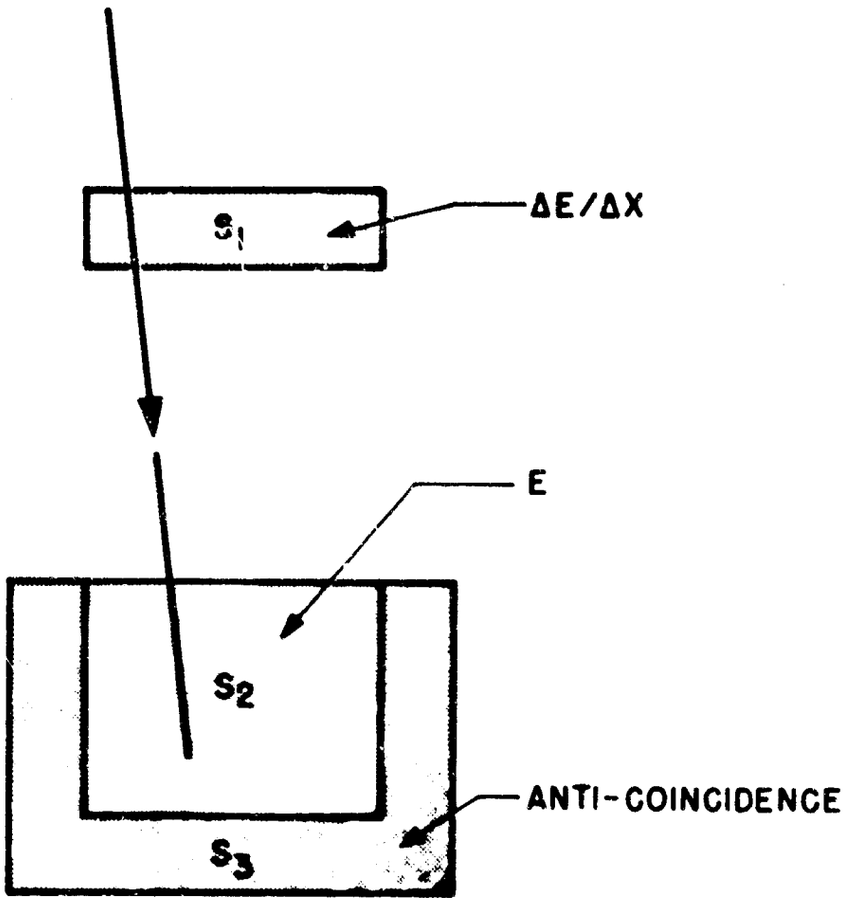

Ⓑ THE MEASUREMENT OF ENERGY E AND RANGE R

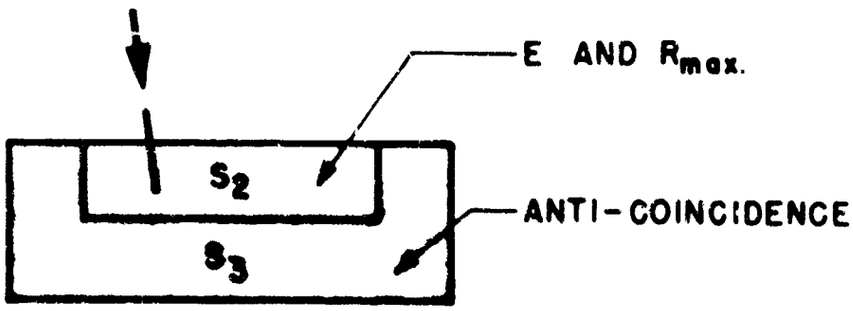

Figure 10

RANGE-ENERGY RELATION

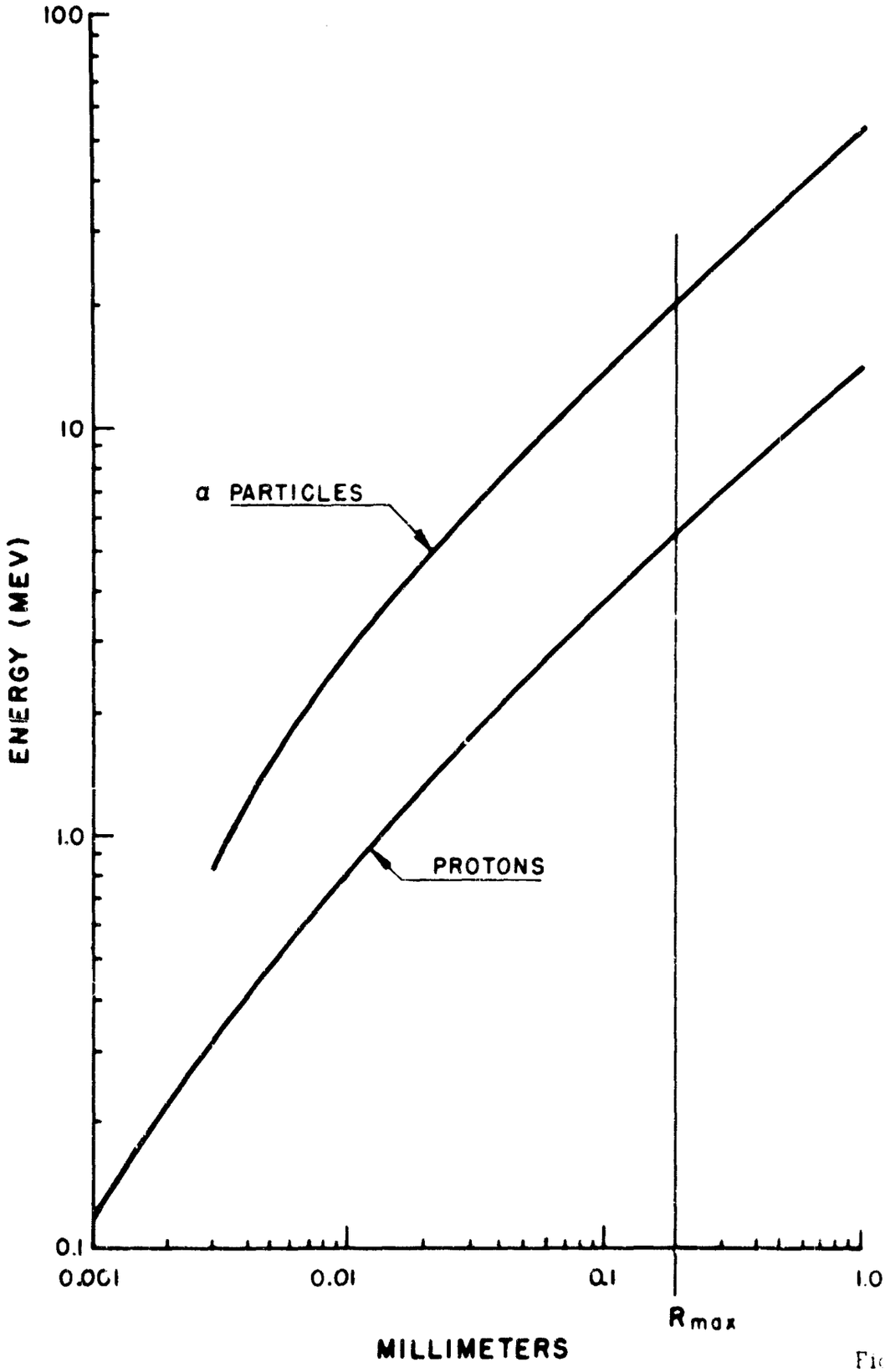

Figure 11

to measure $\Delta E/\Delta x$ is eliminated. One can only measure the total energy, E, lost in S_2. Still, it can be shown that such a detector would, in fact, be able for given energy regions, to distinguish between different kinds of particles besides measuring their energy. Let us assume, for instance, that the scintillator S_2 has a given thickness, R. The maximum range that a particle stopping in S_2 can have is (neglecting straggling) also R. Different particles having the same range have different energies, as evident by inspection of Figure 11. For instance, the maximum energy of a proton stopping in .2 millimeters of CsI(Tl) is about 5 Mev, while the maximum energy of an alpha particle stopping in this thickness is 20 Mev. Therefore, no pulse from S_2 corresponding to an energy loss of more than 5 Mev can be given by a proton. Consequently, with this particular thickness of scintillator, we are able to separate alpha particles of energies between 5 and 20 Mev from protons of any energy, and are also able to measure the α-particle energy spectrum in this region. With other similar detectors having different scintillator thicknesses, other regions of the spectrum could be selected. It should be noted that the higher Z particles could not be separated from the alpha component in this fashion, so that a small contamination of high Z would not be resolved. The same method could, however, be used to separate high Z components from alpha particles in given spectral regions. The design of this particular type of system was adopted for the flight instrumentation.

3.1.4 Rejection of Spurious Events

The available measurements on intensity and composition of radiation in the Van Allen belts of radiation indicate omni-directional intensities in the core of the inner layer of $10^9/cm^2$ sec. for electrons with energies greater than 20 kev and $2 \times 10^4/cm^2$ sec. for protons with energy

greater than about 40 Mev. While the electronics associated with the detector can very effectively distinguish between the pulse heights produced by the electrons and heavier particles, it was felt that the number of electrons present is so high that they might produce a dc background, which would, in effect, jam the counter. One could improve this situation by reducing the solid angle viewed by the detector, but in this way, the fluxes of all types of particles would be reduced by the same amount. We used a different approach to this problem consisting of the use of a magnetic separator capable of reducing the electron fluxes by orders of magnitude without appreciably reducing the proton and alpha fluxes. A magnetic field of about 2000 gauss over a region of 6. cm^2 was used to deflect particles with momenta up to 10 Mev/c by 30°. Electrons up to 10 Mev energies could thereby be removed from the accepted beam, while protons and alphas of the same energy would be deflected by angles of the order of 1°. The advantage of this method is due to the fact that proton and alpha fluxes are not attenuated, while the electron flux is. The magnetic field required was obtained by using small permanent magnets. A diagram of the detector assembly is shown in Figure 12.

Care was exercised in the design of the experiment to discriminate against other possible sources of background as, for instance, nuclear interactions of low and high-energy particles in the detector. By using a thin detector we reduced the probability of occurrence of such interaction to relatively low values.

3.1.5 Flight Instrumentation

Figure 13 is a photograph of the flight instrumentation which was constructed to implement this experiment.

A listing of the design specifications is given below.

ALPHA-PROTON DETECTOR ASSEMBLY

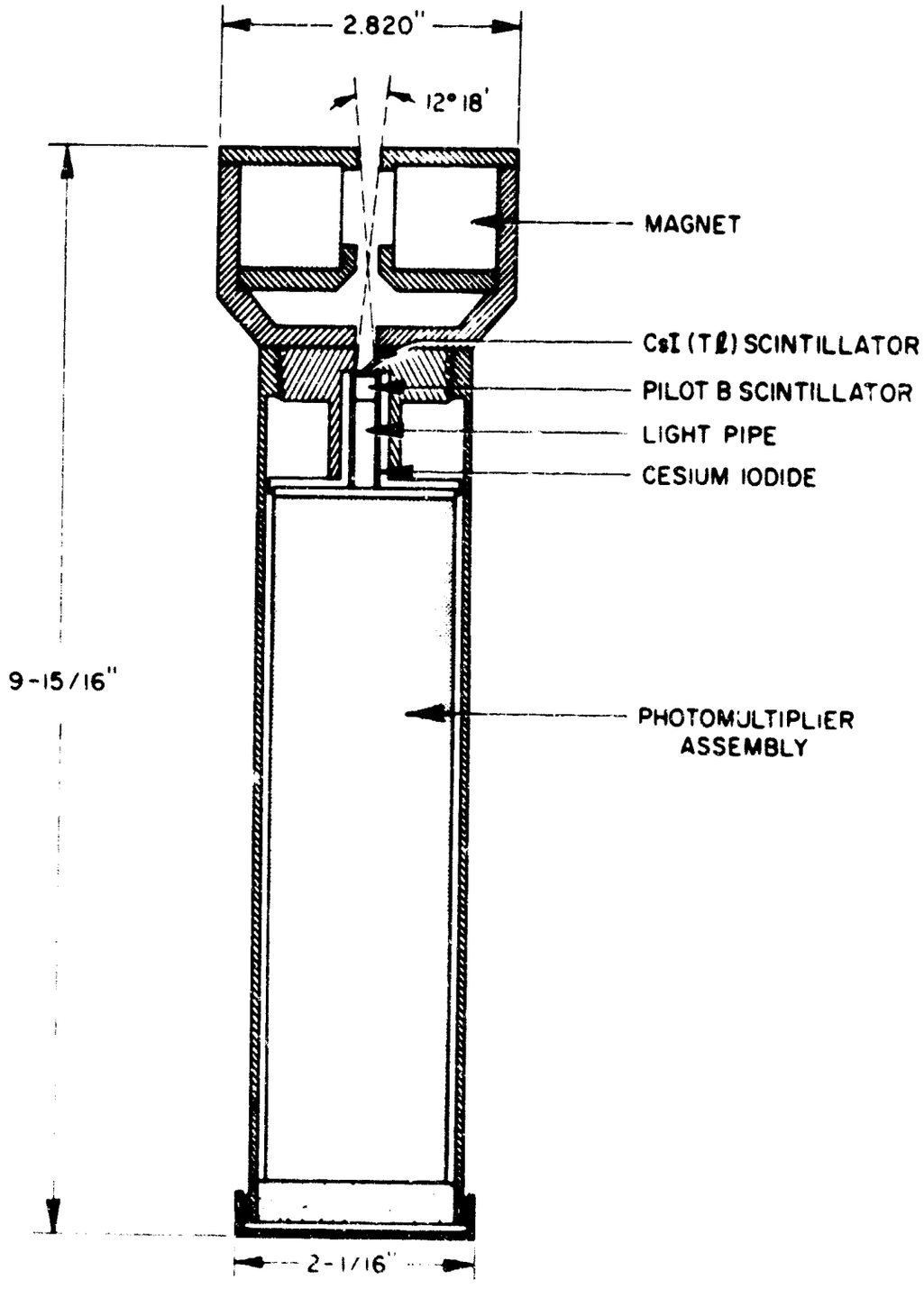

Figure 12

ALPHA-PROTON PARTICLE DETECTOR

Figure 13

Power Requirements:	1 watt, 28 $\pm$VDC.
Weight:	10.8 lbs.
Detector:	6199 photomultiplier with CsI and plastic scintillator sandwich.
Field Strength:	B $\geq$ 500 gauss.
Shielding:	1.5 m gr/cm^2
Geometric Factor:	$A\Omega = 1.5 \times 10^{-3}$ cm^2 ster.
Max. Counting Rate:	10^7 protons/cm^2 sec ster.
Counting Life:	Indefinite.
Outputs:	There are eight outputs fed to the cable connector. These consist of three log count rate meters whose dc output is a linear function of the logarithm of their counting rate. The discriminator circuits in these channels are set to respond to pulses of proton and alpha particle stopping in the CsI. The energy loss required to trigger the discriminators are as follows:

Ch. P1	$\geq$	1 Mev
Ch. P2	$\geq$	2 Mev
Ch. P3	$\geq$	3.5 Mev

In addition to this, there is the output from a cyclic gate (Ch. 1) which internally commutates the outputs from four other log count rate meters and displays each for about four seconds. These channels respond to particles having the following energies:

Ch. α 1a	5.5 - 16 Mev alphas
Ch. α 2a	10 - 16 Mev alphas
Ch. hp 2a	10 - 50 Mev protons
Ch. hp 1a	15 - 30 Mev protons

In conjunction with this output, and having four separate outputs, are four digital readouts, Ch α 1b, Ch. α 2b, Ch. hp 2b, Ch. hp 1b, each operated by an analog staircase and covering the same energy ranges as the above log count rate meters

Environmental Operating Limits:

Temperature:	+20°F to +165°F
Acceleration:	50 G's
Shock:	50 G's in 7 x 10^{-3} sec.
Vibration:	25 G's, 30 - 3000 cps.

A block diagram of the electronics is shown in Figure 14. (Note: Some of the energy ranges indicated differ from those of the previous table; the table indicates the later design values).

Figures 15, 16, 17, 18, 19, 20, and 21, show the wiring of the individual Modules A through G.

A particle in the field of view of the detector is deflected by the static magnetic field. Electrons are deflected enough so that approximately only 1% of the electrons at 1 Mev can reach the detector. Proton and alpha particles are deflected almost inappreciably.

A particle impinging on the detector can penetrate one or both of the scintillators. A mixed light pulse from the Pilot B scintillator with about 5×10^{-8} sec decay time and from the CsI(Tl) with about 3×10^{-7} sec decay time will be detected and amplified by the photomultiplier. Pulses are monitored at the last dynode and at the anode. The dynode pulse is clipped by use of a shorted cable which eliminates the slow component.

The anode pulse is amplified and fed to a linear gate (Module C2) which is triggered by the identical pulse delayed by $.2 \times 10^{-6}$ sec. This allows only the slow portion of the pulse to be transmitted to an antigate (Module B) which is triggered by the fast pulse. If no "fast pulse" is present the slow component from the CsI(Tl) is fed to a 5 channel analyzer (Modules D1 through D5). If a fast pulse is present no output is present from Module B.

On the other hand both pulses are also fed to a linear gate (Module C1). The fast pulse is delayed by $.5 \times 10^{-6}$ sec to allow coincidence between it and the slow portion of the pulse from (Module C2) the previous linear gate which furnishes the slow portion and constitutes the trigger. If coincidence exists the last pulse is analyzed on 2 channels (Modules D6 and D7). The meaning of these operations from the point of view of the measurement is the following. The pulse from a slow particle stopping in the first scintillator CsI(Tl) is analyzed by D1 to D5. The pulse height corresponds to its total energy.

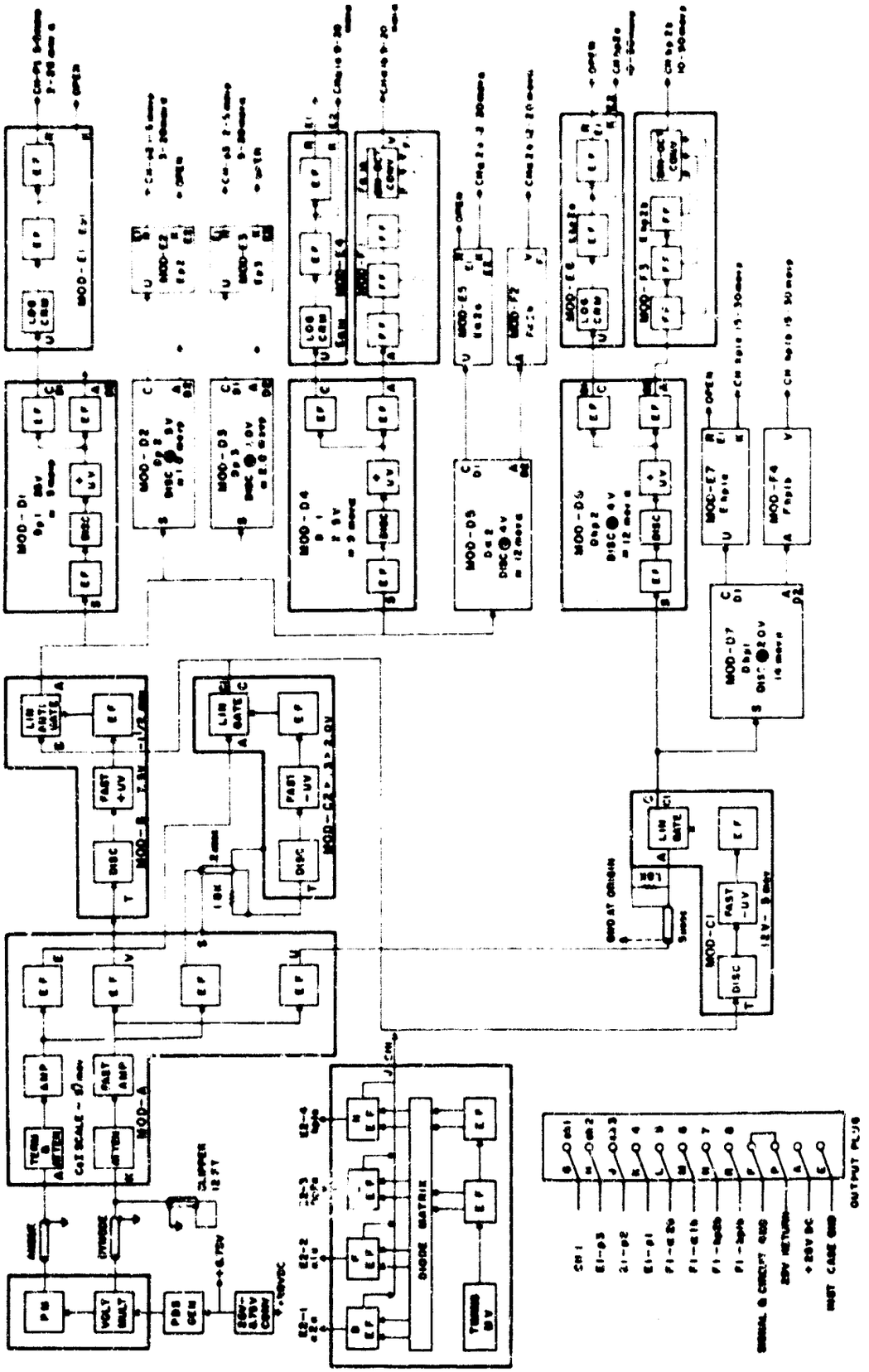

BLOCK DIAGRAM OF ELECTRONICS

Figure 14

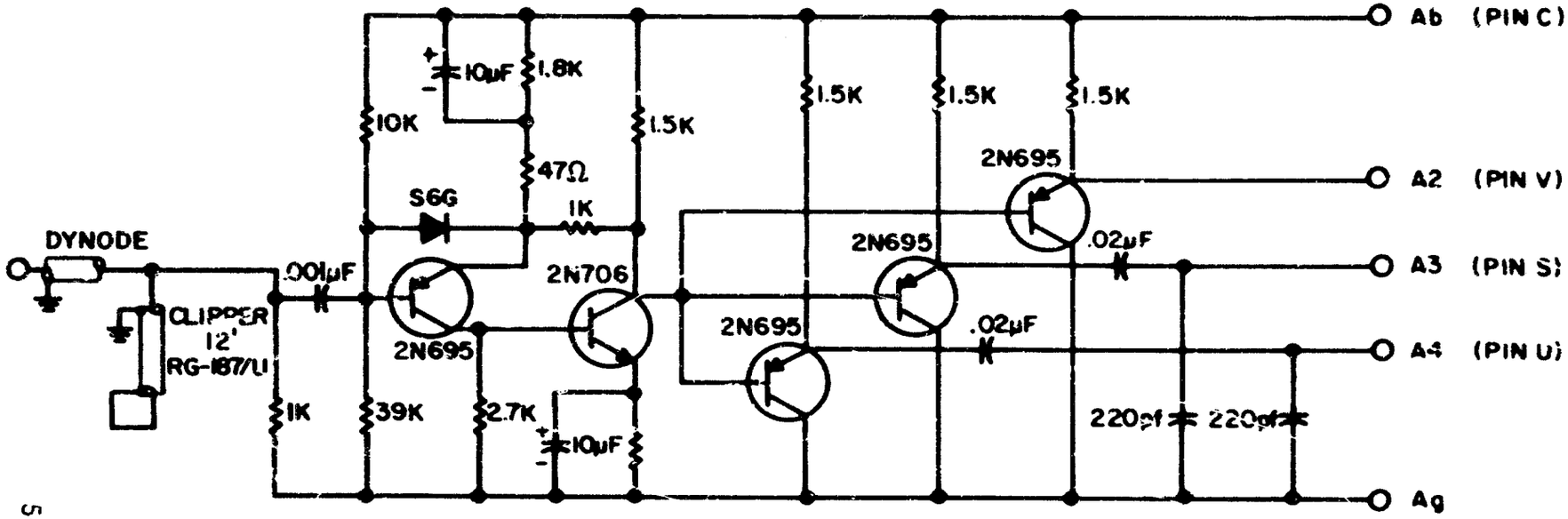

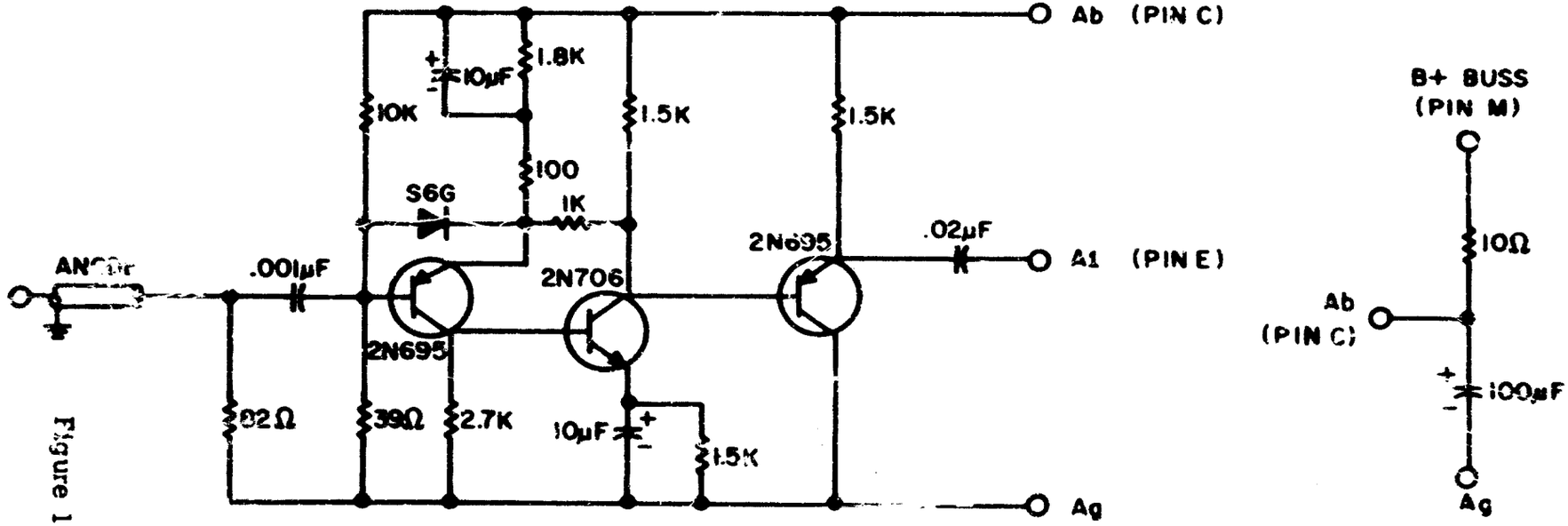

Figure 15

MODULE A

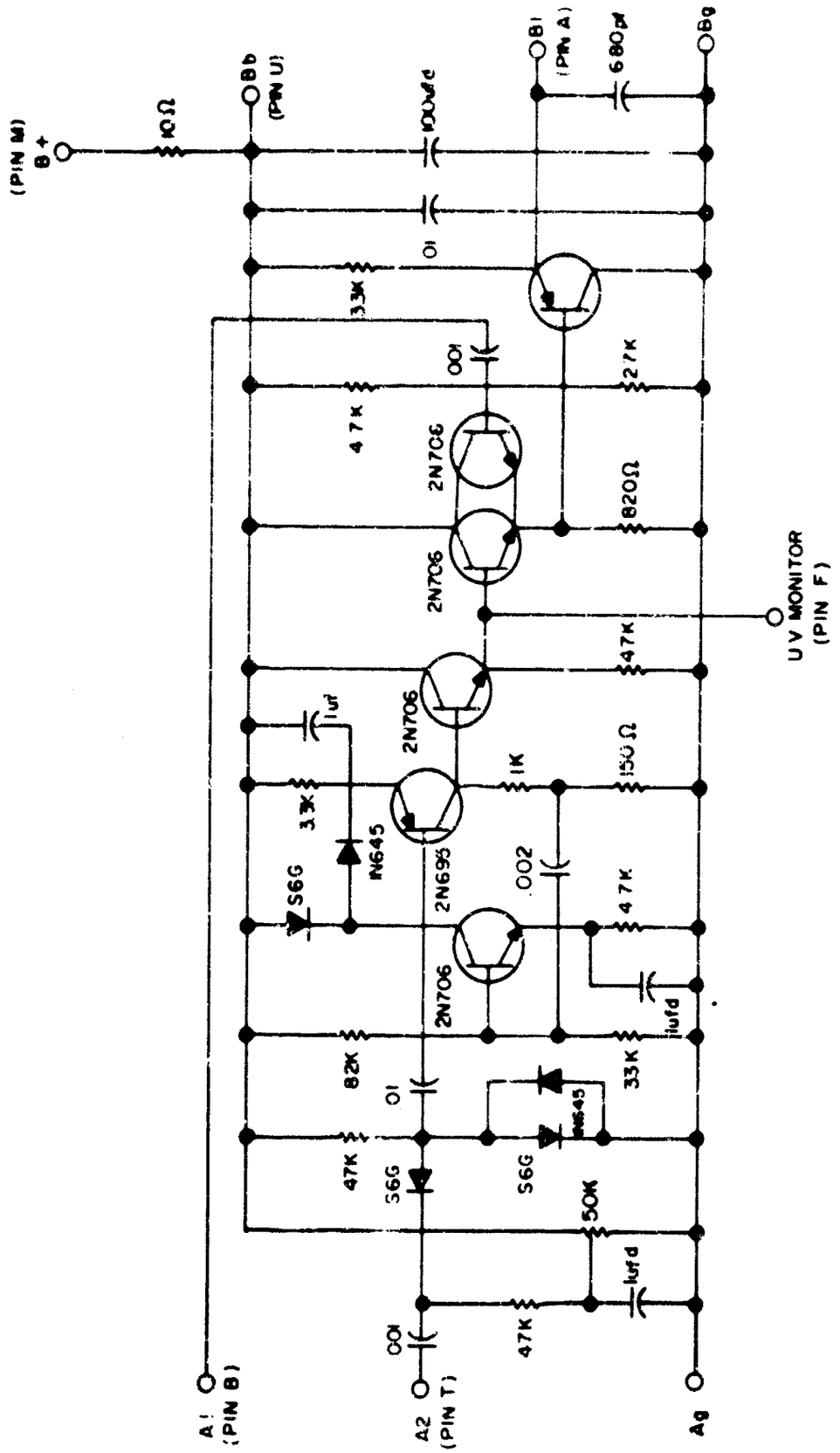

MODULE "B" DISCR. FAST UNIVIBRATOR & LINEAR GATE

Figure 1

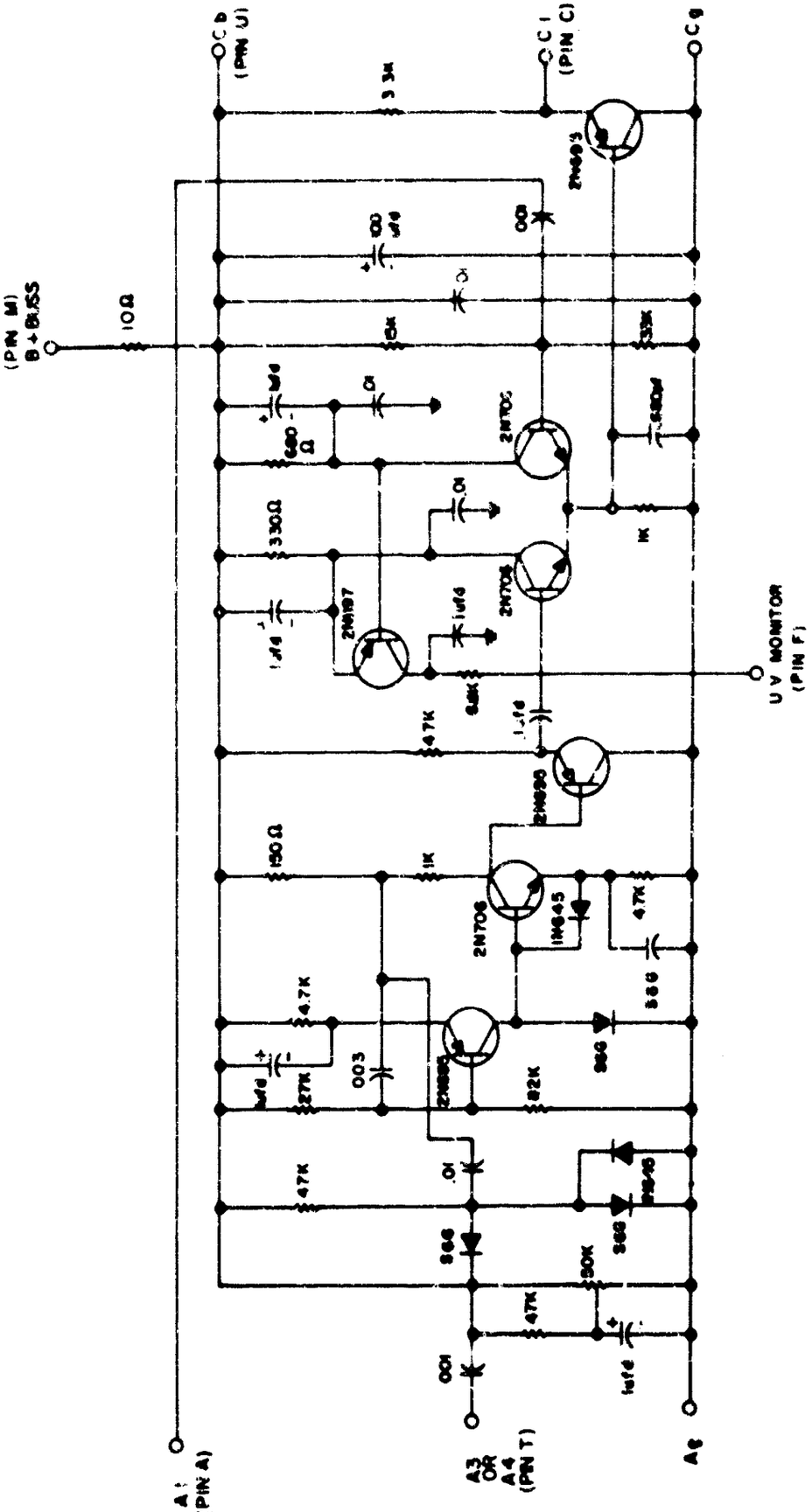

MODULE "C" DISCRIMINATOR FAST UNIVIBRATOR AND LINEAR GATE

Figure 17

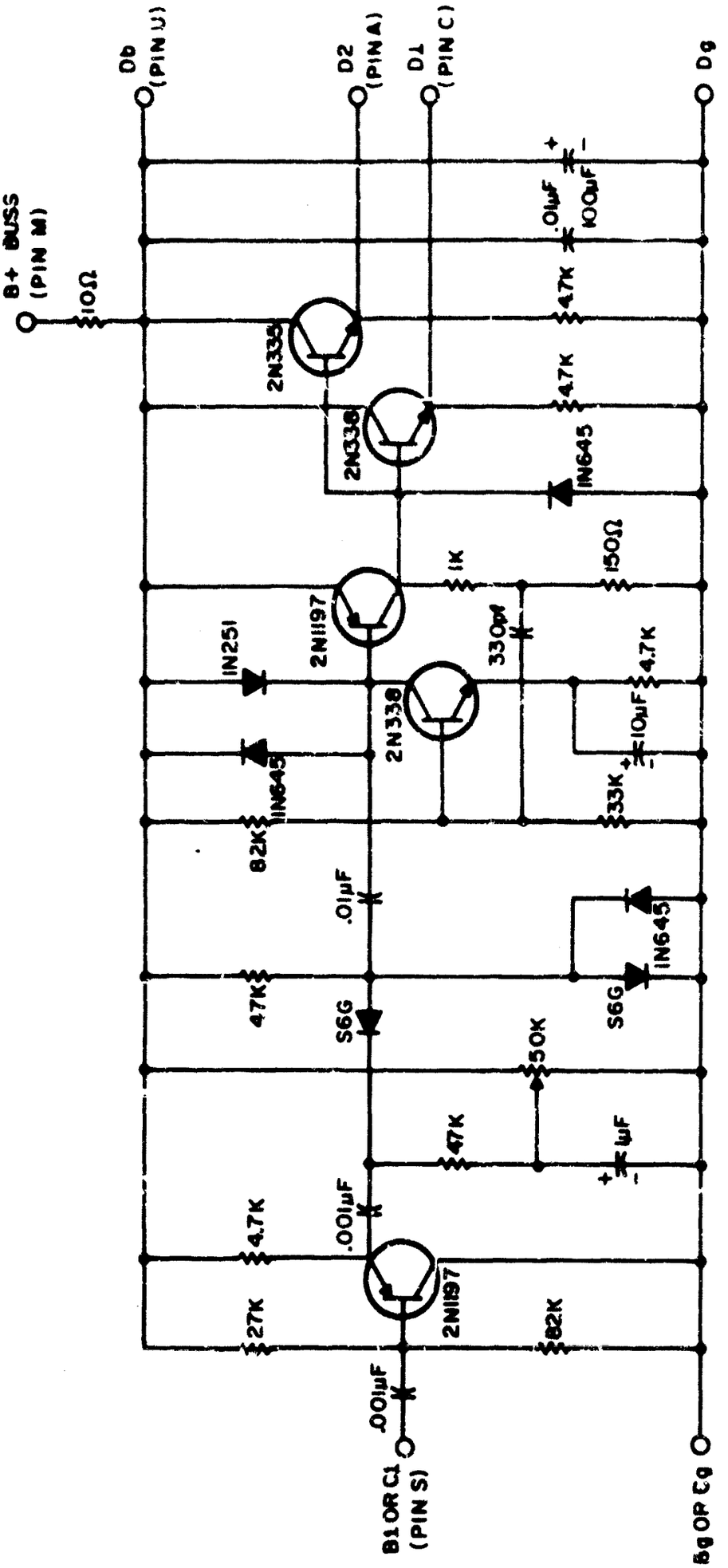

MODULE D DISC UNIVIBRATOR

Figure 18

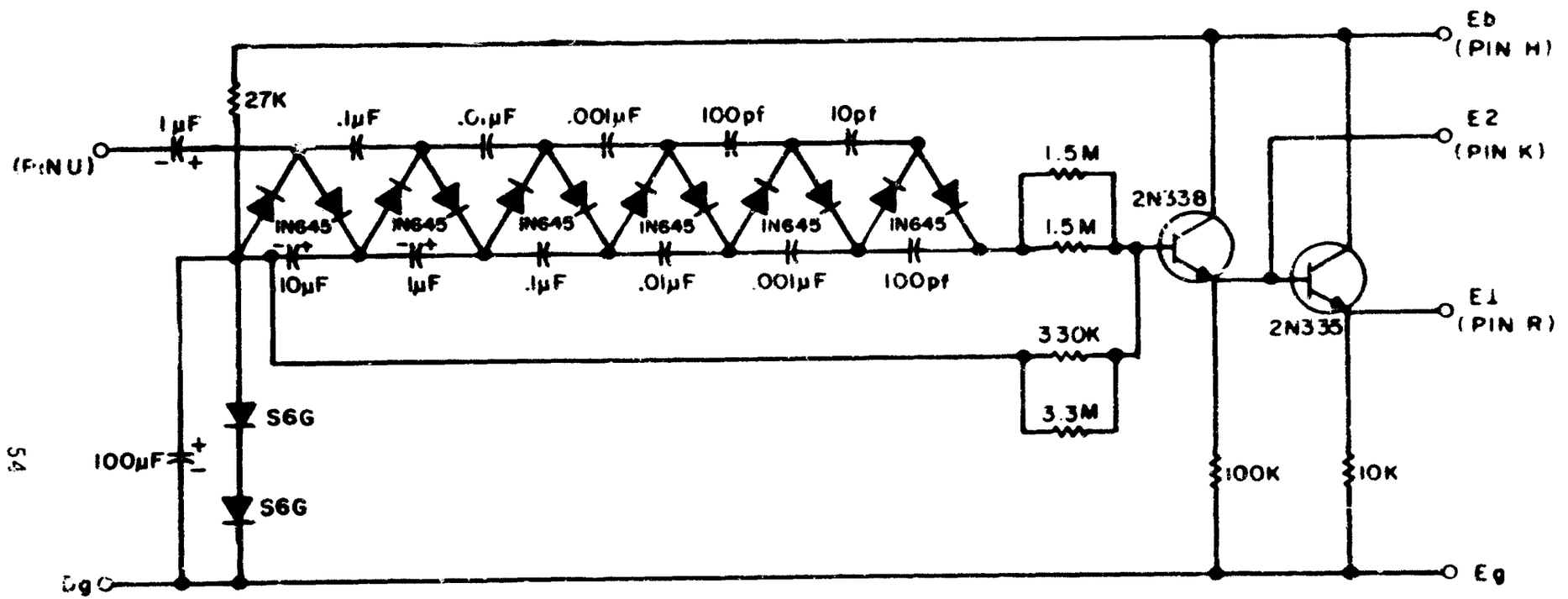

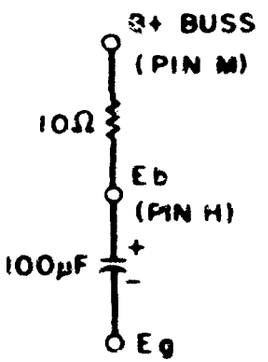

Figure 19

MODULE E

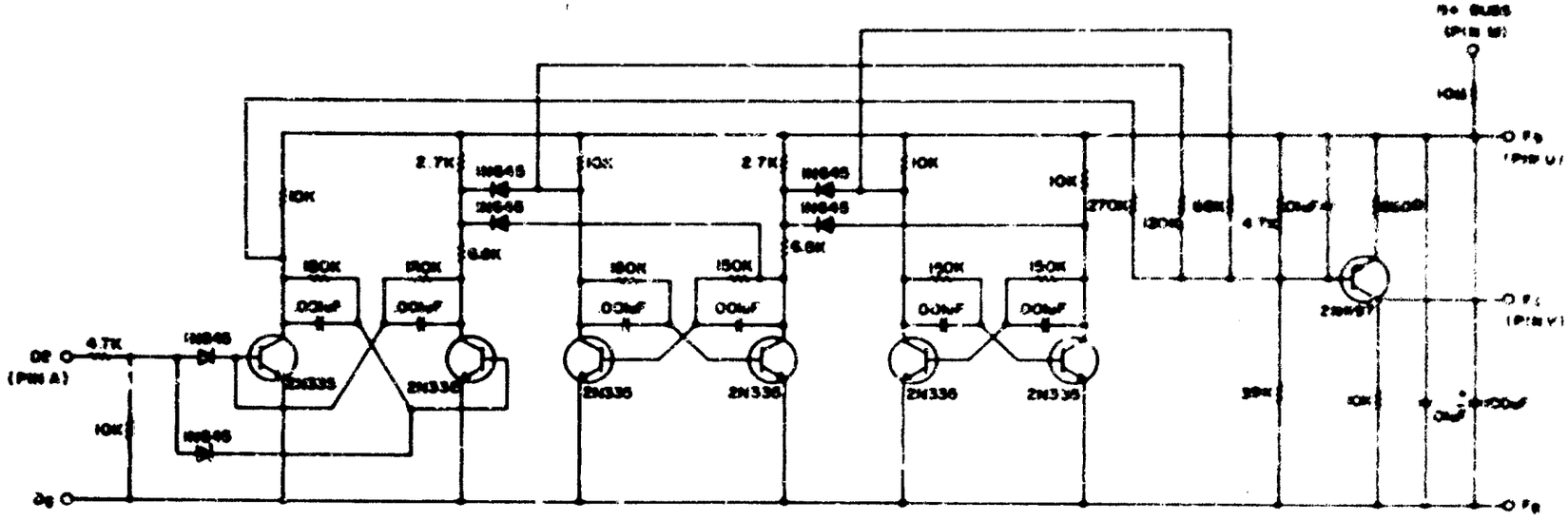

MODULE F
SCALE OF-8 AND BINARY—OCTAL CONVERTER

Figure 20

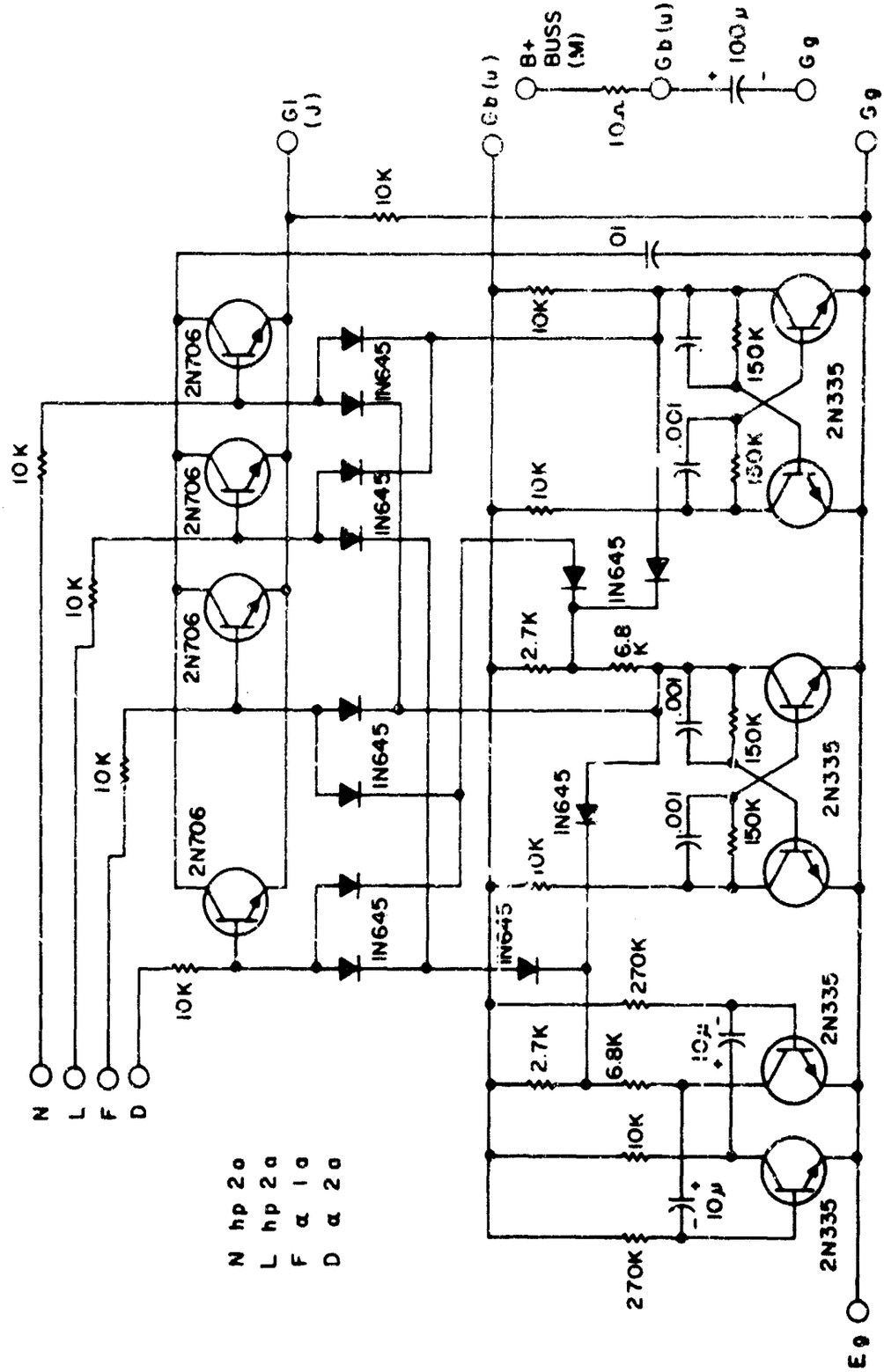
MODULE G COMMUTATOR
N hp 2α
L hp 2α
F α 1α
D α 2α
N
L
F
D
Gl (J)
Eb(u)
B+ BUSS (M)
Gb(u)
Gg
Eg
10K
2N706
IN645
2.7K
6.8K
270K
150K
.001
.01
10µ
100µ
2N335

Figure 21

The pulse from a fast particle which enters both scintillators is analyzed by D6 and D7. The level of discrimination in the linear gate is such that only particles which exhibit a large enough energy loss in the CsI(Tl) are accepted. This corresponds to a $\Delta E/\Delta x$ requirement. The level is such that only particles with energies less than 50 Mev are accepted. These particles will stop in the Pilot B scintillator if they are protons of less than 32 Mev or electrons of less than 2 Mev. By requiring .5 Mev energy loss in the first crystal and greater than 10 and 15 Mev energy loss in the second, we can eliminate electrons and measure the energy of the protons in two bands of 10 to 50 and 15 to 30 Mev. The outputs of all discriminators are fed to count rate meter which furnishes a voltage approximately proportional to the logarithm of the counting rate (Module E). A typical calibration curve is shown in Figure 22. Also on the four highest energy channels the output is fed to octal staircase scalers (Module F) to allow accurate counting at very low fluxes. The output of these scalers were multiplexed within the experiment by means of a cyclic gate (Module G).

Additional electronics included a high voltage supply of the Cockcroft Walton type and a dc to dc converter and voltage regulator shown in Figure 23. Figure 24 shows the wiring diagram of a test panel for testing Modules A through G.

The output from the channels were adjusted to measure particles in the following ranges of energy, given on page 47.

TYPICAL COUNT RATE METER CALIBRATION

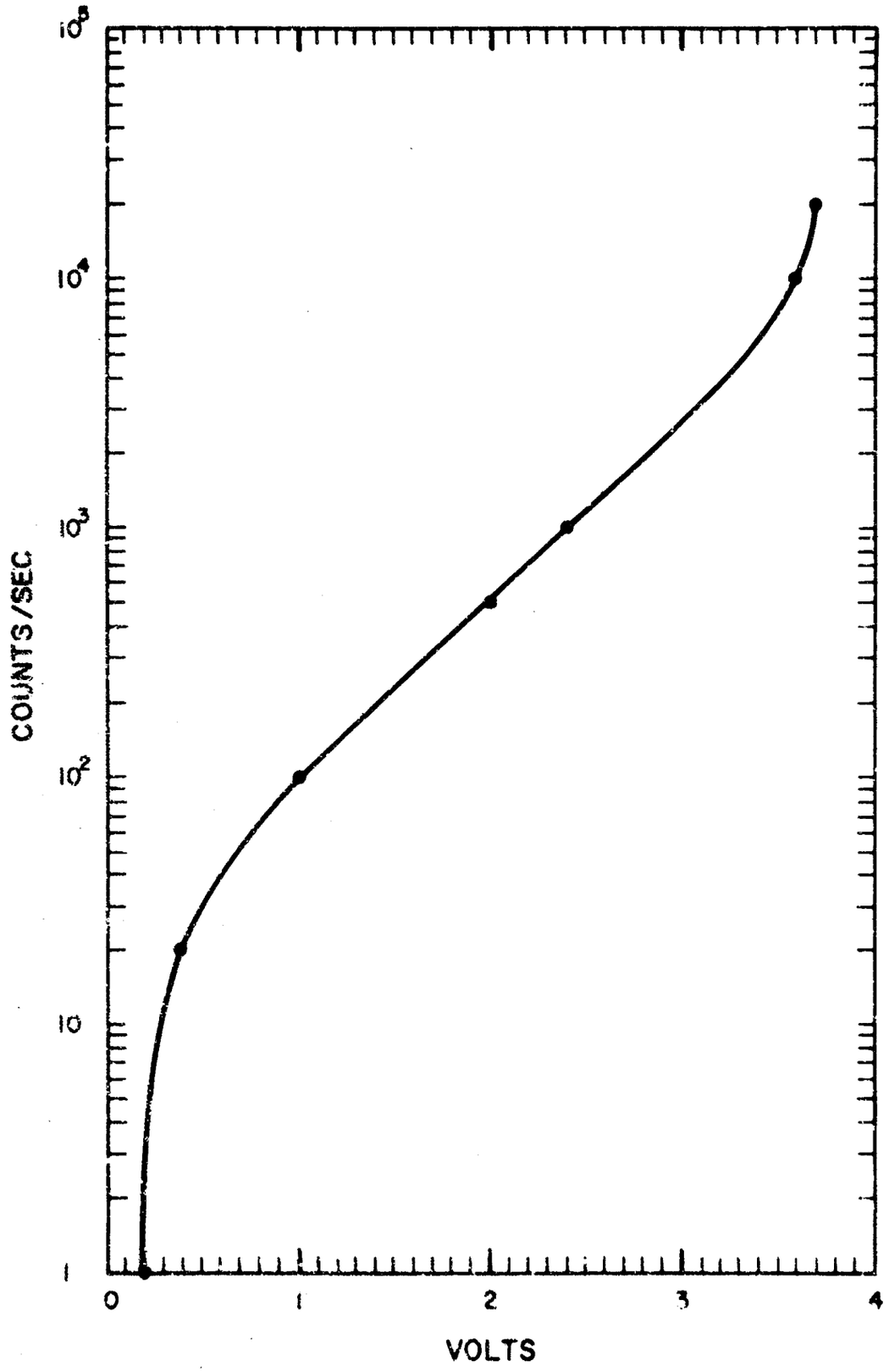

Figure 22

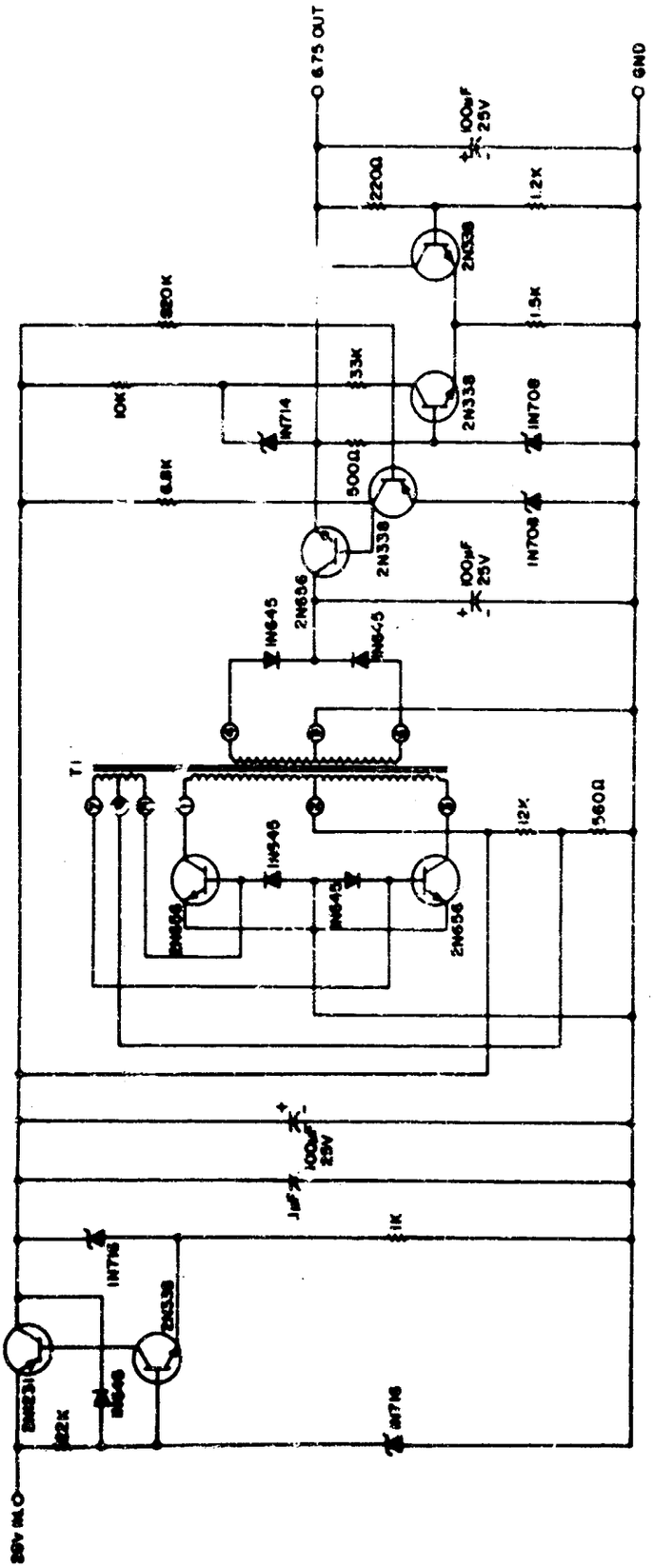

28V TO 6.75V DC-DC CONVERTER

Figure 23

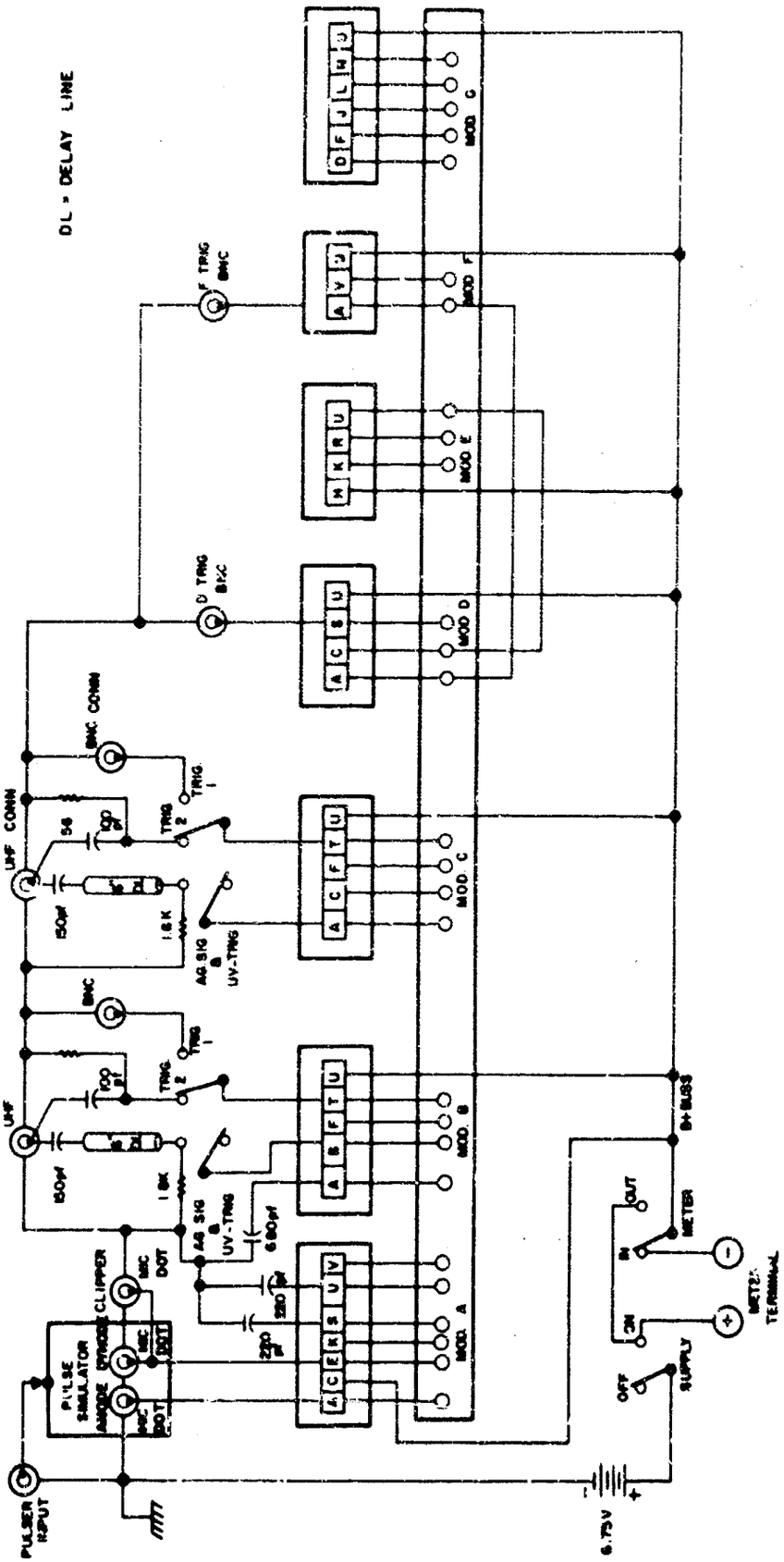

WIRING OF PANEL FOR TEST OF MODULES

Figure 24

3.1.6 Calibrations

The prototype flight instrument was subjected to extensive testing. Exposure at the High Voltage Engineering Van de Graaff electron accelerator was used to study the response of the instrument to very high electron and gamma ray fluxes. Effects such as pile-up and fatigue were studied to assure that conservative criteria had been used in the design of the experiment.

Both in-house calibrations with alpha particle sources and calibration at the 14 Mev M.I.T. Cyclotron were used to set the proper energy discrimination levels. The protons and alpha particles beam was brought outside through a 6.4×10^{-3} gr/cm^2 Au foil. The energy of the particles was then attenuated by use of Al foils .001 inches thick in various amounts. Protons with energy loss as small as .5 Mev in the scintillators were detected. A point calibration was performed to determine linearity of the system to a given energy lost in the CsI(Tl). Figure 25 shows a typical curve obtained in such a test. The vertical error bars are estimated on the basis of inherent statistical accuracy of the detector. The horizontal error bars are due to uncertainty inherent in the method used to degrade the energy. Effects of straggling at very low energies are predominant. The efficiency for measuring alpha particles was determined and a resolution curve obtained with alpha particles showed an energy resolution of about 20 per cent. The rejection efficiency of the anti coincidence was measured and found to be identical, within the measurement error, to 100 per cent. These calibrations were repeated for each flight unit to assure reproducibility. It was found that the individual differences in geometry and crystal efficiencies were negligible.

In the field, calibration was carried out by especially mounted radioactive alpha particle sources which could be brought into close proximity of the CsI(Tl) crystal.

ENERGY CALIBRATION CURVE AT M.I.T. CYCLOTRON

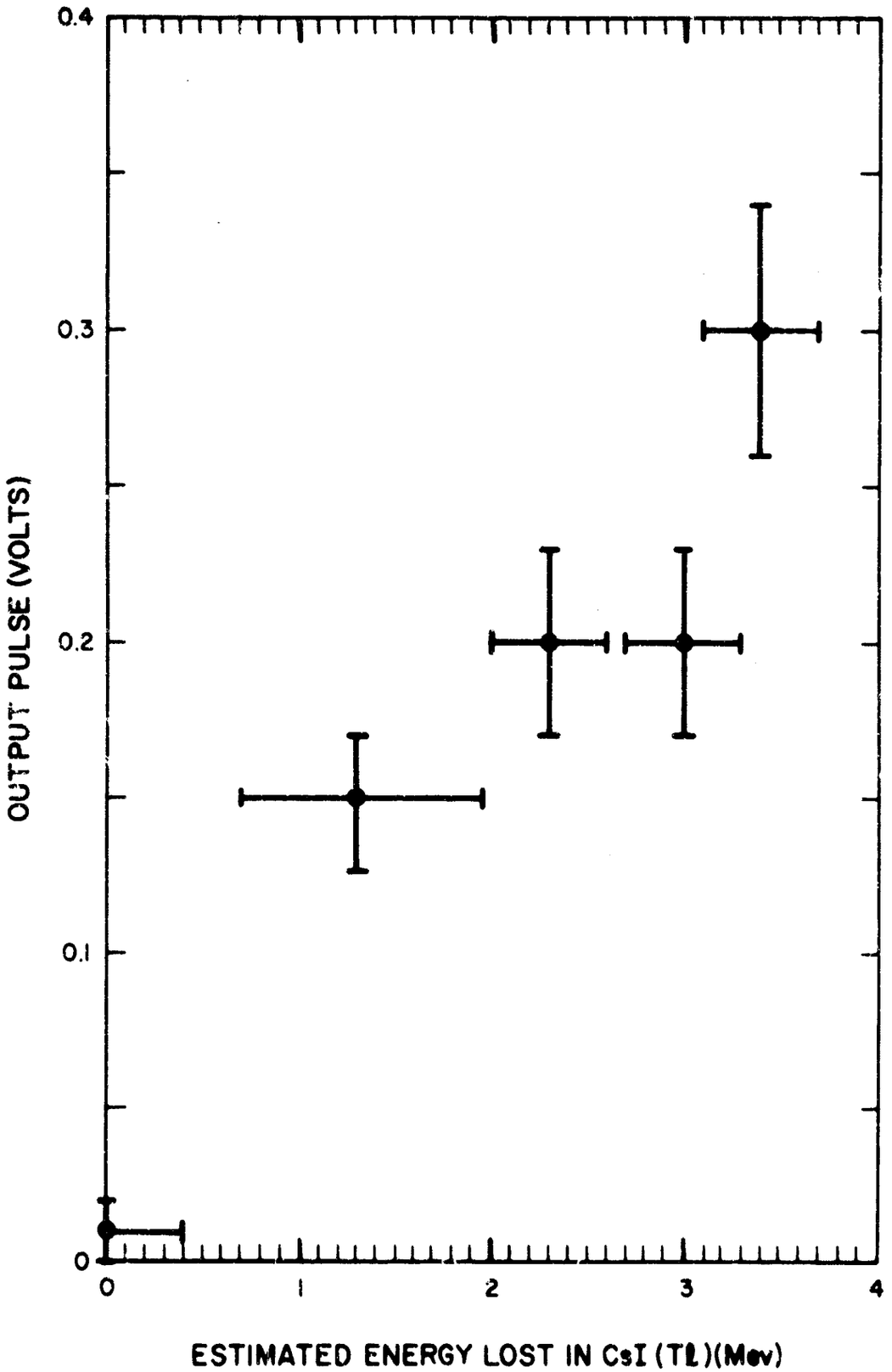

Figure 25

3.1.7 Operational Information

Seven complete units of the proton-alpha experiments (AFCRL designation CRM-2B) were built. The first unit was delivered on 1 February 1961.

Unit ASE-P-32-0 was used in destructive environmental testing.

Unit ASE-P-32-1 was flown on the Atlas Pod 08, at Cape Canaveral on 19 December 1961.

Unit ASE-P-32-4 was flown on an Air Force Satellite launched on 14 December 1962 at VAFB (PMR). The satellite did not achieve orbit.

Unit ASE-P-32-6 was (under the direction of the scientific monitor) modified to fly on the 1962 βk satellite. This unit was working properly up to a few hours before launch when last calibrated. The unit did not however, operate as planned after the boost phase. We ascribe this failure to a malfunction of the high voltage supply. The high voltage supplies of units ASE-P-32-2, ASE-P-32-3, and ASE-P-32-5 were changed to a new supply of the type used on the P-11 instrumentation.

Unit ASE-P-32-5 is presently on board of an orbiting spacecraft launched on 9 May 1963 from VAFB (PMR). No information has yet been received by us on the success of the flight and no data have yet been made available.

Units ASE-P-32-2 and ASE-P-32-3 have not yet been assigned a vehicle. These units are completely tested and calibrated and could be made ready for flight in a matter of hours.

3.1.8 Results

Proton-Alpha unit No. ASE-P32-1 was flown in an engineering test on Atlas Pod 08, 19 December 1961, from Cape Canaveral. The trajectory had an apogee of 1280 km, which took the Pod into the inner

radiation belt. (Figure 26). Since it was primarily an engineering test rather than a scientific data gathering flight, and since there was uncertainty concerning the expected particle intensity the instrument would encounter, the magnetic electron broom was removed, the field of view was increased and the energy thresholds were lowered. This resulted in the detector being sensitive to electrons as well as protons and alphas.

Simple considerations using previously known energy and voltage thres-threshold settings, the newly set voltage threshold settings, and voltage-energy linearity, lead to the following new ranges of sensitivy for the various data channels:

Channel	Protons	Electrons
P_1	3.7 > E > .35 Mev	Insensitive
P_2	3.7 > E > .65 Mev	Insensitive
P_3	3.7 > E > 1.9 Mev	Insensitive
α_1	3.7 > E > 2.82 Mev	Insensitive
α_2	3.7 > E > 3.15 Mev	Insensitive
HP_2	E > 3.4 Mev	E > 0.35 Mev
HP_1	E > 5.3 Mev	E > 0.6 Mev

A complete calibration was done for protons. No calibration was done for electrons. The detector had a 9° half-angle field of view and an area of $\sim 1.25\ cm^2$ giving a geometric factor of $\sim 0.08\ cm^2$-ster. A sample of the type of data retrieved is shown in Figures 27, 28, and 29.

Figure 27 shows the variation of the counting rate in channel P_1 sensitive to protons with energy greater than .35 Mev with respect to $\cos\theta$ where θ is the angle between the axis of the field of view of the detector and the B field. A similar plot for protons with energy greater than .65 Mev is shown in Figure 28.

Figure 29 shows the variation of the rate in one of the fast plastic scintillator (Pilot B) discriminators HP_2. Since the threshold for coincidence

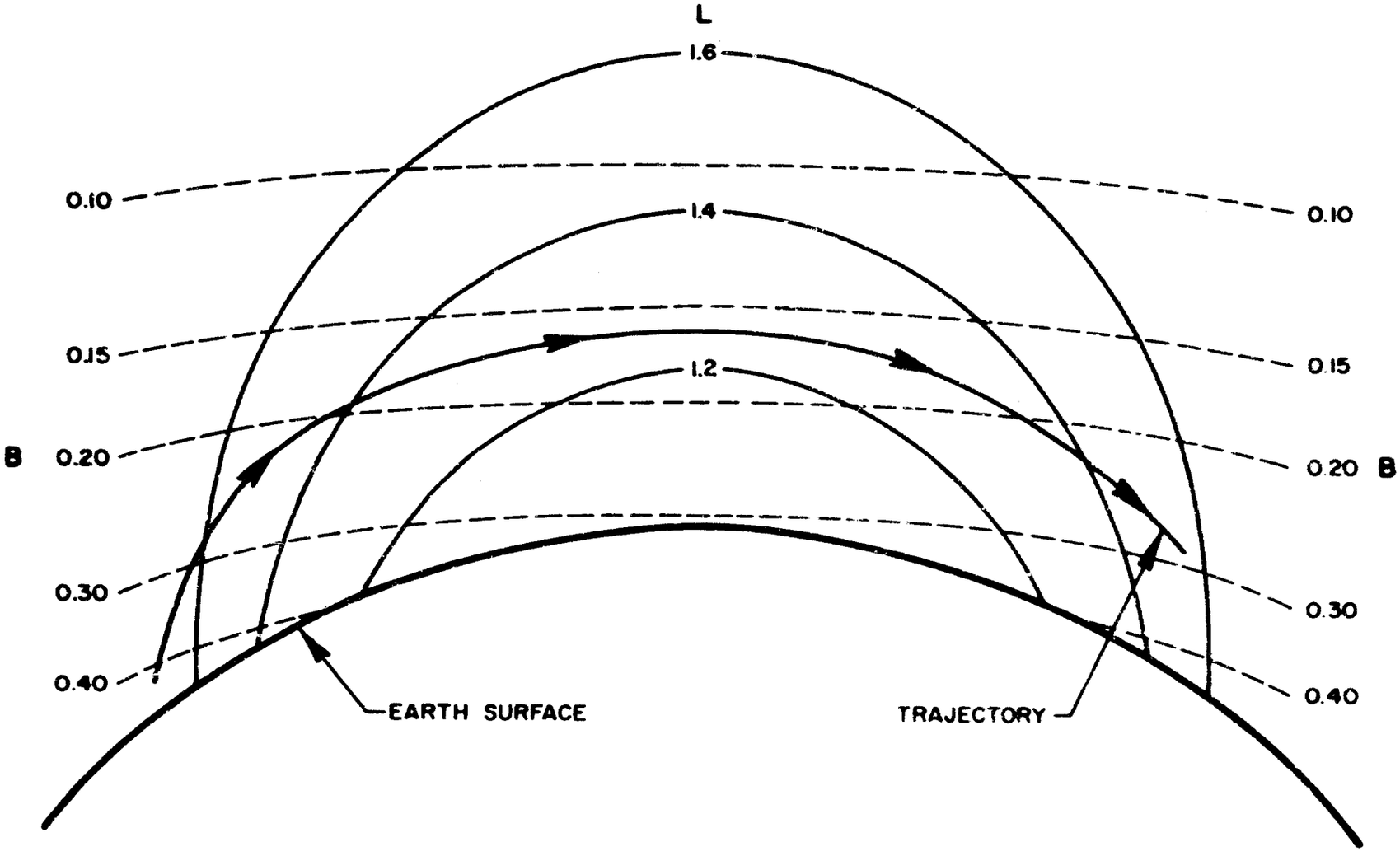

Figure 26

TRAJECTORY OF POD IN B-L COORDINATES

ATLAS POD 08 — 19 DEC. 1961

ANGULAR DEPENDENCE OF CHANNEL P_1 OUTPUT

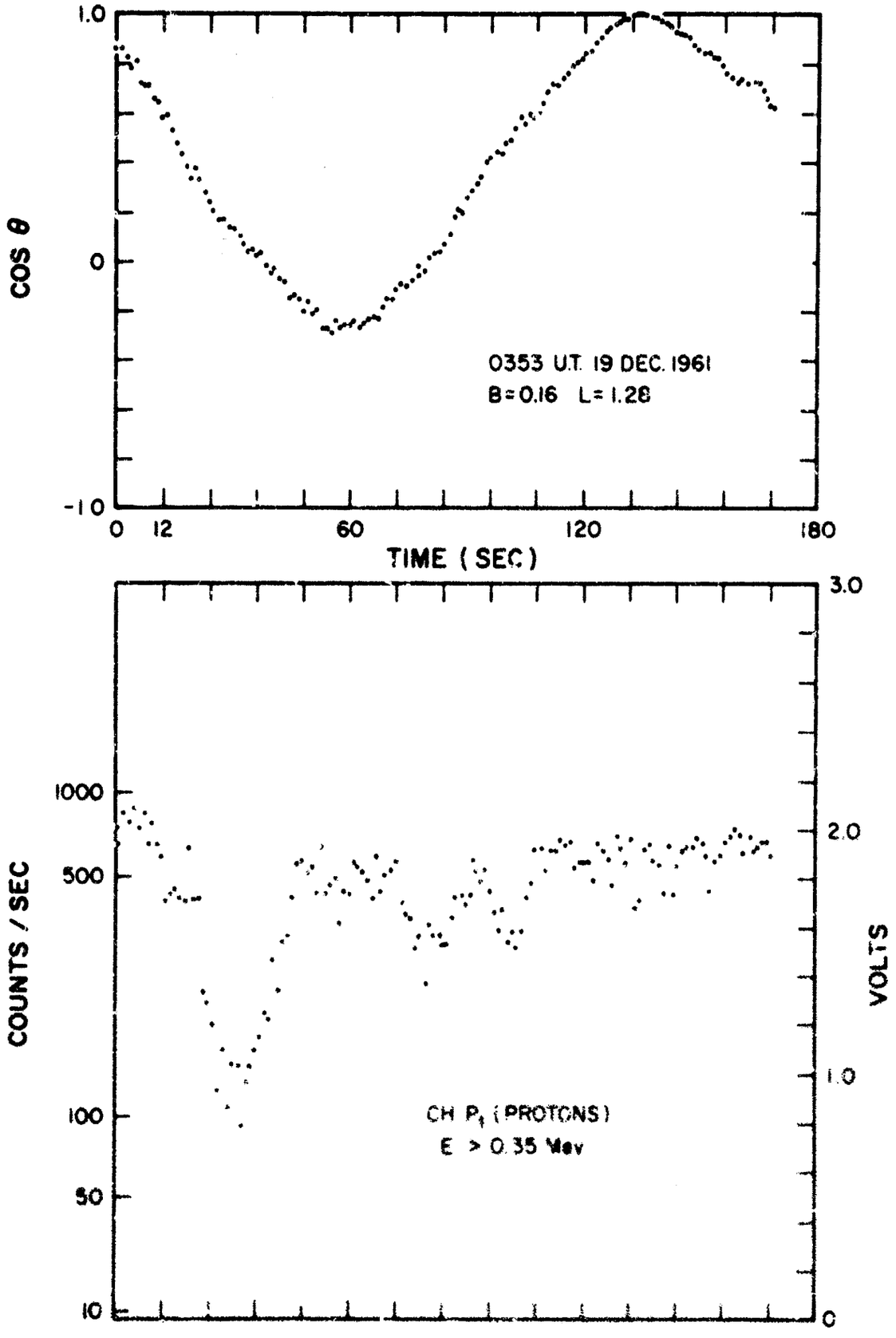

Figure 27

ANGULAR DEPENDENCE OF CHANNEL P_2 OUTPUT

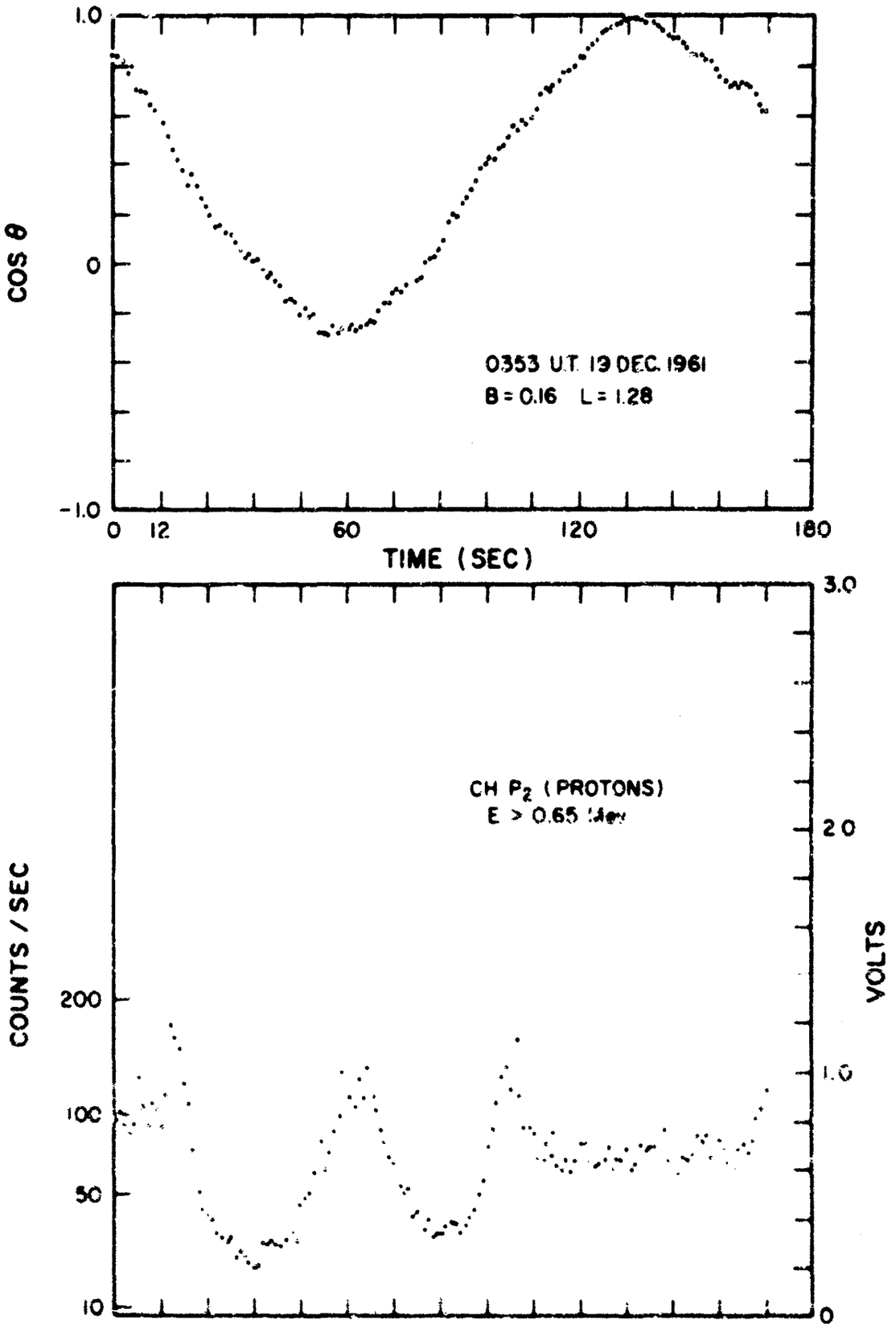

Figure 28

ANGULAR DEPENDENCE OF CHANNEL HP_{2a} OUTPUT

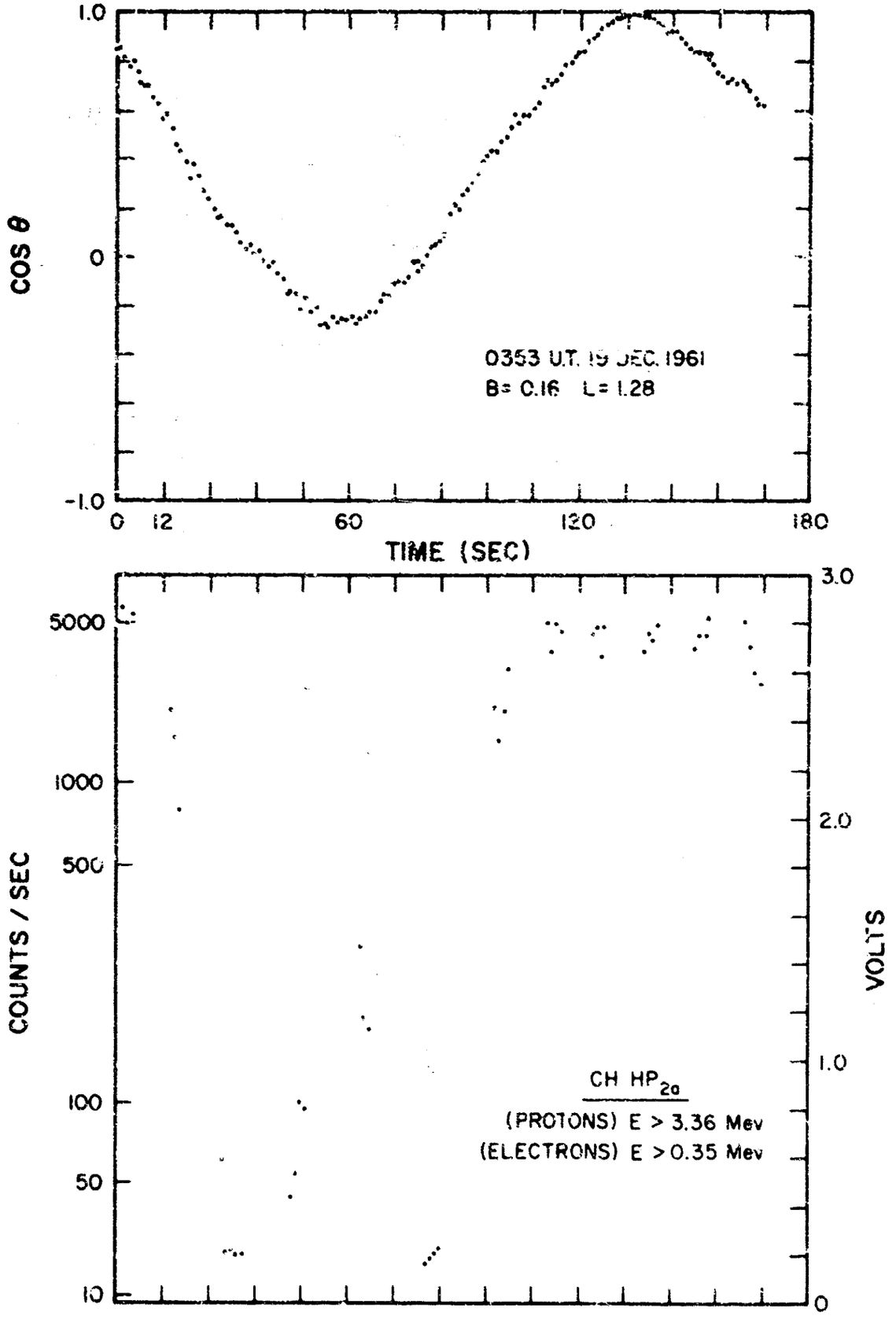

Figure 29

in the CsI(Tl) had been lowered to accept pulses for minimum ionizing particles, this rate can represent the rate either of protons with energy greater than 3.36 Mev or of electrons of energy greater than .35 Mev.

The second possibility is the one we have accepted to explain the inconsistency between the extrapolated energy spectrum at 3 Mev that can be calculated by use of the low energy measurements (which fit a power spectrum of the form $E^{-\gamma}$ with γ between approximately 2.5 and 3.) and the measured intensities in HP2.

We conclude that we have measured in HP2 a mixture of electrons and protons with electrons predominating. We believe that channels P_1, P_2, α_1, and α_2 are measuring protons with perhaps a small contamination of electrons (due to straggling or pile-up).

The rate observed in HP1 is consistent with it being sensitive to protons of energy greater than about 5.3 Mev.

The counting rate shows a sharp rise at an altitude of ~1050 km, B~ .29, L ~ 1.48; reaches a maximum at apogee, 1280 km, B ~ .16 and L ~ 1.28; it decreases sharply around 700 km, B ~ .20, L ~ 1.34. The interpretation is that the pod entered the inner radiation belt at 1050 km, passed through apogee inside the belt and then left at 700 km. These "edges" when plotted on a B-L map correspond to the general outline of the known natural belts.

Below is a table showing the typical counting rates at apogee. The maximum and minimum refer to the maxima and minima of the signal as it is modulated due to tumbling and to changes in B, L with time; units are counts per second.

Channel	Max.	Min.
P_1	700	35
P_2	200	~ 1
P_3	~ 4	~ 0
α_1	~ 3	~ 0
α_2	~ 6	~ 0
HP_2	7900	~ 4
HP_1	~ 5	~ 0

All of these measurements were obtained from the count rate meters. Two of the scalers appear to have operated throughout the flight, α_{2b} and HP_{2b}; HP_{1b} remained constant throughout, and α_{1b} counted for the first 350 seconds and then remained constant for the rest of the flight. These appear to be the only two possible instrumental failures in the entire system.

Preliminary correlations of counting rate with the magnetometers indicate that it may be possible to obtain angular distributions of electrons and protons. The tumbling occurred in such a manner that not all angles were explored; thus it is impossible to get complete angular distributions, but it may be possible to get enough to be of significant interest.

We consider this flight to have been successful beyond expectation both from an engineering and scientific point of view.

A complete study of the angular distributions was not done in the first analysis for we were mainly interested in whether or not the instrument operated correctly under flight conditions — it did, except for the two apparent scaler failures.

APPENDIX C

1.0 BETA, BETA, GAMMA INSTRUMENTATION (CRM 11)

This instrumentation was designed to detect γ-rays and β-rays. As shown in Figure 30, the instrument package contains two β-ray detectors mounted with mutually perpendicular detection vectors and one γ-ray detector. This geometric configuration will allow rough measurements of angular distributions to be performed and correlated with magnetic aspect.

The β-ray detector consists of a plastic scintillator which is covered by a thin aluminum shield and is viewed by a ruggedized photomultiplier. The aluminum shield prevents visible light from impinging on the scintillator and establishes a minimum energy for β-rays which enter the scintillator. The chosen thickness of 6.8 mg/cm^2 corresponds to the practical range of electrons of 70 kev and for protons of 1.5 Mev. The thickness of the plastic scintillator, approximately .31 g/cm^2, corresponds to the practical range of 0.8 Mev electrons. The crystal was chosen so thin to minimize its sensitivity to γ-radiation. The detector is exposed to the environment through a hole in the instrument package. The field of view of this sensor is approximately 1 steradian (Figure 31). The detector is 150 times more sensitive to electrons than to γ-rays. The range of sensitivity of this detector is from approximately 10 to 10^9 electrons/cm^{2}sec. Figure 32 shows the β-sensor unit, and Figure 33, the schematic diagram of the beta-gamma sensor.

The pulse rate and the total current from the detector are measured. A two channel pulse height analyzer is used to furnish crude spectral information for pulse rates from 10 to 10^5 pulses per second. The maximum pulse rate is determined by the fixed dead time of the counter of 10μ sec. The pulse rates measure the number of pulses of energy greater than the threshold energy. Figure 34 shows the beta-gamma logic unit, and Figure 35, the schematic diagram of this unit.

EXPLODED VIEW OF RADIATION EXPERIMENT

MODEL II (DISCOVERER)

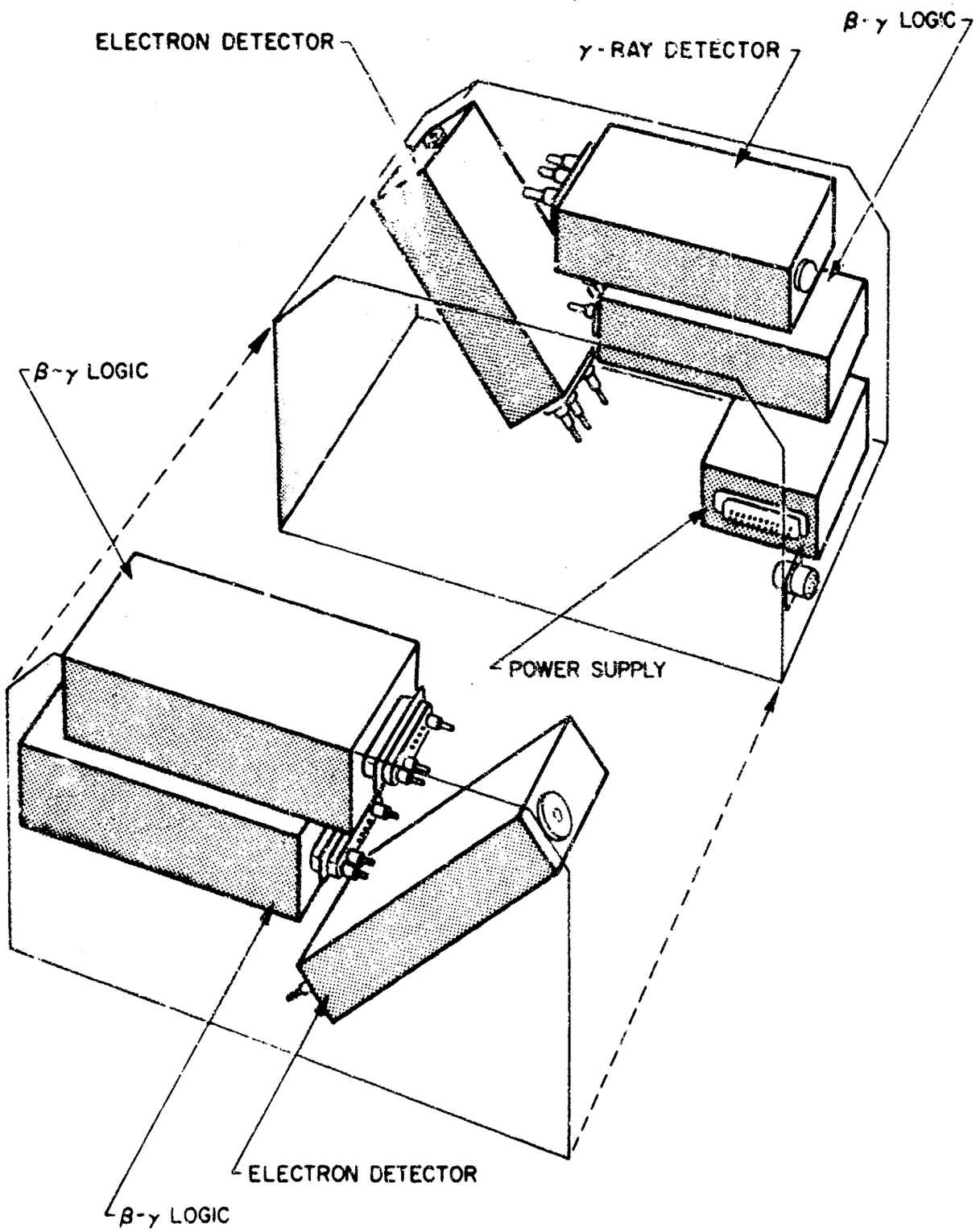

Figure 30

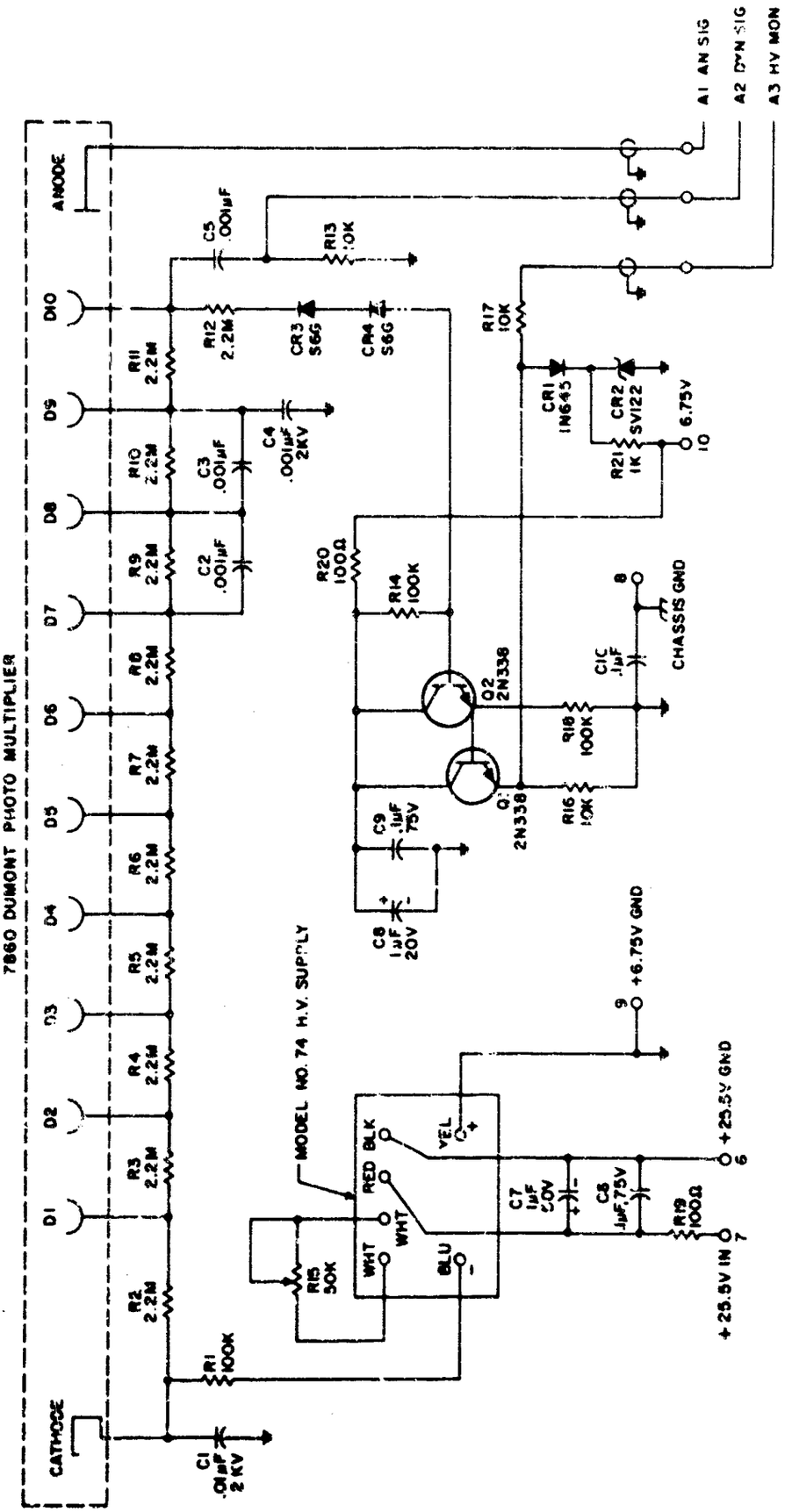

B-T SENSOR

BY-008
EL 232-10

SCHEMATIC DIAGRAM OF BETA-GAMMA SENSOR

Figure 31

RADIATION EXPERIMENT II
β-SENSOR UNIT

Figure 32

GEOMETRY OF BETA RAY DETECTOR

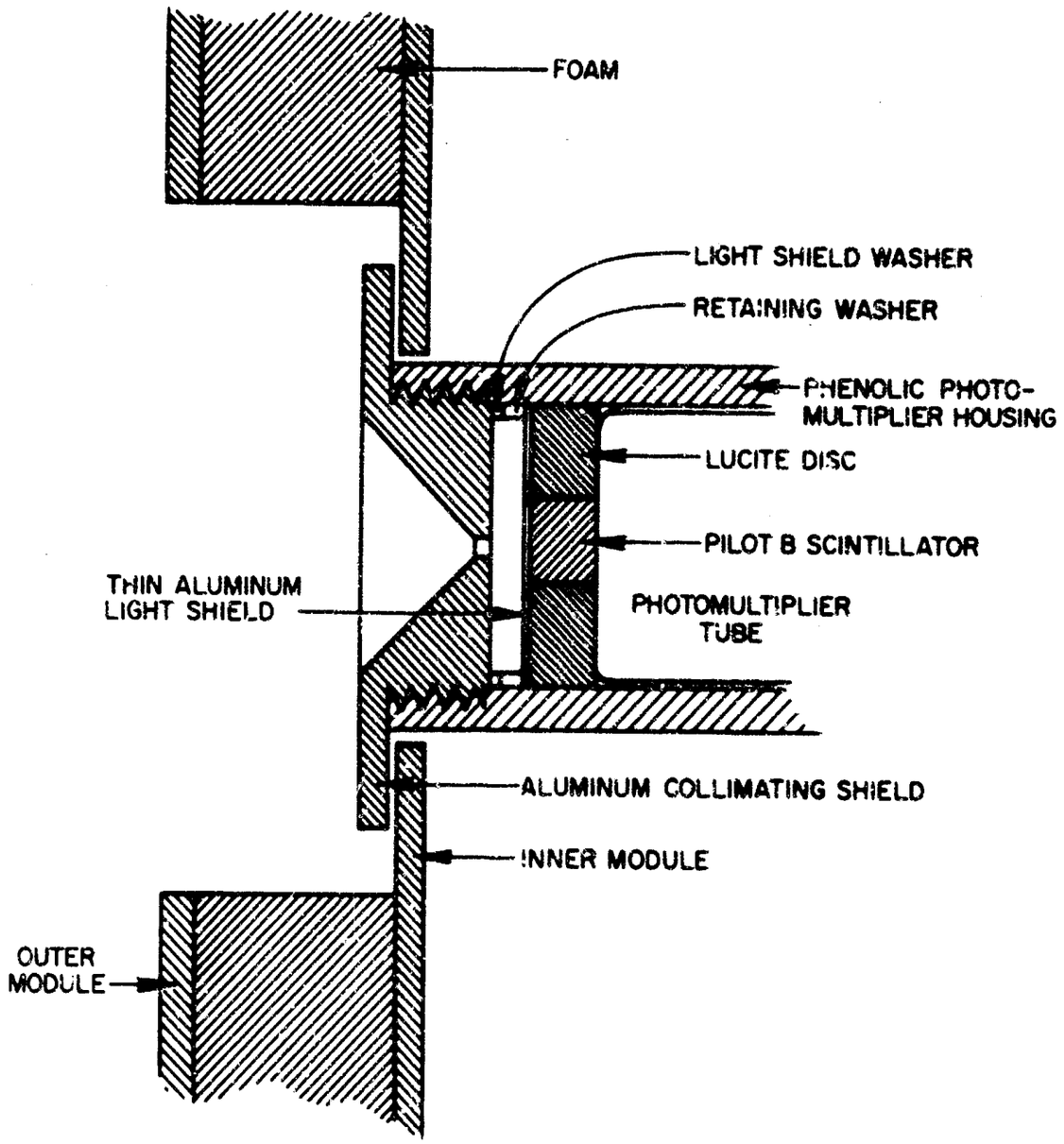

Figure 33

RADIATION EXPERIMENT II
BETA-GAMMA LOGIC UNIT

Figure 34

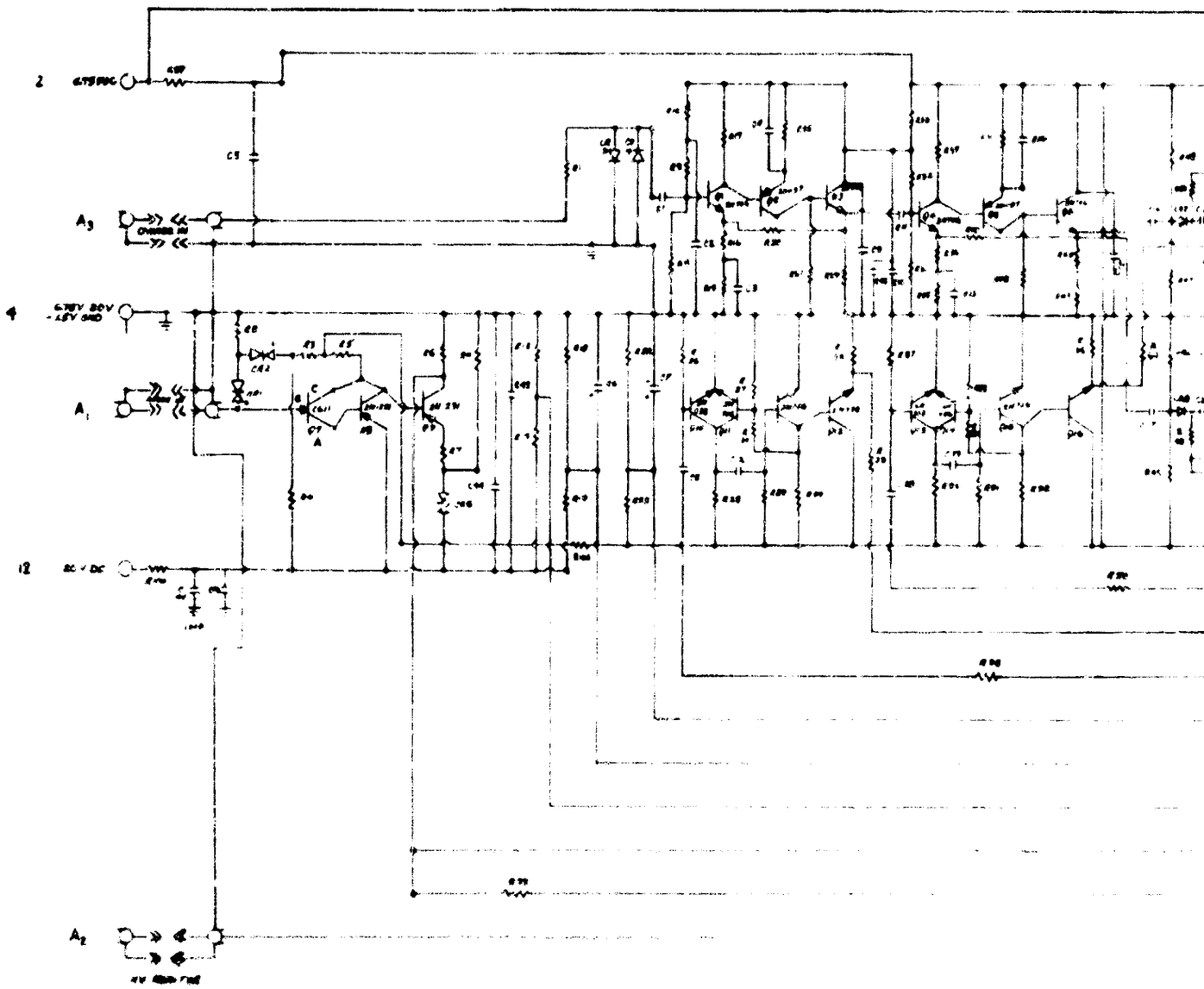

BY-003

SCHEMATIC DIAGRAM OF BETA-G

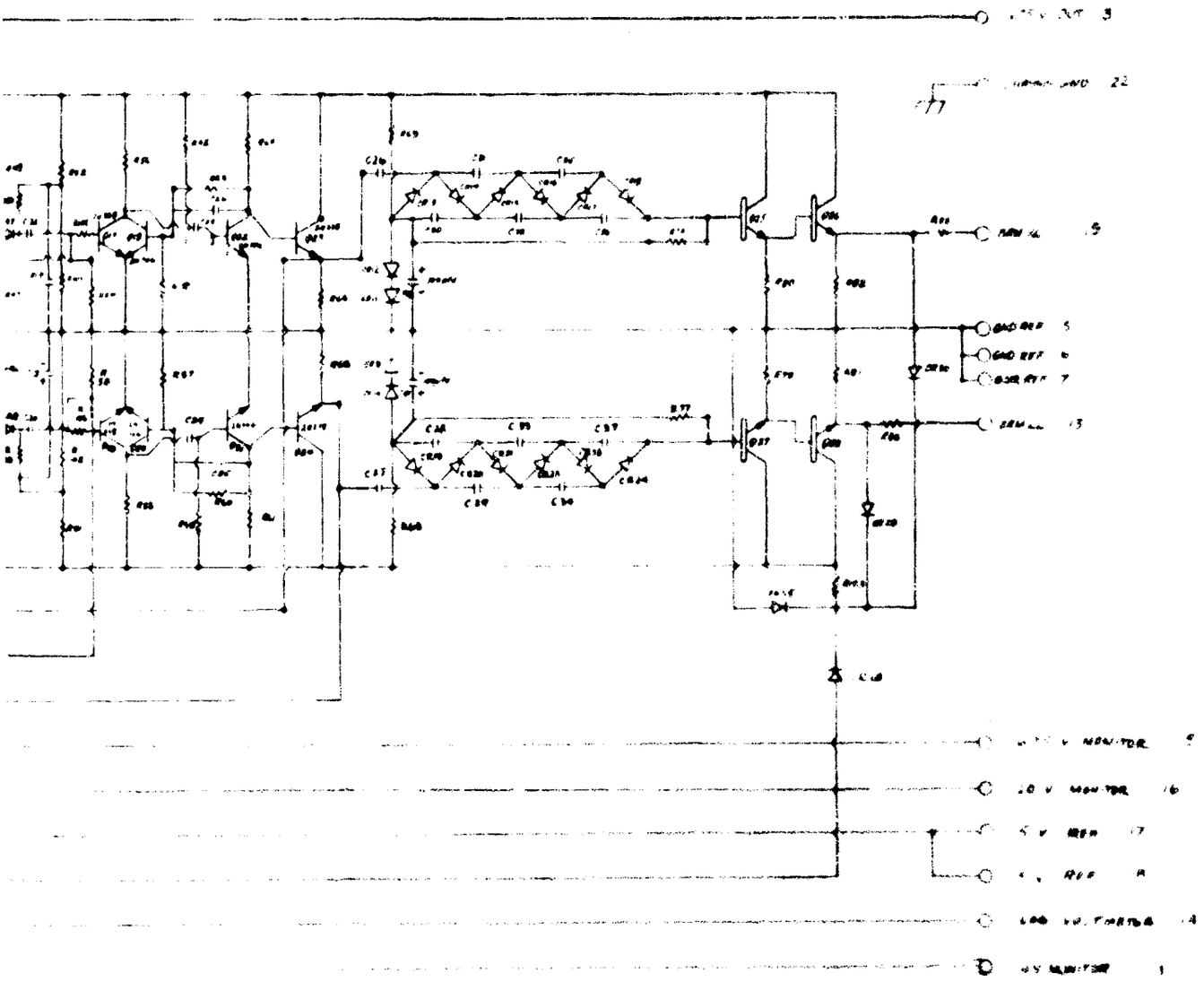

GAMMA LOGIC CIRCUIT

Figure 35

The current monitor measures the rate of energy deposition in the crystal. It is capable of measuring currents equivalent to energy deposition rates from approximately 10^4 Mev/sec to approximately 10^9 Mev/sec.

The γ -ray detector consists of a CsI(Tl) crystal scintillator of approximately 4 g weight covered by a .3 g/cm Al shield and viewed by a ruggedized photomultiplier. This detector is embedded in a foaming compound which is used to support the various components in the instrument package (Figure 36). The detector is, therefore, shielded from the environment by composite materials roughly equivalent to at least 2 g/cm^2 Al. This scintillator is consequently relatively insensitive to electrons of energy lower than 4-5 Mev; it is, however, sensitive to the bremsstrahlung produced by these electrons in the instrumentation case. Therefore, the response of this detector can be used to distinguish between incident photons and electrons. The detector is sensitive to γ -rays of energy greater than about 100 kev over 4π steradians. The range of sensitivity of this detector is from approximately 10 to 10^9 γ -rays/cm^{2}sec. This dynamic range is obtained as in the case of the electron detectors by use of pulse and current measurements. Figure 37 shows the complete experiment, and Figure 38 shows the various beta and gamma sensor logic units inside the case. Figure 39 is the block diagram of the circuit, and Figure 40 is a diagram of the wiring harness.

1.1 Calibration Procedure for Debris Decay Radiation Instrumentation

1.1.1 Calibration of Counting Rate Meters

A variable frequency, variable height pulser producing pulses of 1 microsecond duration was used to establish the discriminator settings of the upper level (UL) and lower level (LL) discriminators. These settings were adjusted for all instruments to be 2.2 and 1.1 volts. Subsequently using a 2.5 volt amplitude, 1 microsecond long pulse, a curve of voltage output of the count rate meter versus pulse rate was obtained.

GEOMETRY OF GAMMA RAY DETECTOR

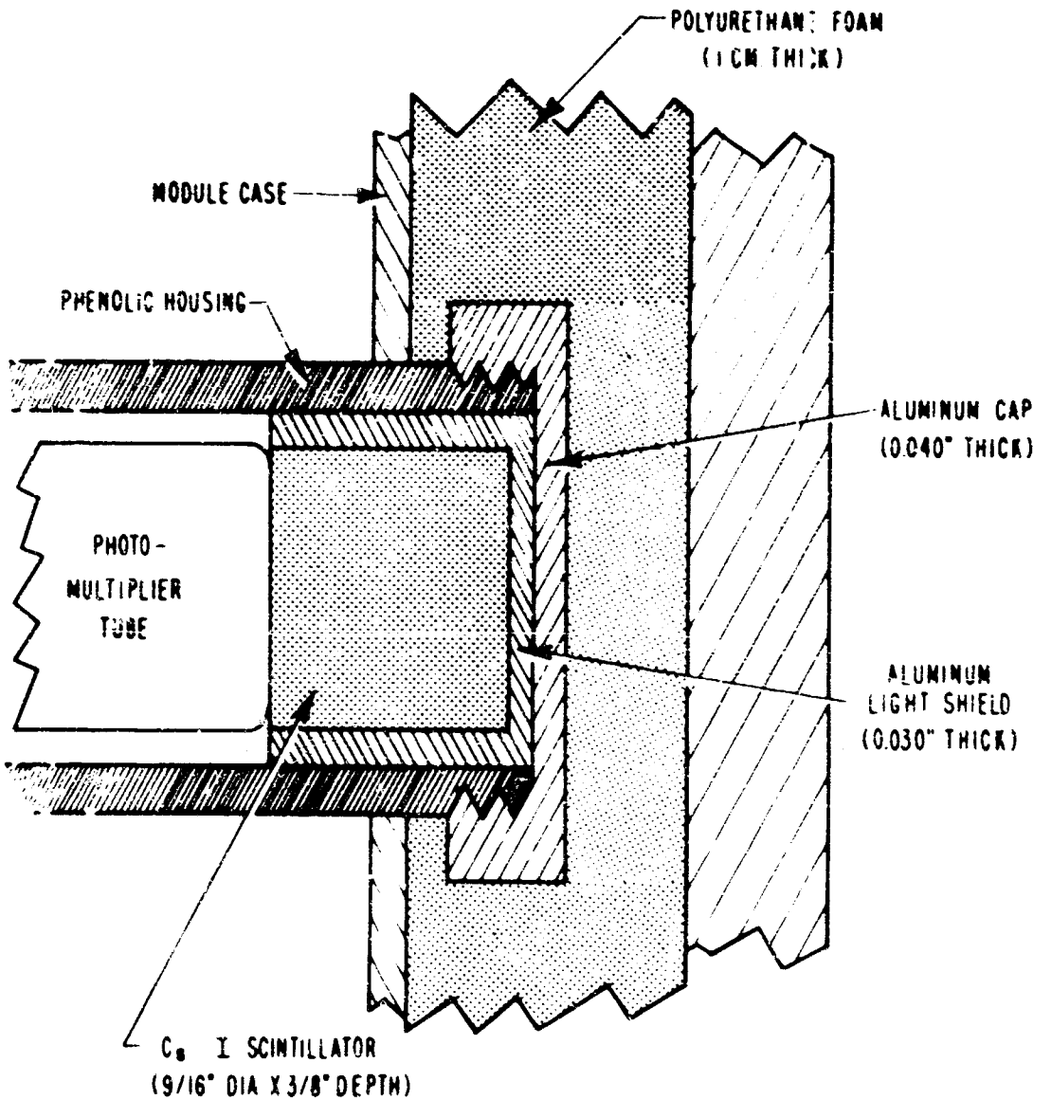

Figure 36

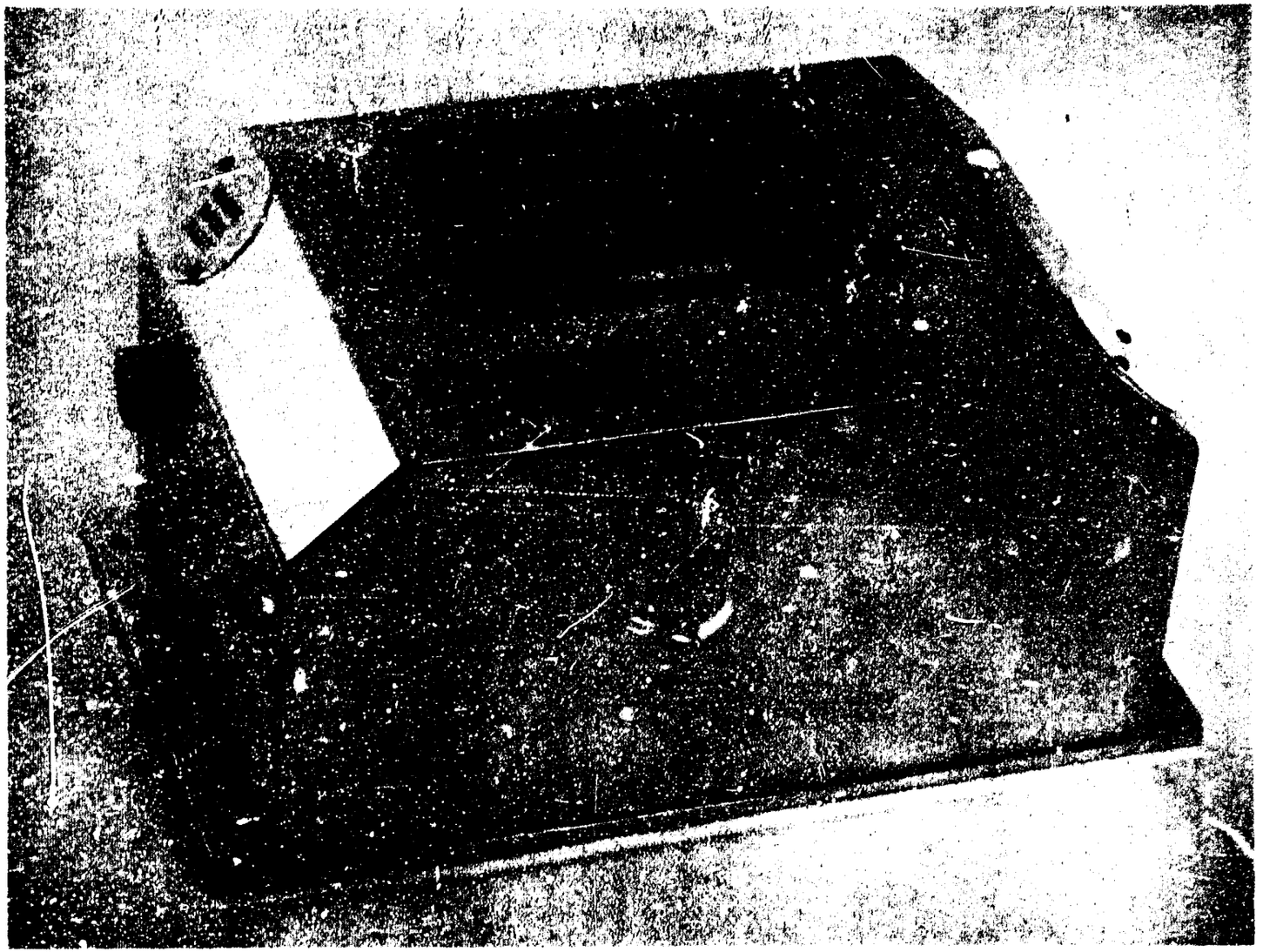

RADIATION EXPERIMENT MODEL 11
BETA BETA GAMMA DETECTOR

Figure 37

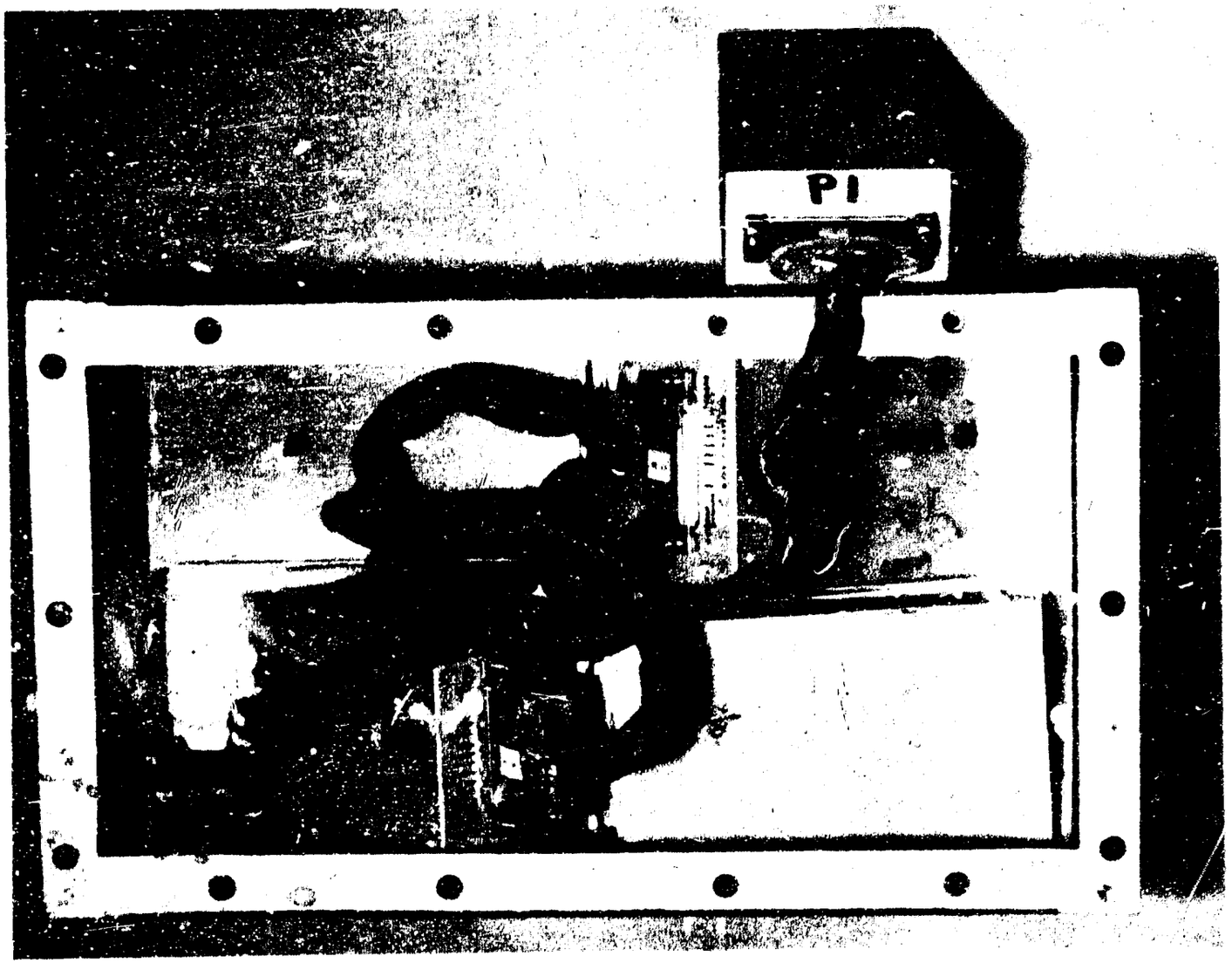

RADIATION EXPERIMENT 11
BETA BETA GAMMA DETECTOR

Figure 38

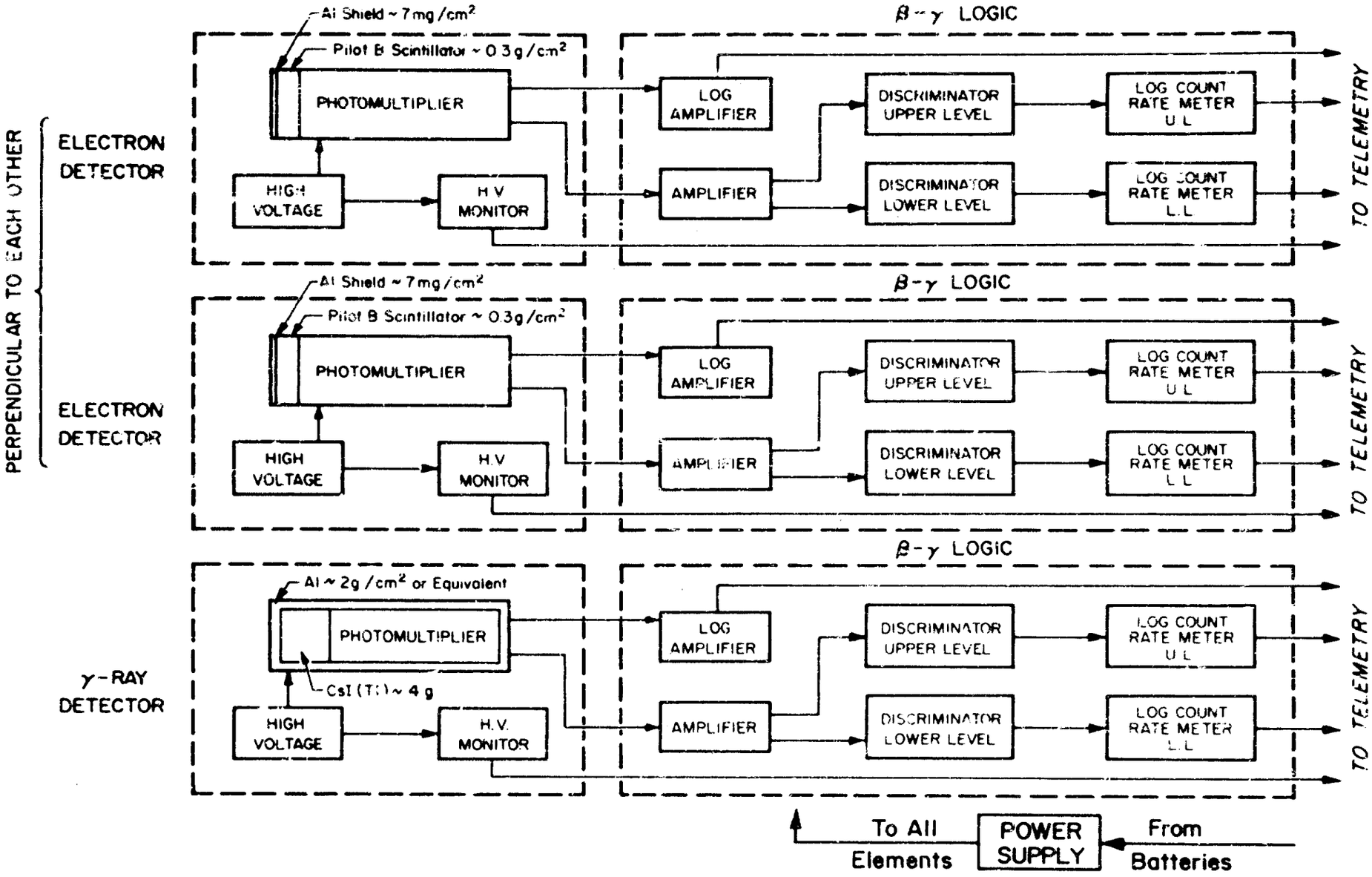

BLOCK DIAGRAM OF RADIATION EXPERIMENT

MODEL II (DISCOVERER)

Figure 39

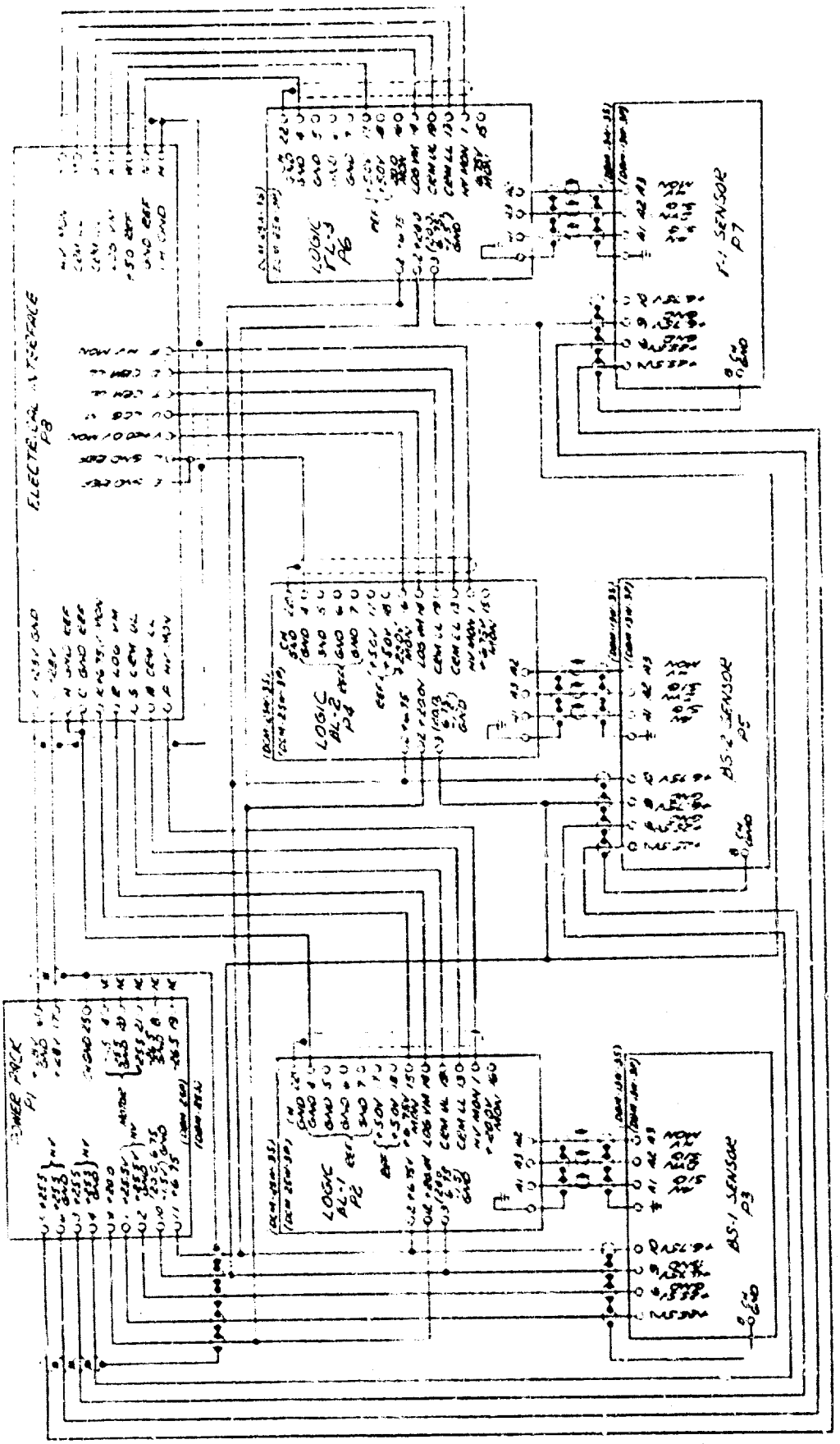

DIAGRAM OF WIRING HARNESS

Figure 40

The pulse rate was obtained by measuring the distance between pulses on a calibrated oscilloscope time base. The method was identical for electron and γ -ray sensor logics.

1.1.2 Determination of Threshold Energies

A Cs^{137} source was used to determine the threshold energies of the two counting rate channels of the electron sensor. A pulse height spectrum of the pulses from the scintillator was obtained to determine the voltage corresponding to the 660 kev internal conversion electron. The gain of the photomultiplier was adjusted until 0.5 Mev energy deposition corresponded to a pulse at the lower level discriminator input of 1.1 volts. The upper level discriminator setting therefore corresponded to approximately 1.0 Mev deposited. The measurement was performed with a known source at a known distance from the detector. A standard logic was used with a standard detector. The count rate meter outputs of the upper and lower level discriminators were recorded.

Subsequently, for all electron sensors, the same source and geometry were used, and the photomultiplier gain was set by simply duplicating the measured rates of the standard unit.

For the γ -ray detector a similar technique, utilizing the 0.51 Mev and 1.28 Mev γ -rays from a Na^{22} source, was employed.

1.1.3 Calibration of Logarithmic Current Meters

The γ -ray detector rate of energy deposition channel was calibrated by use of a Co^{60} source of 10 millicuries. A standard detector was placed at various known distances with respect to the source, and the various anode currents I_i were measured. With the same detector at the same gain, the charge Q_o deposited at the anode by a single

0.51 Mev γ-ray from the Na^{22} source was measured. The charge Q_1 deposited at the anode by 1 Mev was then calculated. The rate of energy deposition R_1 in the standard detector at each position was derived by the equation

$$R_1 = \frac{I_1}{Q_1} \text{ in Mev sec}^{-1}$$

In this manner a tabulation of energy deposited in the standard γ-ray detector as a function of distance was obtained. All γ-ray detectors were then calibrated by measuring the current output at each of the points at which the rate of energy deposition was previously determined. A graph of voltage output versus Mev deposited per second for each γ-ray detector was thus obtained.

The calibration of an electron detector rate of energy deposition channel proceeded in the following manner. The standard γ-ray sensor was used with the electron logic to be calibrated. The logarithmic current meter signal output at each of the standard positions with respect to the Co^{60} source was then recorded. Since all electron and γ-ray sensors had gains adjusted so that a given energy deposited by a single event in the crystal yielded the same pulse height into the discriminator, it can be shown that the rates of equivalent energy deposition R_{ei} in the electron sensor crystal at the standard positions of the Co^{60} source were given by

$$R_{ei} = \frac{1}{f_c} R_1$$

where f_c is a correction, experimentally determined, due to the different characteristic decay times of the CsI(Tl) and the Pilot B scintillators and to the properties of the electronic circuitry. This method was used because it was not practical at the time to use a 10 millicurie electron source and because of the relative low sensitivity of the electron detector to γ-rays. A calibration curve of logarithmic current meter output versus energy deposited R_{el} was thus obtained.

1.1.4 Calibration for Very Large Fluxes

At fluxes in excess of 10^6 particles per second or 10^6 Mev deposited per second, both the counting rate meters and the rate of energy deposition channel (logarithmic current meter) became saturated. In such situations, the photomultiplier used all of the current that the high voltage supply could furnish. The high voltage therefore dropped as the current tried to increase above the power supply's rated maximum in a manner depending on the regulating circuitry of the high voltage supply. One could, therefore, by monitoring the high voltage, measure the rate of energy deposition, thereby increasing the dynamic range of the instrument by about 3 orders of magnitude up to 10^9 Mev deposited per second. This calibration proceeded as follows. Since a 1 curie source was not available (which would have been necessary to produce the desired fluxes), the amounts of incident visible light equivalent to various high rates of energy deposition in the crystal were established. The intensity of a visible light source, covered with neutral density of 10^3 attenuation, was varied until the reading of the logarithmic current meter at the highest energy deposition not yet saturating was reproduced. By removing filters of known attenuation, intensities corresponding to known higher rates of energy deposition could thus be obtained. This calibration was performed on the standard unit. For all other units it was assumed that the high voltage supply and monitor would yield identical results. This assumption was checked in a few samples and found to hold.

1.1.5 Use of Standard Units

All of the calibrations were accomplished by comparison of the units to be calibrated with the standards. This constitutes, of course, a relative calibration. Absolute calibrations were performed on the standard units above. These units have been retained so that if necessary the absolute calibration procedure can be refined and utilized for these data for all units.

The technique of measurement consists of the use of scintillation counters as detectors of the radiation field. A scintillation crystal responds to the incoming radiation by producing light in quantities proportional to the amount of energy lost by ionizing radiation in the crystal. This light is detected by the photosensitive surface of a photomultiplier from which a number of electrons proportional to the incident light flux is produced. The electrons are then accelerated from dynode to dynode of the multiplier structure with a total number gain at the collecting electrode (anode) of approximately one million. Single ionizing particles transversing the crystal will produce a pulse of electrons at the anode whose duration is a function of the crystal properties. In CsI(Tl) this duration is approximately 10^{-6} seconds, Pilot B, approximately 10^{-8} seconds. Particle fluxes impinging on the scintillator can be detected by counting the individual pulses as long as their rate is less than 10^{6} in CsI(Tl) or 10^{8} in Pilot B. If fluxes larger than these occur, then an average current is produced at the anode which is a direct measure of the rate of energy deposition in the crystal.

To utilize fully the information furnished by the detector, the rate of individual pulses as well as the average rate of energy deposition in the crystal was measured. The maximum rate at which single pulses could be counted was determined by the electronics and was of the order of 10^5 per second. At the rates which permitted pulse techniques to be used, pulse height analysis in two channels of different thresholds was performed to obtain rough information on the spectrum of the impinging radiation. For incident fluxes greater than 10^5, measurements were made of the rate of energy deposition. These combined techniques permitted measurements over a range from about 10 Mev deposited per second to 10^9 Mev deposited per second.

In order to carry out the proposed experiment to measure the flux of electrons and γ-rays from radioactive debris decay, two crystals were used — one of CsI(Tl) and the second of Pilot B plastic. The reasons for this choice were as follows: since scintillator crystals respond to ionizing particles, their response to γ-radiation occurs primarily by creation in the crystal of Compton electrons and detection of these electrons. In order to have an efficient detector, one must therefore furnish enough mass for the γ-ray to interact and a material of high atomic number Z to provide a high Compton cross-section. On the other hand, if a low Z, small mass crystal is chosen, its efficiency to γ-radiation is small.

The chosen CsI(Tl) and Pilot B scintillators had masses of approximately 4.0 and 0.31 grams and the ratio of the effective atomic numbers was of the order of 10. Therefore, the CsI(Tl) was approximately two orders of magnitude more efficient in detecting γ-rays than the Pilot B scintillator. Both crystals were approximately equally efficient for detection of electrons. By shielding the CsI(Tl) crystal with about

2.0 g/cm^2 of aluminum and composite materials, the sensitivity of the CsI(Tl) detector to electrons was reduced by orders of magnitude for electrons with energy less than about 4 Mev. The shielding in front of the Pilot B scintillator was made as thin as possible and was of 0.165 g/cm^2 of beryllium. This corresponded to an electron energy threshold of 0.5 Mev. In Figure 41 the calculated fraction of incident energy deposited in the scintillator as a function of the energy of the incident radiation is shown for the electron detector for γ -rays and electrons. The calculation was carried out taking into account the transmission of the beryllium filter and the stopping power of a thickness of carbon equivalent to the thickness of the Pilot B scintillator. In Figure 42 a similar plot is shown for the γ -ray detector. An absorber thickness of 2 g/cm^2 of aluminum was assumed and the stopping power of the CsI(Tl) crystal of about 4.5 g/cm^2 was taken into account. Figure 43 shows, for a given incident gamma ray flux the ratio of the energy deposited in the gamma ray detector to the energy deposited in the electron detector as a function of the gamma photon energy

PERCENTAGE OF IMPINGING FLUX ABSORBED IN ELECTRON DETECTOR VS. ENERGY OF INCIDENT RADIATION

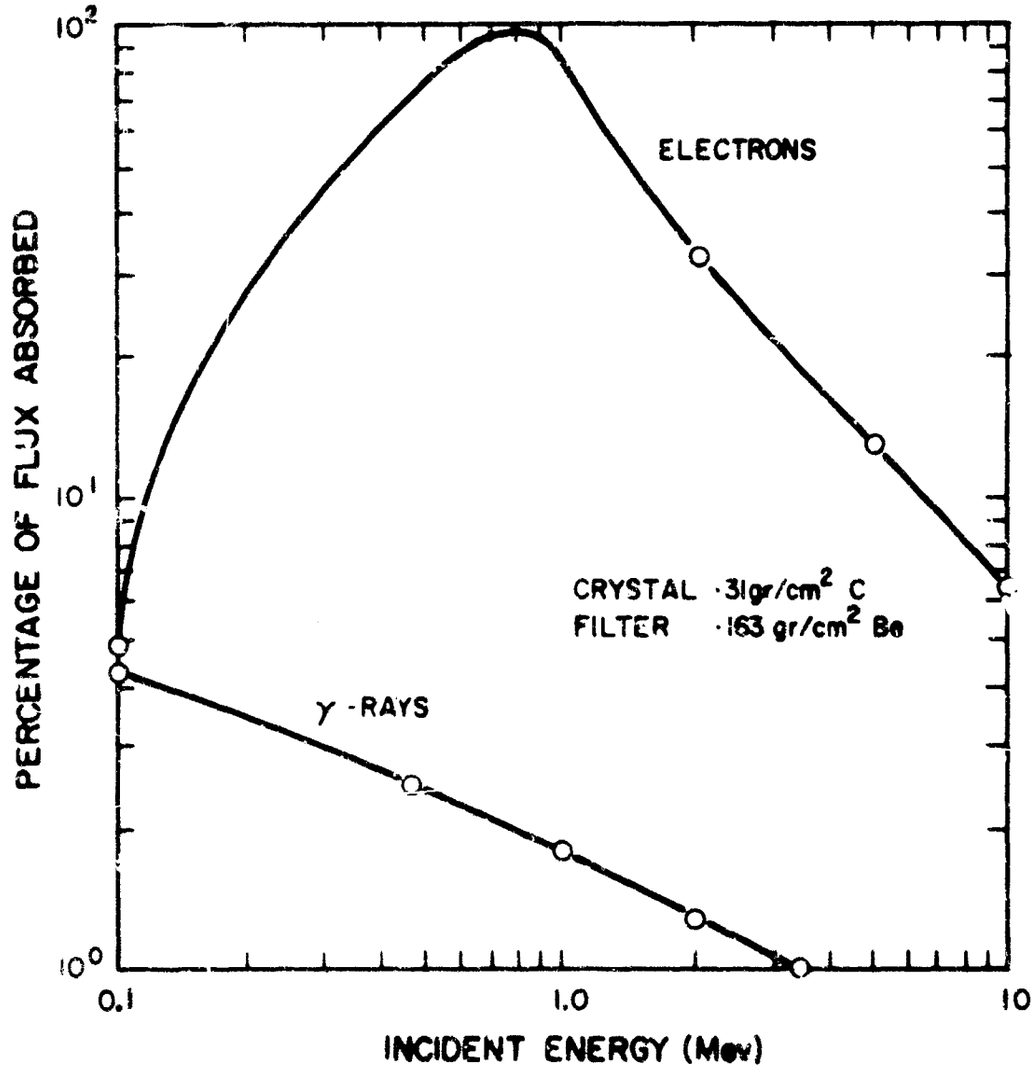

Figure 41

PERCENTAGE OF IMPINGING FLUX ABSORBED IN GAMMA RAY DETECTOR VS ENERGY OF INCIDENT RADIATION

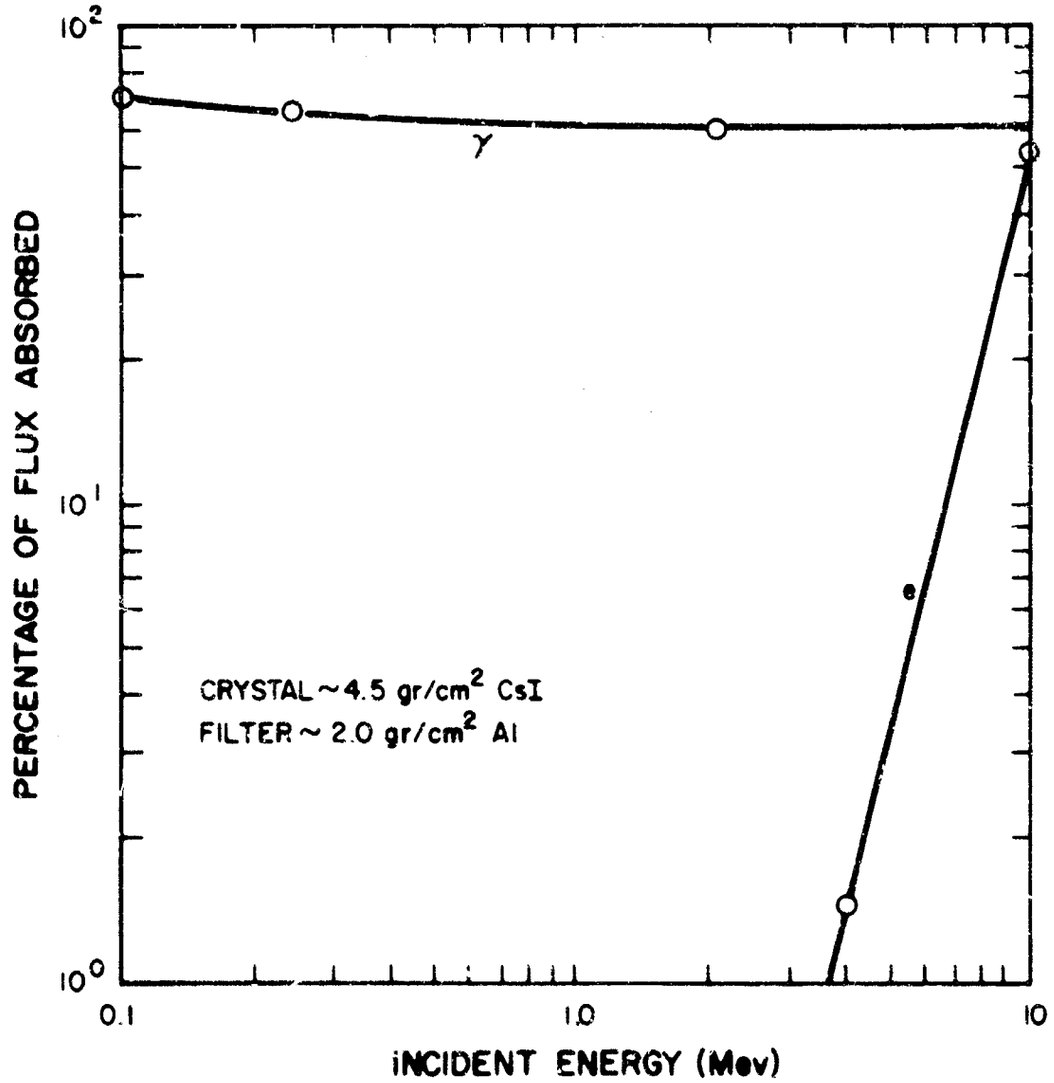

Figure 42

RATIO OF ENERGY DEPOSITED BY GAMMA RAYS IN GAMMA RAY TO ELECTRON DETECTOR VS ENERGY OF INCIDENT RADIATION

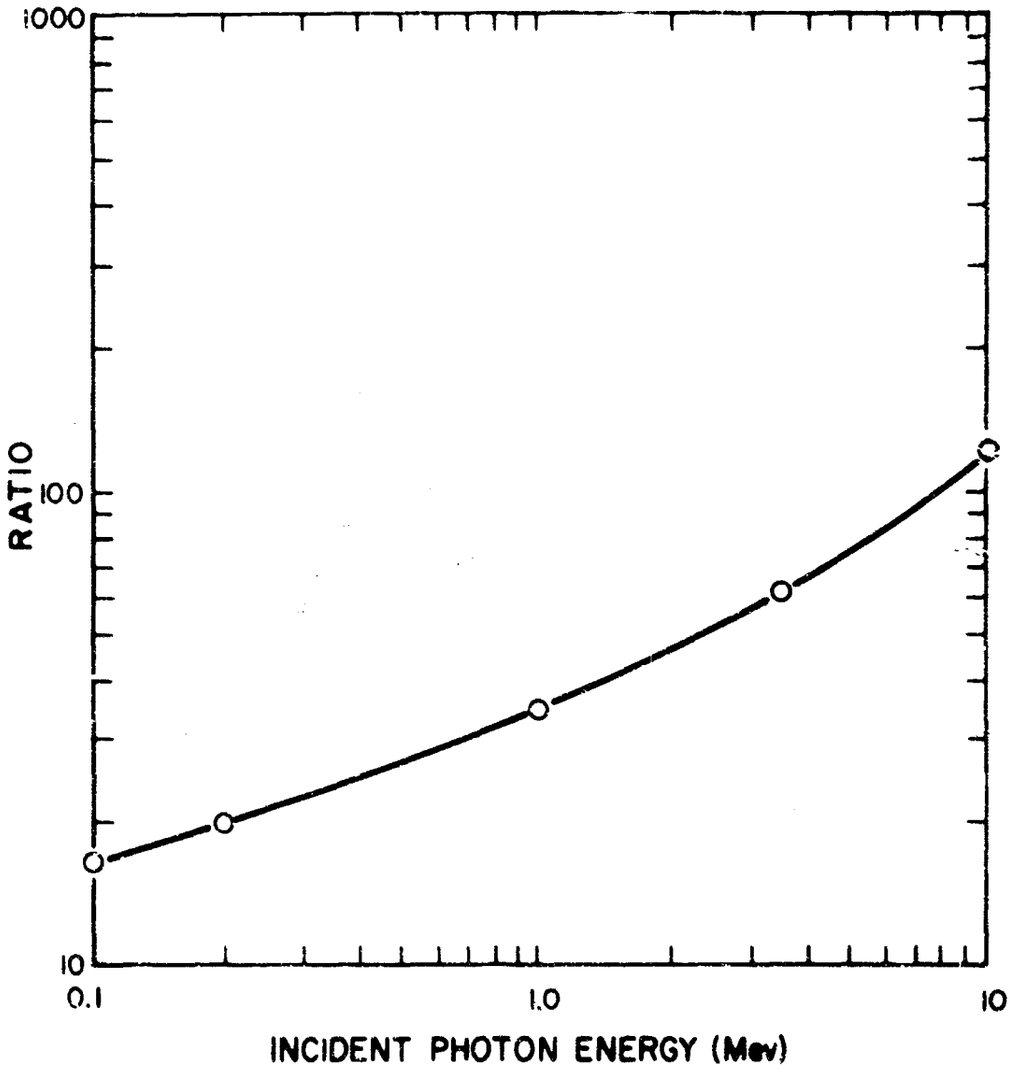

Figure 43

APPENDIX D

DIGITAL COMPUTER PROCESSING

1.0 INTRODUCTION

The telemetered data from the satellite was digitized and initially processed by Lockheed. This processing produced digital magnetic tapes, in a format compatible for reading by the FORTRAN II input-output system on the IBM 7090. These tapes contained voltage readings telemetered from the satellite, with universal times of original instrument reading and merged ephemeris information. During the course of the satellite's lifetime, Lockheed changed the format of these tapes. The two formats are referred to in this document as "Format 1" and "Format 2". Format 2 gives information arranged very differently from Format 1. Therefore, different computer programs had to be rewritten for the two formats.

To aid in the reduction of the data, the following computer programs were written. These programs all run on the IBM 7090, under control of the FORTRAN Monitor System.

1. Tape Inventory Program, Format 1
2. Tape Listing Program, Format 1
3. Count vs. B and L Program, Format 1
4. Time Correction Program, Format 1
5. Alpha vs. N (Pitch Angle vs. Count) Program, Format 1
6. Alpha vs. N (Pitch Angle vs. Count) Program, Format 2

The first program was designed to aid in bookkeeping during the processing of the data. It produced a summary of the information on the Lockheed tapes. The second program produced a detailed listing of selected information from the Lockheed tapes. The third program mapped count rate information in geomagnetic B-L space. The fourth program applied a time correction, which had been computed manually, to the information on the Lockheed tape. The last two programs tabulated voltage readings with their associated count rate values and pitch angles.

Since most of the information received was in Format 1, most of the programs were not rewritten for Format 2.

2.0 LOCKHEED TAPE FORMATS

The following information applies to both formats:

1. Real time channels are 8, 11, 12.
2. Tape recorded channels are 18 and 98 (F)
3. Telemetry Link 1 is used for launch only.
4. Telemetry Link 2 contains all experiment data except SAPUT
5. Telemetry Link 3 is SAPUT only.
6. The station code is:

01 VAFB	23 Ascention Island
07 Kodiak, Alaska	30 New Boston, N. H.
09 Hawaii	

2.1 Format 1

1. The records and files on the tape are arranged in the usual FORTRAN 2 manner, 256 words per record, and as many records as necessary in a file.

2. Each file contains any number of records. The first record contained 2 control words followed by 3 data words (the rest of the 256 words are not used in the record). The first word is a FORTRAN 2 control word. The second word tells how many data words are following in the record. The next three give the vehicle number, channel number, telemetry line number, commutator position, orbit number, station number, and computer run number. For example, this indicitive

might be: 140108020020010091. 1401 vehicle number; 08 channel number; 02 telemetry link number; 002 commutator position; 001 orbit number; 09 station number; and 1 computer run number.

3. The second and succeeding records in the file will contain the following: The first word in the record is a FORTRAN 2 control word, and the second word tells how many words of data follow in the record. Then follow 36 (or fewer) sets of words arranged as TIME, GC LATITUDE. LONGITUDE, ALTITUDE (KM), B. L. These are arranged in groups of seven. Each group gives: time, voltage, readout, geocentric latitude in degrees, terrestrial east longitude in degrees, altitude in kilometers, and geomagnetic coordinates B (gauss), an L (earth radii).

4. Each file contains all the data from one commutator point acquired from one pass. In general the first two words in each record are a FORTRAN control word and the number of data words following in the record. Time is the common base in relating one file to other files and is given to two decimal places, in seconds of Universal Time since 1 October 1962.

2.2 Format 2

The tape contains any number of files. Each file contains:

1. Flight indicative in the first record.
2. Data indicative in the second record.
3. Actual data values from the third up to the last record prior to an end of file.

There is an end of file after each file of data and three (3) end of files after the last file of data on the tape. The following read statement may be used to read all records:

READ TAPE IT, IRM, MG, NSET, [(DATA(I , J), I = 1, MG), J = 1, NSET]

where

IT = Input Tape Unit Number

IRM = which type of record this is:

If IRM = 0, the record contains three (3) words Flight Indicatives.

If IRM = 1, the record contains Data Indicatives. This shows the arrangement of the data in all the following data records.

If IRM = 9, the record contains the actual data values.

MG = Maximum number of the first subscript I in Data (I, J) of the read statement. This value is always equal to the number of merged quantities in the record.

NSET = Maximum number of the second subscript J in Data (I, J). Normal data records except the last partial record have NSET = 60. Therefore, the dimension requires Data (60, 60). MG and NSET are used by the Read Tape statement to read one complete record from the input tape.

DATA (I, J) = Locations, where the actual indicative information or data values are stored.

The format can best be described by an example:

Suppose a file of data to be read in, from the input tape, contains the following data:

A. Flight 1401

Channel 8

Link 2

Orbit 30

Station 30

Run Number 1

B. Pin #3, #4, #11, #38, and #41 data from Channel 8, Link 2 commutator are written together with ephemeris data on each data record.

After reading each record, test IRM value.

1. If IRM = 0, the Flight Indicative gives BCD information as follows:

Flight	Ch	Link	Pin	Orbit	Sta.	Run
1401	08	0 2	0 0 0	0 3 0	3 0	1
Data (1, 1)		Data(2, 1)		Data (3, 1)		

This record contains all the information in Item A above.

MG = 3, NSET = 1 in this case.

2. If IRM = 1, Data Indicative gives BCD information as follows:

DATA (1, 1) = TIME**

DATA (2, 1) = 2*****

DATA (3, 1) = 4*****

DATA (4, 1) = 11****

DATA (5, 1) = 36****

DATA (6, 1) = 41****

DATA (7, 1) = GC*LAT

DATA (8, 1) = LONG.*

DATA (9, 1) = ALT.**

DATA (10, 1) = **B**

DATA (11, 1) = **L***

This record should give all the information on the order of all merged data in Item B. MG = 11, NSET = 1.

3. If IRM = 9, this record contains the actual data which looks like: (all data between the dotted lines are omitted for convenience)

One Record of Data

			Data Indicatives	
DATA (1, 1)	=	13209.05	Time in seconds.	First Merged Data Set
DATA (2, 1)	=	1.46	Pin #2 data value.	
DATA (3, 1)	=	4.35	Pin #4 data value.	
Data (4, 1)	=	18.40	Pin #11 data value.	
.				
.				
.				
DATA (11, 1)	=	9.34	Ephemeris L value	
.				
.				
.				
DATA (1, 2)	=	13210.05	Time.	Second Merged Data Set
DATA (2, 2)	=	2.08	Pin #2	
.				
.				
.				
DATA (11, 2)	=	15.03	L value	
.				
.				
.				
DATA (1, NSET)	=	14093.00	Time	
(2, NSET)	=	1.68	Pin #2	
(11,NSET)	=	11.05	L value of the last set in the record.	

MG = 11 -- (one time word) + (5 data pin words) + (5 ephemeris words)

NSET = 60 -- (last record may be partial)

3.0 LOCKHEED TAPE INVENTORY PROGRAM (FORMAT 1)

This program produces a printed summary of the contents of the Lockheed tapes. For each file, the program prints:

1. Summary of the indicative record. This gives the 3 data words in the record in their original packed BCD form, and also in an unpacked form with labels to show the meanings of each quantity given. If the indicative record contains more than three data words, the program prints an error comment and gives the first few words converted to floating point decimal.

2. Total number of words and records (not counting the indicative in the file.

If any record after the first in the file contains 3 or fewer data words, the program assumes that this is intended to be the start of a new file, prints an error comment, and treats this record as an indicative record.

The program can process up to 3 Lockheed tapes simultaneously. It cannot handle two-reel tapes, but will handle the second reel as a separate Lockheed tape. This simply means that the first file on the tape, which will probably be a continuation of a file on the previous tape, will be treated as an independent file.

The program uses no sense switches. It reads one input card, which has data fields in columns 1-6, 7-12, and 13-18. In each of these fields the user may punch, right adjusted, the logical tape number where a Lockheed tape will be mounted. The first blank or zero field on the card will signal the end of the list of tape numbers. Columns 19-24 must be blank.

4.0 LOCKHEED TAPE LISTING PROGRAM (FORMAT 1)

This program is designed to produce a summary of the contents of the Lockheed tape that is more detailed than that produced by the tape inventory program. Like the tape inventory program, it uses no sense switches, and reads as input a single card, which is identical to the card read by the tape inventory program. For each file, it produces the following output:

1. A summary of the indicative record. This summary is identical to that produced by the tape inventory program.

2. Every 30 records in the file. It prints out the time, ephemeris, and voltage information for the first 5 voltage readouts in the record. These groups of 5 voltage readouts are separated by a blank line.

Like the tape inventory program this program can detect the occurrence of indicative records in the middle of data files.

5.0 COUNT VS B + L PROGRAM (FORMAT 1)

5.1 Purpose

The program processes data from the Lockheed satellite tapes (Format 1) to produce the following printouts:

1. A group of tables showing the calibrated voltage readouts (count numbers) as received from the satellite as a function of the geomagnetic coordinates of (B and L) the satellite. Each of these tables represents one voltage point or commutator position, and one range in B and L. This information is specified in input cards. So is the calibration tables used to convert voltage to count number. Any number of these tables may be produced per computer run, but only nine will be produced during one pass through the Lockheed tape.

2. For each of the tables above, an accompanying table in the same format showing the number of points averaged to produce each quantity in the above tables.
   (1) and (2) above are referred to as "Table 2".

3. A straight tabulation of information on the Lockheed tape. This lists time, geocentric coordinates, geomagnetic coordinates, and raw voltage readouts for requested commutator positions during a requested time interval. This is referred to as "Table 1". It is generally not requested.

4. A listing, for a requested item in Table 2, of the count numbers and associated times used to produce this average.

5. Other information that is useful in interpreting the run. This includes:

   a) Tape inventory, a summary of the files on the tape.

   b) Monitor performance, summarizing the occurrence of noise as indicated from monitor voltages.

   c) Summary of handling of voltage readouts during Table 2 processing. This tells how many voltage readouts had B + L values that were outside the range of the B-L table, and how many were rejected due to monitor failure.

6. When there are errors in the Lockheed tape or in the input cards, comments to enable diagnosis of the errors.

While producing Table 2, the program rejects all points during times of noise, as indicated from monitor voltages which should remain steady. Monitor voltage points and nominal voltages are indicated in the input cards.

The Lockheed tape may be in one or two reels.

5.2 Functional Description

The program is essentially a straightforward data processing program, and the functions that it performs are described in Section 4.0 in the text of this report. However, the user should be aware of a few additional points:

1. Conversion from voltage readout to count rate is performed by linear interpolation using the calibration curves supplied as input.

2. Voltage readouts are considered by the program to be "noise-free" if no monitor voltage failure has been detected within T seconds of the time of the voltage readout. The value of T is read as input.

3. Each B-L box in Table 2 represents the average of count rates that fell within this B-L interval. To compute each individual count rate value, the average of 5 successive voltage readouts is used. When, due to occurrence of noise, less than 5 consecutive readouts are available, then these readouts are not used.

5.3 Operating Instructions

Sense Switches:

ON - If 2 binary tapes are in use;

OFF - If 1 binary tape is in use.

Tapes:

Tape A-6 is the binary tape prepared by Lockheed which includes satellite ephemeris in both geographic and geomagnetic coordinates, plus voltage readouts. If this tape is in two reels, the second reel must be mounted on unit B-6, and sense switch 2 must be on.

Input Cards:

Tape A-2 is prepared from a card deck, which may be stacked with other FMS jobs. The makeup of this deck is as follows:

FMS ID card*

XEQ card*

PROGRAM BINARY DECK

FMS DATA CARD *

Deck of control cards read by the program

The control card deck tells the program what data to process from the

* These are standard FMS control cards.

Lockheed tape, and how to process it. It contains the following sets of cards, in the following order:

1. Channel specification cards
2. Table 2 specification cards (There may be any number of sets of these after a set of channel specification cards.
3. Recycle card

The sequence above is referred to as a Channel Deck, and may be repeated any number of times.

Set (1), Channel specification cards, contains the following cards:

1. 1 Page Heading card
2. 1 Channel Request card
3. 1 Table 1 Request card
4. Up to 10 Monitor Specification cards. [The last Monitor Specification card is differentiated by the presence of data in the 4th field, which must be blank in the previous Monitor Specification cards. (See Card Formats, below).]

Set (2), Table 2 specification cards, contains the following cards:

1. 1 Table 2 Request card. (This gives the commutator position number and limits for the B-L table).
2. A block of cards which specify the Calibration Curve

   This block of cards contains:

   a) Calibration Curve Size card
   b) Enough Calibration Curve Table cards to represent all the voltages (ordinates of the curve)

c) Enough Calibration Curve Table cards to represent all the particle counts (abscissas of the curve).

This block of cards may be omitted altogether if the following conditions are met:

a) This same calibration curve was given previously for this commutator position.

b) No recycle card has appeared since giving the calibration curve.

3. 1 B-L Box Detail Request card (This specifies number of B-L box lists to be printed out.)

4. N B-L Box List Request cards, where N = the number of lists specified in the B-L Box Detail Request card. These cards must be omitted if the B-L Box Detail Request card is blank.

Card Formats:

The above formats of the above cards are given below:

Page Heading Card

Columns 1 - 72: Anything punched here will appear as the first line of each page of output. It is suggested that identifying information from the tape label be punched here.

Channel Request card

Columns 1 - 2: Channel numbers of data desired from the binary tape. This number must be right adjusted and filled in with a leading zero if appropriate.

3 - 12: Must be blank.

13 - 22: Start time for printed voltage tabulation (Table 1).

23 - 32: Stop time for printed voltage tabulation (Table 1). These times must be in the same units as used on the binary tape, and must be punched with a decimal point, anywhere in the field.

33 - 40: Must be blank.

41 - 44: Punch any integer here to cause printing of messages whenever a voltage point, specified in any of the Table 2 requests below, has B-L coordinates outside the specified B-L table. Leave blank to suppress such printing.

Table 1 Request Card

Columns 1 - 6
7 - 12
13 - 18
19 - 24
25 - 30
31 - 36
37 - 42
43 - 48
49 - 54
55 - 60
61 - 66
67 - 72

Each of these fields may be punched with a right adjusted integer, which specifies a commutator position whose voltage readings are to be tabulated in Table 1. As many of these fields as desired may be used, but the first blank or zero field (scanning from left to right) will signal the end of the Table 1 requests.

Monitor Specification Card

Columns 1 - 6:	Ignored.
7 - 12:	Commutator position number for this monitor. (Right adjusted integer)
13 - 20:	Nominal voltage reading for this monitor. (Punch with decimal point)
21 - 28:	Allowable deviation from the nominal voltage reading. (Punch with decimal point).
29 - 36:	This field must be blank for all but the last Monitor Specification card in a series. In the last Monitor Specification card in the series, this must be punched with a non-zero time interval (punch with decimal point) T, such that any data reading within T time units of a monitor failure will be discarded. This will be punched as a negative number if it is desired to print messages about each monitor failure. It will be punched as a positive number to suppress such printing.

Table 2 Request Card

Columns 1 - 4:	Commutator position number for this table. (Right adjusted integer)
5 - 10:	Lower table limit in B. (Punch with decimal point)
11 - 16:	Upper table limit in B. (Punch with decimal point)

17 - 22: Lower table limit in L. (Punch with decimal point)

23 - 28: Upper table limit in L. (Punch with decimal point)

29 - 48: Name of point

Calibration Curve Size Card

Columns 1 - 12: N, the number of points given in the calibration Table cards that follow. This must be punched as a right-adjusted integer.

Calibration Curve Table Card

Columns 1 - 12:
13 - 24:
25 - 36:
37 - 48:
49 - 60: Each of these fields may contain a coordinate of one of the points on the calibration curve. Numbers should be punched with a decimal point. A decimal exponent may be punched, in the form E $\pm$ xx, and it must be right-adjusted, in the field. There are two sets of these cards for each curve. The first gives the ordinates, or voltages, in numerical order, and the second set gives the corresponding abscissas or particle counts. Each set will start a new card. Numbers must be punched in successive fields from left to right across the card, and continued onto successive cards until all N points are represented.

B - L Box Detail Request Card

Column 1: Minus sign. (11 punch) (May be blank if rest of card is blank)

2 - 12: The number of B-L Box List Request cards that follow. (Right-adjusted integer).

B - L Box List Request card

Columns 1 - 12: Column number of B-L box to be listed in detail. (Punch as right-adjusted integer).

13 - 24: Row number of B-L box to be listed in detail. (Punch as right-adjusted integer).

Recycle card

There are two possible formats for this card:

Format 1:

Column 4: 1

Rest of Card: Must be blank

The Format 1 Recycle card must be immediately followed by another Channel Deck, unless it is the last card in the input deck.

Format 2:

Column 4: 2

Rest of Card: Must be blank

This card is used to instruct the operator to mount a new tape on unit A-6 (and B-6 if in use). It must always be followed by another card, which may contain in columns 1 - 72 any instructions to the operator.

Upon recognizing a Format 2 Recycle card, the program will read the next card, print its contents on the on-line printer, and halt. Pressing start will cause the machine to read another Channel Deck.

Restrictions on Program

Due to the limited table sizes, certain restrictions exist and are given below:

Restrictions on Monitors

No more than 10 monitors may be specified in any one set of Channel Specification cards.

No commutator position higher than 60 may be specified.

Restrictions on Table 1

No more than 12 voltage points may be listed in Table 1.

No commutator position higher than 60 may be specified.

Restrictions on Calibration Curves

No calibration curve may contain more than 50 points.

For any one Channel Deck there may be no more than 20 different Calibration Curves input. The total combined size of all Calibration Curves may not exceed 250 points.

Restrictions on Table 2 Requests

No commutator point higher than 60 may be specified.

Restrictions on B- L Box Detail Requests

For any one Channel Deck there may be no more than 20 B - L Box List Request cards.

6.0 LOCKHEED TAPE TIME CORRECTION PROGRAM (FORMAT 1)

This program is designed to apply a universal time correction to selected data from the Lockheed tapes. It does not compute the time correction. That must be done manually, and given to this program as input.

6.1 Operating Instructions

1. Data Deck

a) Time correction card, columns 1 - 6, $\pm$ XXXX, where XXXX is an integral number of seconds.

\+ means that the voltage should occur XXXX seconds later down the tape.

\- means that the time and ephemeris correspond to a voltage occurring XXXX seconds later down the tape.

b) Channel selection card, columns 1 - 6, XX, channel no.

c) Commutator position selection card, columns 1 - 40. (In any column N, a "1" indicates that commutator position N is desired to be saved.

2. Sense Switches

#2	OFF, if input tape is 1 reel.
	ON, if input tape is 2 or 3 reels.
#3	OFF, if input tape is 1 or 2 reels.
	ON, if input tape is 3 reels.

3. Tapes Required

FMS Systems Tapes, plus A-7 for Reel 1 in input; A-6 for binary output (SAVE); B-6 for Reel 2 of input; B-7 for Reel 3 of input.

7.0 ALPHA VS N (PITCH ANGLE VS COUNT RATE) PROGRAM, FORMAT 1

7.1 Program Description

This program tabulates particle counting rate with corresponding pitch angle. Input cards specify what areas of time and what experiment voltage points are to be tabulated. A fifth order divided difference table technique is used to interpolate in calibration curve tables, to convert from voltage readout to count rate. The calibration curve tables are read as input.

Voltage readouts are considered by the program to be "noise-free" if no monitor voltage failure has been detected within 10 seconds of the time of the voltage readout.

Since the satellite tumbles with a period that is much less than the commutator revolution rate, successive readouts of the same magnetometer voltage output should show a slow variation. Therefore, the program smooths the magnetometer data, to reduce the effect of undetected noise in the magnetometer readouts. Taking each magnetometer axis independently, it fits each group of 7 consecutive readouts to a second order polynomial, using a least squares technique.

These magnetometer readouts are then used to compute a unit vector describing the direction of the magnetic field. Cosine pitch angle is then computed as the dot product of this vector with another unit vector, read as input, describing the orientation of the instrument in the magnetometer coordinate system.

Data is printed in the following format: TIME, GLAT, GLON, ALT, B, L, BM, ALPHA, COSINE ALPHA, VOLT, COUNTING RATE. The time is in seconds and free-running from 1 October.

GLAT	Geodetic latitude accurate to 1 place.
GLON	Geodetic longitude accurate to 1 place.
ALT	Geodetic altitude in kilometers accurate to 1 place.
B	Theoretical B field in Gauss accurate to 3 places.
L	Geomagnetic L coordinates, measured in earth radii at the equator, accurate to 3 places.
BM	Measured B field (in Gauss) accurate to 3 places.
ALPHA	Pitch angle.
COSINE ALPHA	Cosine pitch angle.
VOLT	Voltage reading of the specified commutator point, accurate to 3 places.
COUNTING RATE	Particle count rate of the specified commutator point.

7.2 Operating Instructions

Sense Switch 2 -

ON if 2 reel binary tape on units A-6 and B-6;

OFF if 1 reel binary tape on unit A-6

Input: Tape A-5 is the binary tape in Lockheed Tape

Format 1: If it is a two-reel tape, the second reel is mounted on B-6.

Tape A-5 is prepared from card deck as follows:

FMS ID Card

XEQ Card

Binary Deck

FMS Data Card

DATA DECK

The makeup of the data deck is as follows:

1. Identification
2. Experiment number, order of accuracy, and specification
3. Channel request
4. Time intervals
5. Direction cosines for all four instruments
6. Magnetometer conversion coefficients
7. Calibration curves
8. Monitor data
9. Commutator positions of magnetometer data

A data deck may consist of any number of sets of data; each set contains the nine types of cards specified above, as long as the end specification on the last, and only the last set, is not zero.

Formats:

1. Identification —

Columns	Description
1 - 6	Flight number
7 - 12	Orbit number
13 - 18	Station identification
19 - 24	Computer run number

2. Experiment card —

Columns	Description
1 - 6	Experiment number (any number from 1 - 4) integer, right-adjusted.
7 - 12	Order of polynomial interpolation desired, integer, right-adjusted.
13 - 18	End specification, integer, right-adjusted — 1 if this is the last data set; 0 otherwise.

3. Channel request —

Columns	Description
1 - 2	Channel number of two digit integer

4. Time intervals —

Columns	Description
1 - 12	Minimum time.
12 - 24	Maximum time.

In the format XX...X.X. there may be as many as 10 time intervals requested in a data set. The last request must be followed by a blank card.

5. Direction cosines —

Columns	Description
1 - 10	x
11 - 20	y direction cosines
21 - 30	z

In the format ± XX...X.XXX there are four such cards, one for each instrument. The order of the cards must correspond to the order assigned to the instruments as experiment numbers.

6. Calibration for magnetometer data —

Columns	Description
1 - 10	x
11 - 20	y Factor, in the format XXX...X.XXX
21 - 30	z

Here are two cards; the first gives the numbers which are subtracted from the magnetometer voltage and the second gives the division factor.

7. Calibration curves —

A. Size Card

Columns	Description
1 - 12	Number of points in the calibration curve
13 - 18	Number of the commutator position for which the calibration curve follows.
19 - 24	Experiment number for this commutator position.

B. Curves —

Columns	Description
1 - 12	Each field may contain a coordinate of a point on the calibration curve.
13 - 24	Numbers should be punched in the form XXX.XXE±XX and right-adjusted in the field. There are two sets of these cards for each curve. The first gives the ordinates, or voltages, in numerical order, and the second gives the corresponding abscissas or particle counts. Each set starts a new card. Numbers must be punched in successive fields from left to right. A blank card must follow the last curve to be read in.

8. Monitor data —

There are two cards for each monitor. The first card contains the commutator position of the monitor as a right-adjusted integer in columns 1-4.

The second card contains:

Columns	Description
1 - 4	Anything except 0
5 - 16	Nominal value of the monitor voltage.
17 - 28	Allowed deviation of the voltage. The first field is an integer, the last two are in the format X...X.XXX. The last monitor request must be followed by a blank card.

9. Magnetometer commutator positions —

Columns	Description	
1 - 6	x	commutator position
7 - 12	y	
13 - 18	z	

Restrictions

Only one channel may be requested in any data set. A maximum of ten time intervals may be requested. Calibration curves may contain a maximum of 25 points each.

A maximum of 7 monitors may be used. Up to 10 non-monitors, non-magnetometer commutator positions may be requested per data set.

If a total of more than 2,000 seconds of time is included in the time intervals, the program will have to make two extra passes of the tape.

The first pass compiles monitor and magnetometer data. The second pass correlates this with requested commutator positions.

If the time intervals of two succeeding data sets are exactly the same, the monitor, magnetometer pass will be by-passed. Care should be taken so that this does not occur if the first of these data sets required more than 2,000 seconds, because the first 1,000 seconds of magnetometer data will be lost for the second set.

8.0 ALPHA VS (PITCH ANGLE VS COUNT RATE) PROGRAM, FORMAT 2

8.1 Program Description

This program tabulates voltage readouts from commutator position 5 on channels 11 and 98 with cosine of pitch angle. The output gives ephemeris quantities, including B and L from the ephemeris; value of B computed from the magnetometer readouts, cosine pitch angle, and voltage readouts.

The program tabulates the following commutator positions which represent experimental data: 2, 3, 4, 6, 7, 19, 20, 21, 23, 24, 25, 27, 28, 29 from channels 11 and 98, but does not give pitch angles for these positions. Magnetometer coefficients and direction cosine of instrument are read as input.

8.2 Operating Instructions

The program reads three input cards. Each of these cards has three numeric fields, as follows: columns 1 - 10, 11 - 20, and 21 - 30. Data must be punched with explicit decimal point in each of these three fields.

The first card gives the bias voltage values for the x, y, and z axis magnetometers, in that order.

The second card gives slope values for three magnetometers. Together, these cards allow B component to be computed as a function of magnetometer

voltage, as follows:

$$B = (v - v_o)/a$$

where v_o is bias and a is slope.

The third card gives x, y, and z axis direction cosines for the direction of the instrument pointing in the magnetometer coordinate system.

APPENDIX E

A reprint of a paper entitled,

"Measurements on Trapped Particles Injected by Nuclear Detonations"

L. Katz, D. Smart, F. R. Paolini, R. Giacconi and R. J. Talbot, Jr., Space Research IV, Proceedings of the Fourth International Space Science Symposium, Warsaw, June 3-12, 1963, North-Holland Publishing Company, Amsterdam.

REPRINTED FROM:

SPACE RESEARCH IV

PROCEEDINGS

OF THE FOURTH INTERNATIONAL SPACE SCIENCE SYMPOSIUM
WARSAW, JUNE 3–12, 1963

EDITED BY

P. MULLER

MEASUREMENTS ON TRAPPED PARTICLES INJECTED BY NUCLEAR DETONATIONS

L. KATZ and D. SMART
Air Force Cambridge Research Laboratories, Bedford, Massachusetts, USA

and

F. R. PAOLINI, R. GIACCONI and R. J. TALBOT JR.
American Science and Engineering, Inc., Cambridge, Massachusetts, USA

1964

NORTH-HOLLAND PUBLISHING COMPANY – AMSTERDAM

MEASUREMENTS ON TRAPPED PARTICLES INJECTED BY NUCLEAR DETONATIONS

L. KATZ and D. SMART
Air Force Cambridge Research Laboratories, Bedford, Mass., USA
and
F. R. PAOLINI, R. GIACCONI and R. J. TALBOT, Jr.
American Science and Engineering, Inc., Cambridge, Mass., USA *

Abstract: A polar-orbiting Air Force satellite carried aloft a payload, shared by many experimenters, of radiation detection instruments for studying artificially produced trapped-radiation belts. Pertinent information on the satellite's orbit and capabilities is given. Data from four scintillation detectors are presented. The detectors have capabilities for discriminating among types of particles, and for measuring both energy and angular distributions of trapped particles. Data showing spatial distributions of trapped radiation, both as omni-directional flux versus L-shell plots and as iso-intensity contour plots, are presented. The major portion of data presented emphasizes electron pitch angle distributions and derived parameters. Both spatial and temporal variations of the pitch angle distributions (measured with a 6° angular resolution) are given. Some tentative conclusions are drawn.

Резюме: На спутнике ВВС, запущенном на полярную орбиту, была установлена аппаратура, смонтированная несколькими исследователями. Она представляет собою детекторы излучения, предназначенные для изучения искусственно создаваемых радиационных поясов. Приводятся параметры орбиты спутника, а также его технические характеристики. Приводятся данные по четырем сцинтилляционным детекторам. Детекторы способны различать характер частицы и измерять как энергию, так и угловое распределение захваченных частиц. Приведены данные, показывающие пространственные распределения захваченной радиации: как график потока, всенаправленного по отношению к оболочке L, так и контуры областей, ограниченных линиями равной интенсивности. Основная часть приведенных данных дает распределение электронов по питч – углу и другие параметры. Даются как пространственные, так и временные вариации распределений по питч – углу (измеренные с угловым разрешением 6°). Сделаны некоторые предварительные выводы.

1. Introduction

In the fall of 1962, an Air Force satellite, given the international designation, 1962 $\beta\kappa$, was launched into orbit. The satellite carried instrumentation to study artificial radiation belts created by the injection of electrons from

* This work was performed under Contract AF 19 (628) – 2799 with the Air Force Cambridge Research Laboratories, Bedford, Massachusetts.

nuclear detonations into the magnetosphere. Under the scientific direction of Air Force Cambridge Research Laboratories, a number of instruments were chosen for inclusion in the payload. In addition to Air Force Cambridge Research Laboratories, the following organizations participated in the experiment: American Science and Engineering, Inc., Lawrence Radiation Laboratory, Johns Hopkins University, the University of Utah, Air Force Special Weapons Center, and Lockheed Missiles and Space Company.

The pertinent parameters for the satellite orbit at early times were the following: apogee, 3000 n.m.; perigee, 115 n.m.; orbit inclination, 71°; orbital period, 147 min; apsidal rate, 0.8° per day. Fig. 1 illustrates these

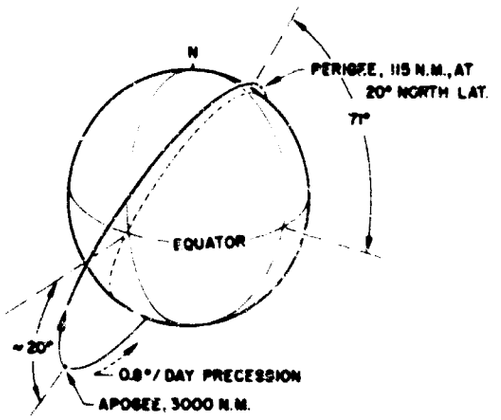

Fig. 1. Satellite orbit.

orbital parameters. The satellite pitch period was 127 sec, and the roll period was 53 sec. The satellite parameters were well suited to study the phenomena of interest. For example, the high eccentricity of the orbit enabled the acquisition of data at large L values near the equatorial plane. Slow tumbling rates, along with the chosen data sampling rate of about one per second, permitted the use of instruments which could measure accurately the angular distributions of trapped particles.

Fig. 2 shows the projection of an early orbit on a dipole field. The coordinates are the usual "natural" B L coordinates of McIlwain [2]. The squares and circles show regions of data acquisition in the 1.2 and 1.9 L shells, shells of interest with respect to artificial radiation belts.

The instruments comprising the total payload were selected to yield redundant measurements in the energy range corresponding to fission electrons, and to include narrow acceptance angle detectors as well as omnidirectional detectors. Instruments obtained their power from a large capacity battery pack to avoid degradation of the experiment due to possible solar

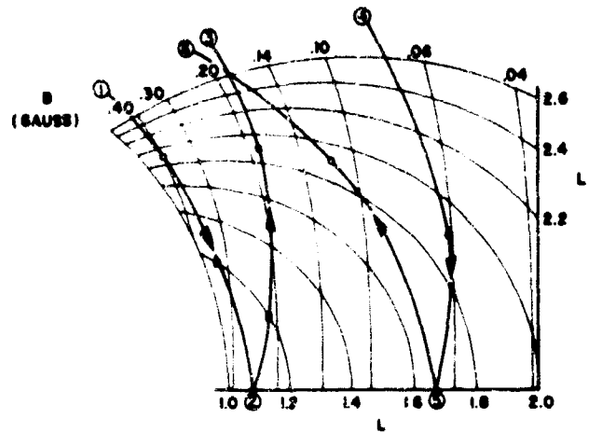

Fig. 2. Locus of an orbit in B-L space.

cell damage. Data could be acquired both by direct "real-time" read-out and by command read-out of a tape recorder capable of storing data from all instruments for a time longer than the orbital period.

This paper will deal with the data obtained from the AFCRL-ASE portion of the payload only. Data obtained by other experimenters are reported elsewhere [8]. At this time, only a small portion of the available data has been analyzed. This is especially true of data referring to spectral information. In a previous paper [1] the authors presented data illustrating the gross aspects of the artificial belts. This paper emphasizes the measured pitch angle distributions as functions of both time and magnetic shell, and the information derived from them. Efforts of analysis have been concentrated on data obtained between 27 October and 30 October. As a result, the effects of primarily a single nuclear detonation are investigated, albeit fairly completely.

Programs for both 7090 and 1620 IBM computers have been developed and used whenever possible in data reduction. Digitized tapes with merged ephemerides, including B, L coordinates derived from McIlwain's model [2], and punched cards bearing detector calibrations are primary data inputs for such programs. Outputs include a B, L matrix with detector counting rates as elements. Programs also exist for yielding pitch angle distributions directly when magnetometer data are added to the input.

2. Instrumentation

The five scintillation detectors comprising the AFCRL-ASE portion of the payload were designated Beta 1, Beta 2, Gamma, P and P alpha. There is evidence that the P alpha detector malfunctioned shortly after

TABLE 1
Instrument characteristics

Instrument	Field of view		Scintillator (g/cm²)	Shielding: Window; Sides			Detector threshold (MeV)		
	$\Delta\theta$ (deg.)	$\Delta A\,\Delta\Omega$ (cm²·ster)					γ	e	P
Beta–1	90	1.8×10^{-2}	0.3 "B" Plastic	3 mg/cm² Al; ≥ 3 g/cm² Al	A	ϕ		0.5	2.0
					B	ϕ		1.0	2.8
Beta–2					C*	W		0.05	1.4
Gamma	120	1.8	4.5 CsI(Tl)	2 g/cm² Al; ≥ 4 g/cm² Al	A*	ϕ	0.5	4.5	40.+
					B	ϕ	1.0	5.0	40.+
					C	W	0.04	4.0	40.
P	6	1.7×10^{-3}	12.5 CsI(Tl)	70 mg/cm² Al; 25 g/cm² Fe	A*	ϕ	1.0	1.0	6.2
					B	ϕ	2.0	2.0	6.5
					C	ϕ	4.0	4.0	7.6
					D	ϕ	8.0	8.0	10.5
					E	ϕ	20.	20.	21.
					F	ϕ	30.	30.	31.
					G	ϕ	50.	50.	51.
					H	ϕ	70.	70.	70.
					J	W	0.012	0.3	6.0

Key: ϕ: Flux measurement.
W: Rate of energy deposition measurement.
A thru J: Channel identification.

launch. The most salient features of the remaining four instruments are summarized in table 1.

It will be observed that detectors Beta-1, Beta-2 and Gamma have extremely wide fields of view for charged particles (detector Gamma has essentially a 4π field for gamma radiation). These instruments were utilized in determining the gross aspects of the artificial belts. Detector P has an extremely narrow field of view, and is essentially a "directional differential intensity" detector. This detector was used in obtaining pitch angle distributions. Output channels most used for the data presented in this paper are marked with an asterisk.

All detectors obtained energy spectra information by means of pulse

height discrimination performed in the various electronic logics of each output channel. Threshold discrimination was utilized, hence the output counting rates are integral counting rates. All counting ratemeters and photomultiplier current meters had logarithmic responses in order to achieve wide dynamic range. Time constants of the circuits, in the ranges of counting rate encountered, were less than 1 sec.

Discrimination among types of particles (electrons, protons or gammas) is achieved by a comparison of the observed counting rates and the rates of energy deposition in several channels, and by roll-modulation observations. In artificial radiation belts produced by high altitude nuclear detonations, the detected particles are predominantly electrons.

3. Presentation of preliminary data; discussion

Figs. 3, 4 and 5 indicate some of the gross aspects of the observed artificial radiation belts. The data serve to give a semi-quantitative picture of the changes occurring in certain regions of the magnetosphere at that time.

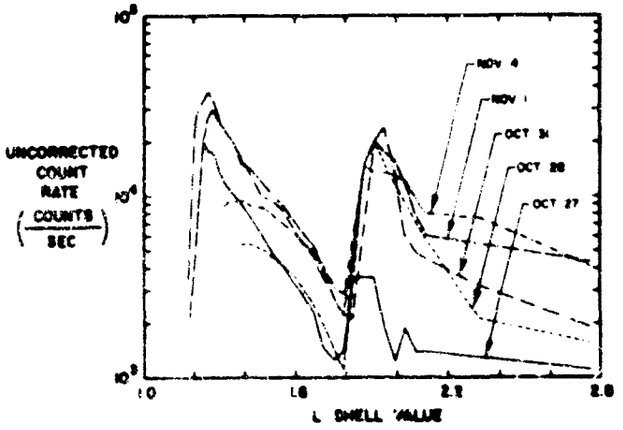

Fig. 3. High energy electrons ($E > 4.5$ MeV); $B = 0.170$–0.205.

In fig. 3, the uncorrected peak counting rate of detector Gamma is given as a function of the L-shell for different times of observation. The peak counting rate is the maximum counting rate measured during a tumble period of the satellite. In cases where dwelling time in a particular L-shell was sufficiently long, an average peak value was used. The counting rate is thus a measure of, but not necessarily linearly proportional to, for all B, L values, the omni directional flux. All data were taken for an interval of magnetic field intensity B between 0.170 and 0.205 gauss. The disagree-

ment in counting rates shown in figs. 3 and 4 for L-shells less than 1.8 are probably due to this large B interval. The particles observed by this detector are deduced to be electrons rather than gamma radiation since: (a) strong roll-modulation is apparent in the raw data; (b) channels A and B read very much the same; and (c) the rate of energy deposition indicated in channel C is consistent with the measured flux and with each particle depositing a few MeV of energy in the scintillator. Protons of energy greater than 40 MeV are ruled out by the absence of a signal in channel F and by the low counting rates in channels D and E of detector P. In the preparation of fig. 3, time corrections were applied to ephemeris data to make all peaks coincide at $L \approx 1.9$. This action was deemed necessary by the following observations. In each complete satellite orbit, there were three distinct regions in which extremely high fluxes were encountered. In some orbits, ephemeris data led to a unique value of $L \approx 1.9$ for each of these regions. On other orbits, three different L values were deduced. This shift in L values occurred in some cases even for consecutive orbits. In all of these latter cases, a unique time shift for all data of an orbit, usually of the order of 10–30 sec (although sometimes in the hundreds of seconds), led to the same $L \approx 1.9$ assignment for all three regions. If this correction is not made, unrealistic models must be invoked to explain the apparent violent vertical shifts of an entire radiation belt.

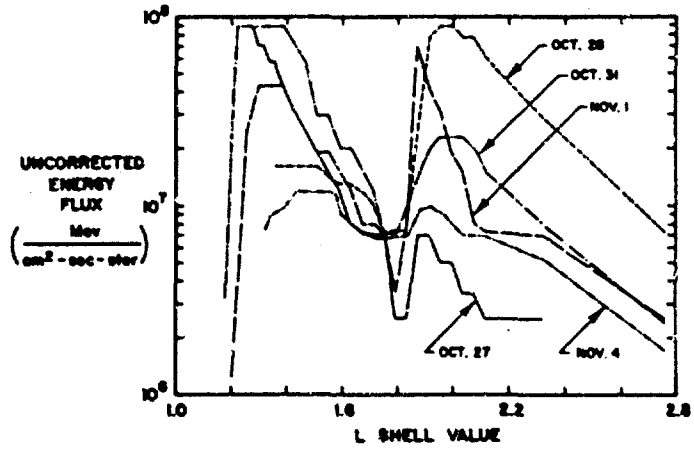

Fig. 4. Integral energy flux ($E > 50$ keV); $B = 0.170$–0.205.

Fig. 3 illustrates qualitatively the existence on 27 October of a radiation belt between L values of 1.2 and 1.7, and another around 1.9. The creation of a new belt around $L \approx 1.9$ on 28 October is evident. There is some evidence

of further injection into the $L \approx 1.9$ belt on 1 November. These dates can be correlated with known times of nuclear detonations. All new artificial belts peak around $L = 1.9$, and all exhibit tails extending well into higher L regions.

In fig. 4. the uncorrected peak rate of energy deposition in detectors Beta 1 and 2 is given as a function of L, for the same times as fig. 3. Comments made concerning data handling in the preparation of fig. 3 hold for these data also. The identification of the particles as predominantly electrons rather than gammas is inferred from: (a) the roll-modulation; (b) the extremely low efficiency of the detector for gammas coupled with the high counting rates observed in channels A and B; and (c) the consistency of the latter counting rates with the counting rate of detector Gamma channels A and B. The identification of the particles as electrons rather than protons is implied again by the physics of nuclear detonations, at least in the regions of the newly created belts. This latter statement requires some qualification. For L values less than about 1.7, channels A and B of detector P read essentially the same. This indicates the existence of some protons in these regions.

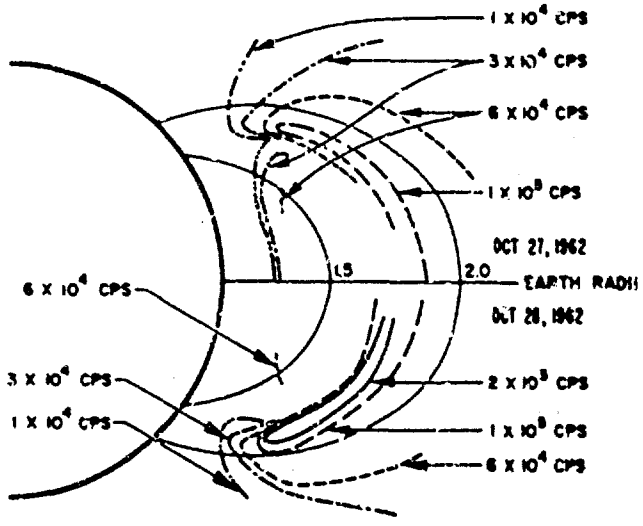

Fig. 5. Isointensity contours for high energy electrons (> 4.5 MeV), uncorrected rates.

Fig. 4 leaves no doubt about the creation of new artificial radiation belts on 28 October, and again on 1 November, in the $L \approx 1.9$ shell. An additional interesting observation is that the decay of the $L \approx 1.9$ belt between 28 and 31 October and again between 1 and 4 November is much more pronounced than in fig. 3. This suggests a relative hardening of the radiation

in that belt – an effect not inconsistent with dumping through the process of scattering in the atmosphere at high B values.

Fig. 5 gives iso-intensity contours for electrons of energy greater than 4.5 MeV measured by detector Gamma. The upper half of the figure gives contours observed on 27 October; the lower half, those observed on the 28th. The contours were obtained by sampling peak counting rates throughout the region. This figure indicates the "boundaries" for the artificial belt created on the 28th and those previously in existence, accredited to an earlier Soviet shot, and to an American shot of the summer of 1962 [3, 4]. Comment on fig. 5 will be curtailed since better data pertaining to iso-intensity contours have since been obtained and will be discussed later.

The remaining data presented in what follows are all concerned with pitch angle distributions and derived parameters such as omni-directional flux. The pitch angle distributions were calculated from the channel A output of the narrow (about 6°) field of view detector (detector P) coupled with satellite aspect relative to the magnetic field vector as derived from the magnetometer signals.

Fig. 6 shows, as a function of time, a typical portion of the raw data from detector P and the corresponding calculated value of the cosine of the pitch angle θ. If we accept these pitch angle curves at face value, we would

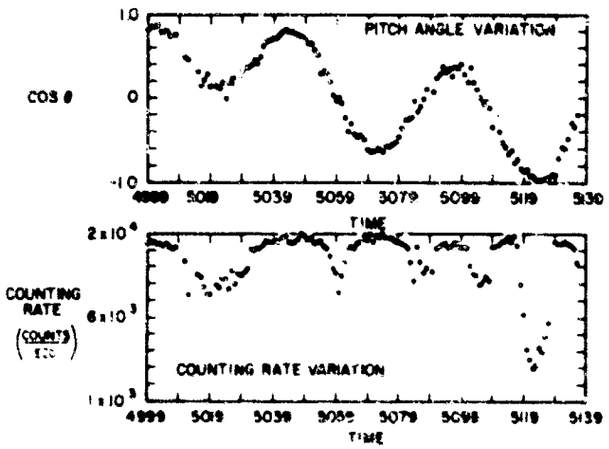

Fig. 6. Typical data.

obtain inconsistent distributions from the left and right portions about a maximum or minimum of the cos θ curve. We demand consistency about maxima and minima in our analysis, attributing the apparent angular discrepancies to magnetometer error. This amounts to assuming axial symmetry about a B-field line.

There is little doubt that the magnetometer data are in error. The angular discrepancy is always greater in low B-field regions. Furthermore, if we plot the difference in absolute values between the magnetic field strength given in the ephemeris (calculated from the Jensen and Cain model) and the magnetic field strength derived from the magnetometers, we obtain an oscillatory function with a time behavior characteristic of the pitch-and-roll behavior of the satellite. Such an apparent magnetometer error may be due to the residual magnetic field of the satellite or to magnetometer calibration drifts. Insufficient magnetometer data have been analyzed, so far, to enable a definite conclusion in this respect, although the latter type of error seems to be indicated. The angular discrepancy does not seem to be due to timing errors since in the same orbit the angular shift required to bring about data consistency is just as apt to be positive as negative. We have, therefore, in our treatment of the data, shifted the aspect function by the amount required to bring about data consistency. The magnitude of such a shift seldom exceeds 6° and, as stated, tends to be larger in the low B-field regions of the orbit. The counting rate curve in fig. 6 gives many examples of the so-called "butterfly" distribution, which is characteristic of radiation belts generated by the injection of particles off the equatorial plane.

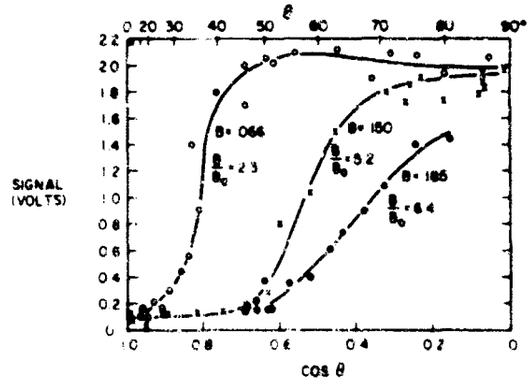

Fig. 7. Pitch angle distributions; electrons of $E > 1$ MeV, 1000–1200 UT, 28 Oct. '62; $2.189 < L < 2.212$.

Fig. 7 gives pitch angle distributions obtained on 28 October in the $L = 2.14$ to 2.32 shell at three different B values. The ordinate is the raw output signal from channel A of detector P and is very nearly proportional to the logarithm of the particle counting rate. Errors in individual data point signals amount to errors in counting rate of the order of $\pm 10\%$

(except in cases of telemetry noise). Smoothed curves are probably dependable to within 5 %. All curves in the vicinity of the low pitch angle cut-off are somewhat questionable however, not only because of the 6° field of view of the detector P, but more important because of errors in the determination of the value of the cosine of the pitch angle. The abscissa is the absolute value of the cosine of the pitch angle, $\cos\theta$, plotted from $|\cos\theta| = 1$ to $|\cos\theta| = 0$, so that pitch angles read from 0 to 90°, left to right, on a non-linear scale. Data points obtained for $90° < \theta < 180°$ have been reflected about 90° before plotting. This amounts to assuming fore-and-aft symmetry with respect to a B-field line. This assumption appears to be valid (at long enough times after a nuclear detonation) in that the data points for $90 < \theta < 180$ plotted separately (when such points are available) do indeed define the same curve, with fluctuations, as those for $0 < \theta < 90°$.

We have adopted the convention of plotting angular distributions as a function of the cosine for two reasons: first, solution of the aspect problem leads directly to the determination of $\cos\theta$; second, and most important, it can be shown that the area under such curves (when the ordinate is plotted linearly as detector counting rate) is proportional to the omni-directional flux.

The curves shown obey the well-known transformation law for directional differential intensities [5]:

$$I_1(\theta_1, B_1, L) = I_2(\theta_2, B_2, L).$$

This is a direct consequence of Liouville's Theorem. The intensity I has the units of particles/sec·cm²·ster and is linearly proportional to the counting rate seen by a "differential" detector such as detector P. The subscripts 1 and 2 refer to the angular distributions in different regions of the same L-shell. The pitch angles θ_1 and θ_2 are related by

$$\frac{\sin^2\theta_1}{B_1} = \frac{\sin^2\theta_2}{B_2}.$$

This results from the adiabatic invariance of the magnetic moment. The angular distributions at different B values can be transformed to partial angular distributions in the equatorial plane by using these equations. Fig. 8 shows the results of such a transformation; the equatorial value of B is denoted by the subscript 0. As is apparent, all data points lie on a single curve, "universal" for this shell. The distribution of fig. 8 goes through a maximum; the peak counting rate is about 1000 counts/sec.

The authors of this paper have adopted as a standard practice, in dealing with pitch angle distributions, the immediate transformation of all distri-

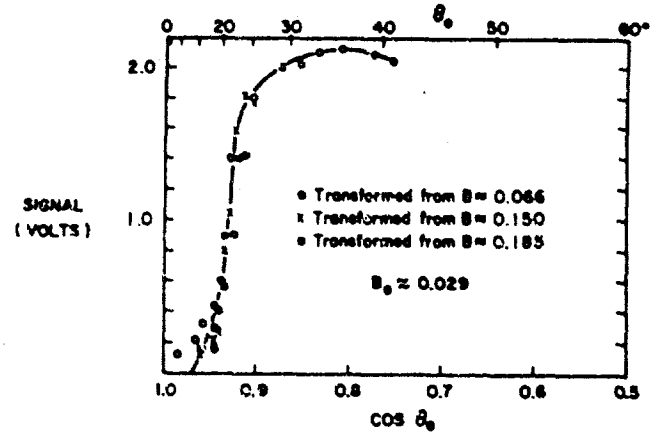

Fig. 8. Equatorial pitch angle distribution; electrons of $E > 1$ MeV; 1000–1200 UT· 28 Oct. '62; $2.189 \leqslant L \leqslant 2.212$.

butions obtained to the equatorial plane of the shell concerned. All data presented below have been so treated. With few exceptions, all such equatorial distributions are the result of at least two separate (generally three) data acquisitions within the shell, usually from the same orbit. Other than corrections previously mentioned, no others were applied in deriving the equatorial distributions. This procedure leads to incomplete equatorial distribution functions, since a distribution (even if complete) taken at a field value B in a given shell can only define the equatorial distribution up to a "cut-off" angle $\theta_0^{\max}$ given by

$$\sin^2 \theta_0^{\max} = B_0/B.$$

That is, no information can be obtained on the pitch angle distributions of those particles which mirror within the shell between the region of B (or its conjugate point) and the equatorial plane at B_0. A few distributions are incomplete because of incomplete pitch angle coverage by the satellite pitch and roll. A complete distribution at some point B_1 will always lead to a complete distribution at all points in the same shell which have a $B > B_1$, of course.

We have found the aforementioned procedure very useful. Besides limiting the number of variables which must be considered (to E, I, $\cos \theta_0$, L in equatorial plane) it facilitates identification of artificial belts, and allows checking of data consistency in a standard way. (All distributions obtained from a given L-shell at essentially the same time must transform to the same equatorial-plane distribution.) It further provides a convenient function for generating and determining omni-directional fluxes in regions of space

inaccessible to a satellite. This is accomplished by first transforming the distribution from (B_0, L) to (B, L), and then integrating over angle.

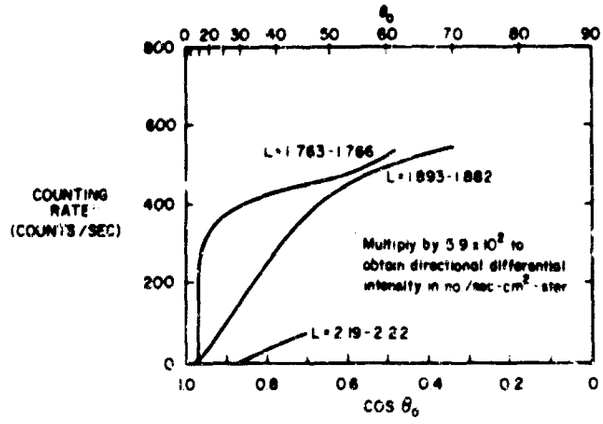

Fig. 9. Equatorial pitch angle distributions; electrons of $E \geq 1$ MeV; 1710–1930 UT 27 Oct. '62.

Fig. 9 gives equatorial pitch angle distributions for L shells in the vicinity of 1.8, obtained on 27 October. The detector P calibration has been incorporated, so that the ordinate is in units of actual detector counting rate. This can be converted to directional differential intensity (in units of particles/sec·cm²·ster) by multiplication by 5.9×10^2. All curves are smoothed, but the scatter of data points is about the same as shown in fig. 8. All the angular distributions exhibit what may be called a "predetonation" shape. This distribution favors pitch angles closer to 90° and has a low angle cut-off.

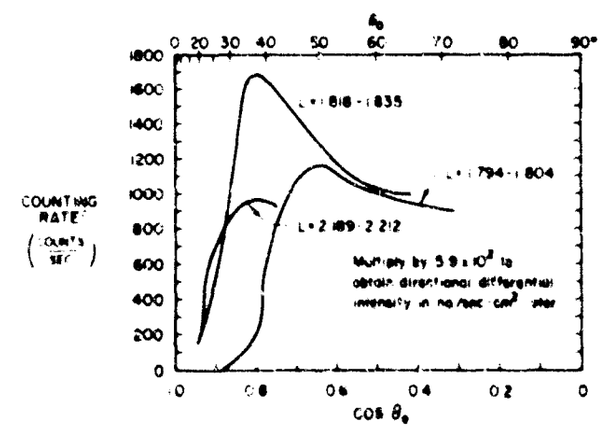

Fig. 10. Equatorial pitch angle distributions, electrons of $E \geq 1$ MeV, 1000–1300 UT 28 Oct. '62.

Fig. 10 also shows distributions for L-shells in the vicinity of 1.8, but obtained a day later on 28 October. A comparison with fig. 9 indicates the injection of particles into the shells in this vicinity which occurred sometime between the two data acquisitions. The major injection is localized within the $L = 1.818$ to 1.835 shell, although some injection into both the $L \approx 1.80$ and the $L \approx 2.20$ shell is also obvious. (The curve for $L \approx 2.20$ is the same as that shown in fig. 8.) The time can be correlated with the detonation of a Soviet nuclear device. All distributions illustrate the "butterfly" shape mentioned earlier, being most pronounced for $L = 1.818$ to 1.835.

Simple qualitative arguments can be used to explain the "butterfly" shape, and it may be well to point them out here. Assume point injection of electrons following the detonation of a nuclear device at an extremely high altitude well above the tangible atmosphere. Assume that the atmosphere can be represented by a slab and that any particle striking the top of this slab is lost. Let B_T, B_I and B_0, be the magnetic field strengths at the top of the slab, at the point of injection and in the equatorial plane, respectively, of the shell of injection. Then the equatorial pitch angle distribution of electrons will be characterized by a low angle cut-off, θ_T, given by

$$\sin^2 \theta_T = B_0/B_T$$

(i.e., no particle mirrors below the top of the slab) and a high angle cut-off, θ_I, given by

$$\sin^2 \theta_I = B_0/B_I$$

(i.e., no particle mirrors between B_I or its conjugate point and B_0). The sharpness of the low angle cut-off is smeared out since the atmosphere is not an ideal slab with a definite top. The sharpness of the high angle cut-off is smeared out since the injection does not occur at a point but has very significant extent in space due to the expansion and possible trapping of the fission debris. Radiation previously trapped in the shell with a more "normal" distribution, (pitch angles nearer 90° favored) completes the smearing out of the high angle cut-off to 90°.

Consider next a detonation at a low altitude within the atmosphere. The only major contribution to the radiation populating the belt for any appreciable period of time will be that due to the β-decay of fission debris isotopes which have been transported out of the dense region of the atmosphere. In this case we obtain a distribution of the same "butterfly" shape as before.

It will be noted in fig. 10 that the distribution for $L = 1.818$ to 1.835 peaks at about 37°; another distribution obtained for this shell earlier on

28 October peaks around 32°. Particles of pitch angle 35° mirror at a magnetic latitude of 30° and mean altitude of about 2300 km. The direct physical significance of this is not obvious since the measurements were performed at relatively late times after the detonation. The measurement of the angular distribution of the injected particles at early times after detonation may presumably yield information on the injection mechanism.

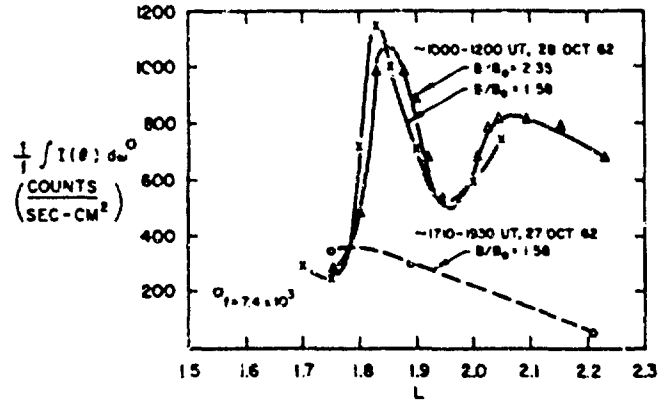

Fig. 11. Omni-directional flux; electrons of $E > 1$ MeV.

Fig. 11 is derived from the data presented in figs. 9, 10 and 12, and gives the omni-directional flux as a function of L-shell before the detonation for B/B_0 equal to 1.58, and after the detonation for B/B_0 equal to 1.58 and 2.35. B/B_0 equal to unity cannot be used since the equatorial pitch angle distributions are incomplete, and it is desirable to avoid extrapolation. The choice of a cut through L-shells at a constant B/B_0 is made because for identical equatorial pitch angle distributions in various shells, such a cut yields also identical pitch angle distributions. This choice thus seems the natural basis for comparison when it is desired to show the effects of shell number only. Fig. 11 is the "correct" version of figs. 3 and 4 shown earlier. Again, the belt created on 28 October is clearly evident, with a peak omni-directional flux in $L = 1.83$.

Fig. 11 shows a feature not evident in figs. 3 or 4 although suggested by the structure beyond $L = 2.0$. Differences between these representations should not be unexpected, however, since the figures represent different modes of cutting through L-shells and the figures refer to different threshold energies. Moreover, the narrow field detector yields a more accurate measurement of omni-directional flux. The $B/B_0 = 1.58$ curve shows a slot at $L = 1.95$ and a subsequent rise in counting rate which presumably goes through a peak beyond $L = 2.05$. The $B/B_0 = 2.35$ curve shows clearly the existence of

a second belt, peaked at $L \approx 2.10$, and somewhat broader than that at $L = 1.83$. Both belts were apparently generated by the same nuclear detonation, judging from the 1.58 curve taken on the 27th of October.

Fig. 12 gives iso-intensity contours, on a dipole field, for 28 October. The number defining the contours are omni-directional fluxes derived by first transforming the equatorial pitch angle distribution of each L-shell to various B values in that shell, and then integrating over pitch angle at each B value. Each number used is probably good to within 10 % considering only statistical accuracy. Larger systematic errors previously discussed may exist in the determination of position. The omni-directional flux J at a point (B, L) is given explicitly by

$$J(B, L) = 4\pi \int_{\lambda}^{0} I(\cos 0, B, L)\, \mathrm{d}(\cos \theta).$$

Fig. 12 is the "correct" version of fig. 5. One feature that at first glance may seem surprising – namely a region of maximum intensity in the 1.83 shell off the equator, around $B = 0.08$ – is a natural consequence of the "butterfly" shape of the distribution. In fact, any distribution that presents a peak at an angle different from 90° in the equatorial plane will lead to a maximum omni-directional flux at some high B value in the shell. The

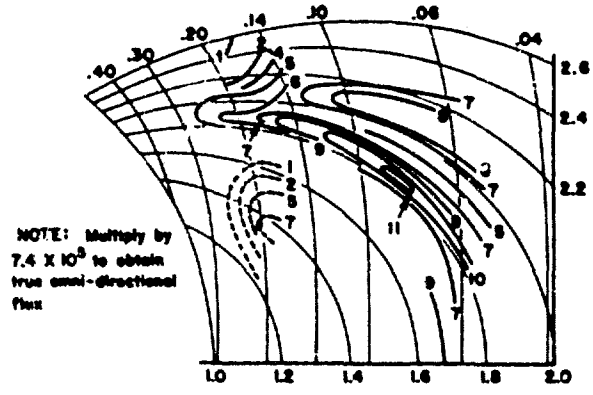

Fig. 12. Iso-intensity contours; electrons of $E > 1$ MeV; 1000-1200 UT. 28 Oct. '62.

contours in the region defined by $1.2 < L < 1.6$, and $0.26 < B < 0.16$ are shown as "uncertain" since there are indications from our data that these are due to an admixture of both protons and electrons. Insufficient analysis has been performed for an accurate determination of the relative abundance of each particle. These are probably contours of the natural inner belt. Omni-directional fluxes observed are not inconsistent with an $E^{-1.6}$ proton

integral spectrum, with $E = 6$ MeV, where fluxes observed from protons of $E > 40$ MeV by Van Allen [6] are used to determine the scaling factor (about 5×10^7).

Fig. 12 indicates clearly the existence of two well defined belts on 28 October. A Soviet detonation was known to occur in the vicinity of $L = 1.83$ on this date. The belt at $L = 1.83$ is the sharper of the two, and the one most easily recognizable. The shell at $L = 2.1$ is nevertheless, also quite real, and new, as data from 27 October (see e.g. figs. 7 and 9) show low particle counting rates in this shell.

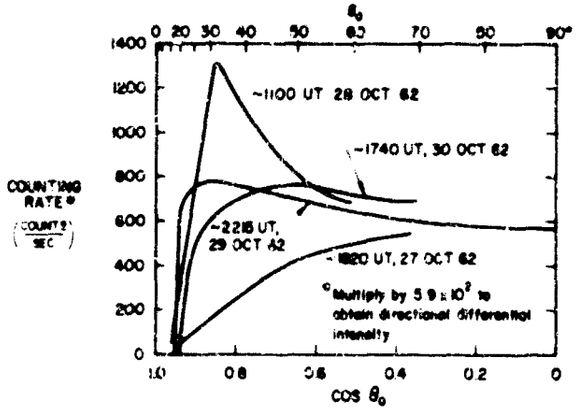

Fig. 13. Equatorial pitch angle distributions; $L \approx 1.83$.

Figs. 13 through 15 pertain to the time behavior of the L 1.83 radiation belt between 28 and 30 October. The ordinates of figs. 13 and 14 are dependable to within 5 %, except, as usual, in the vicinity of the cut-off; the ordinate of fig. 15 is probably good to 7 %. Fig. 13 gives the equatorial distribution at L 1.83 at three different times after the event, and on the day before the event. The most obvious features are the shift of the peak towards 90° and the decrease in the peak (a tendency towards isotropy) in qualitative agreement with the more pronounced effect of atmospheric scattering on particles of lower pitch angle. The question of whether these decay rates are consistent with removal by scattering on atmospheric particles alone is being studied and is obviously of geophysical significance.

Fig. 14 is a plot of intensities in the L 1.83 shell versus time for different pitch angles. Changes are seen to occur most rapidly at early times, particle intensities at the smaller pitch angles tend to change the fastest, and distributions at late times tend to approach isotropy (as indicated by the groupings of points at 35 and 55 hr). The extremely fast decay of the intensity

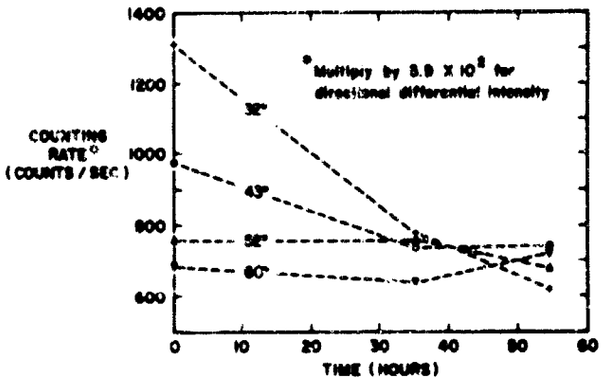

Fig. 14. Time behavior of $L = 1.83$ belt at constant pitch angle.

at pitch angle 32°, which mirrors at a mean altitude of 1909 km, is not too surprising. The initial fast decay of the intensity at pitch angle 43°, which mirrors at a mean altitude of 3100 km, is surprising. If the data are believed, this suggests a removal mechanism other than atmospheric scattering for this L-shell region although a definite conclusion must be reserved until atmospheric scattering calculations are performed. It would also be well to look closely at pitch angle distributions of radiation in unperturbed shells,

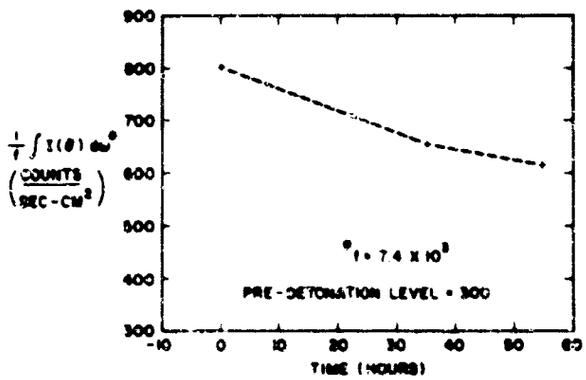

Fig. 15. Decay of $I = 1.83$ belt omnidirectional flux $B/B_0 = 1.58$.

and study them for long periods of time. The relative time independence of the intensities at pitch angles 52° and 60° (and higher, as indicated in fig. 13) is understandable. There may even be a tendency for intensities at very large pitch angles to increase with time (as suggested by the 60° curve), an effect consistent with the theoretical calculations of Walt [7] showing upward as well as downward diffusion of mirror points of particles scattered in the atmosphere.

Fig. 15 is a replot of the data of fig. 13, giving omni-directional fluxes in the $L = 1.83$ belt as a function of time. The decay of the radiation component injected into this shell on 28 October is not inconsistent, for the three day interval of observation, with an exponential decay half-life of approximately 75 hr. However, the decay rate is certainly very dependent on pitch angle distribution. Since all distributions tend ultimately toward the "normal" shape, with pitch angles towards 90° favored, the decay rate should certainly decrease with time. Comparison of figs. 14 and 15 shows that the drastic effects indicated in fig. 14 tend to be masked by the integration over pitch angle, and strongly implies that curves like fig. 14, derived from pitch angle distributions are most useful in time behavior studies.

4. Closing remarks

The possibility of the creation of double belts by a single nuclear detonation is indicated by the data. We have as an example, in the present case, the generation of two well defined belts, at $L \approx 1.83$ and $L \approx 2.1$, by the burst of 28 October.

Mechanisms for electron removal other than atmospheric scattering may be at work. In any event, the most profitable means of studying the time behavior of artificial belts seems to be by intensity at constant pitch angle versus time data.

Information on omni-directional flux and iso-intensity contour maps alone have limited usefulness as a means of studying the dynamics of radiation belts. Data of prime importance are pitch angle distributions obtained at various L values in the equatorial plane. These can be used to obtain the omni-directional flux and iso-intensity contours as well.

This report may serve to illustrate the methods of data handling used by the authors, and may give some indication of the nature of the information to be learned from satellite data analysis, in particular from pitch angle distributions. Work will continue in all aspects of data reduction. Of particular interest will be data obtained subsequent to the latest observed nuclear detonation which will allow a long time study of the artificial belt created by that detonation without complication by further injection. Data pertaining to energy spectra, so far almost completely untouched, will be analyzed. Derivation of iso-intensity contours, using the methods of pitch angle transformation described in this report, are in progress for various times of interest. Attempts will be made to calculate the effects of atmospheric scattering on pitch angle distributions, and to check the consistency of the results of such calculations with the experimentally observed data.

A minor program to detect systematic errors in the magnetometer calibrations will also be attempted in hopes of improving aspect determination.

References

1. L. Katz, D. Smart, F. R. Paolini, R. Giacconi and R. J. Talbot Jr., Recent Changes in the Artificial Radiation Belts. Presentation at the 44th Annual Meeting, American Geophysical Union, Washington DC, 18 April 1963
2. C. E. McIlwain, J. Geophys. Research 66 (1961) 3681
3. W. L. Brown and J. D. Gabbe, J. Geophys. Research 68 (1963) 607
4. L. A. Frank, B. J. O'Brien and J. A. Van Allen, J. Geophys. Research 68 (1963) 619
5. S. Olbert and B. Rossi, Particles and Fields in Outer Space, Lecture Notes on a course given at M.I.T., Section V (1961), unpublished
6. J. A. Van Allen, Transactions of the International Astronomical Union 11B (1962) 99
7. W. M. MacDonald and M. Walt, J. Geophys. Research 67 (1962) 5025
8. H. I. West Jr., L. G. Mann and S. D. Bloom; B. Clark and D. A. Adams; R. V. Smith; Various Papers, 44th Annual Meeting, American Geophysical Union, Washington DC, 18 April 1963.

Unclassified
Security Classification

DOCUMENT CONTROL DATA - R&D

(Security classification of title, body of abstract and indexing annotation must be entered when the overall report is classified)

1. ORIGINATING ACTIVITY *(Corporate author)*
American Science and Engineering, Inc.
11 Carleton St., Cambridge, Mass.

2a. REPORT SECURITY CLASSIFICATION
Unclassified

2b. GROUP

3. REPORT TITLE
A RESEARCH PROGRAM TO INVESTIGATE ARTIFICIALLY INJECTED TRAPPED RADIATION

4. DESCRIPTIVE NOTES *(Type of report and inclusive dates)*
Final Report

5. AUTHOR(S) *(Last name, first name, initial)*
Giacconi, R.; Paolini, F. R.; Hadley, W. C.; Talbot, R., Jr.

6. REPORT DATE	7a. TOTAL NO OF PAGES	7b. NO. OF REFS
30 October 1964	149	11

8a. CONTRACT OR GRANT NO. AF 19(628)-2799	9a. ORIGINATOR'S REPORT NUMBER(S)
b. PROJECT NO. 8600	ASE-759
c. TASK 860006	9b. OTHER REPORT NO(S) *(Any other numbers that may be assigned this report)*
d.	AFCRL-64-917

10. AVAILABILITY/LIMITATION NOTICES
Qualified requestors may obtain copies of this report from DDC.

11. SUPPLEMENTARY NOTES	12. SPONSORING MILITARY ACTIVITY
	Office of Aerospace Research Air Force Cambridge Research Labs. Bedford, Massachusetts

13. ABSTRACT

This document describes an experimental research program to measure the intensity, angular distribution, and energy spectra of particles trapped in the Earth's magnetic field. Particular attention has been focused on the measurement of particles artificially injected by high altitude nuclear detonations during the series of nuclear tests conducted by the USSR and the USA during the summer and fall of 1962. A detailed description of the instrumentation and calibration procedures are given. Measurements obtained by instrumentation identical to the one here described, flown on an Air Force satellite (1962 βk) are given. The method of data handling is discussed and machine programs for data reduction are described. Results from these measurements have appeared in several documents, a listing of which is included in the text. A summary of the results and conclusions is given.

DD FORM 1 JAN 64 1473

Unclassified
Security Classification

Unclassified
Security Classification

14. KEY WORDS	LINK A		LINK B		LINK C	
	ROLE	WT	ROLE	WT	ROLE	WT
1 Artificial Radiation Belts						
2 Trapped Radiation in Earth's Magnetosphere						
3 Effects of Soviet High Altitude Nuclear Tests on Radiation Belts (Oct. 1962)						
4 Satellite 1962βk Measurements in the Magnetosphere						

INSTRUCTIONS

1. ORIGINATING ACTIVITY: Enter the name and address of the contractor, subcontractor, grantee, Department of Defense activity or other organization *(corporate author)* issuing the report.

2a. REPORT SECURITY CLASSIFICATION: Enter the overall security classification of the report. Indicate whether "Restricted Data" is included. Marking is to be in accordance with appropriate security regulations.

2b. GROUP: Automatic downgrading is specified in DoD Directive 5200.10 and Armed Forces Industrial Manual. Enter the group number. Also, when applicable, show that optional markings have been used for Group 3 and Group 4 as authorized.

3. REPORT TITLE: Enter the complete report title in all capital letters. Titles in all cases should be unclassified. If a meaningful title cannot be selected without classification, show title classification in all capitals in parenthesis immediately following the title.

4. DESCRIPTIVE NOTES: If appropriate, enter the type of report, e.g., interim, progress, summary, annual, or final. Give the inclusive dates when a specific reporting period is covered.

5. AUTHOR(S): Enter the name(s) of author(s) as shown on or in the report. Enter last name, first name, middle initial. If military, show rank and branch of service. The name of the principal author is an absolute minimum requirement.

6. REPORT DATE: Enter the date of the report as day, month, year, or month, year. If more than one date appears on the report, use date of publication.

7a. TOTAL NUMBER OF PAGES: The total page count should follow normal pagination procedures, i.e., enter the number of pages containing information.

7b. NUMBER OF REFERENCES: Enter the total number of references cited in the report.

8a. CONTRACT OR GRANT NUMBER: If appropriate, enter the applicable number of the contract or grant under which the report was written.

8b, 8c, & 8d. PROJECT NUMBER: Enter the appropriate military department identification, such as project number, subproject number, system numbers, task number, etc.

9a. ORIGINATOR'S REPORT NUMBER(S): Enter the official report number by which the document will be identified and controlled by the originating activity. This number must be unique to this report.

9b. OTHER REPORT NUMBER(S): If the report has been assigned any other report numbers *(either by the originator or by the sponsor)*, also enter this number(s).

10. AVAILABILITY/LIMITATION NOTICES: Enter any limitations on further dissemination of the report, other than those imposed by security classification, using standard statements such as:

(1) "Qualified requesters may obtain copies of this report from DDC."

(2) "Foreign announcement and dissemination of this report by DDC is not authorized."

(3) "U. S. Government agencies may obtain copies of this report directly from DDC. Other qualified DDC users shall request through _____."

(4) "U. S. military agencies may obtain copies of this report directly from DDC. Other qualified users shall request through _____."

(5) "All distribution of this report is controlled. Qualified DDC users shall request through _____."

If the report has been furnished to the Office of Technical Services, Department of Commerce, for sale to the public, indicate this fact and enter the price, if known.

11. SUPPLEMENTARY NOTES: Use for additional explanatory notes.

12. SPONSORING MILITARY ACTIVITY: Enter the name of the departmental project office or laboratory sponsoring *(paying for)* the research and development. Include address.

13. ABSTRACT: Enter an abstract giving a brief and factual summary of the document indicative of the report, even though it may also appear elsewhere in the body of the technical report. If additional space is required, a continuation sheet shall be attached.

It is highly desirable that the abstract of classified reports be unclassified. Each paragraph of the abstract shall end with an indication of the military security classification of the information in the paragraph, represented as *(TS), (S), (C), or (U).*

There is no limitation on the length of the abstract. However, the suggested length is from 150 to 225 words.

14. KEY WORDS: Key words are technically meaningful terms or short phrases that characterize a report and may be used as index entries for cataloging the report. Key words must be selected so that no security classification is required. Identifiers, such as equipment model designation, trade name, military project code name, geographic location, may be used as key words but will be followed by an indication of technical context. The assignment of links, rules, and weights is optional.

Unclassified
Security Classification